University of Alberta

Structure, function and evolution of enzymes involved in poxviral nucleotide metabolism

by

John-Paul Bacik ©

A thesis submitted to the Faculty of Graduate Studies and Research
in partial fulfillment of the requirements for the degree of

Doctor of Philosophy

in

Macromolecular Crystallography

Department of Medical Microbiology & Immunology

Edmonton, Alberta
Fall, 2008

And David put his hand in the bag and took out a stone and slung it. And it struck the Philistine on the head and he fell to the ground.

Samuel 17:49

"Seen in the light of evolution, biology is, perhaps, intellectually the most satisfying and inspiring science."

- Theodosius Dobzhansky

"No amount of experimentation can ever prove me right; a single experiment can prove me wrong."

- Albert Einstein

Acknowledgements

I would like to thank my Mum and Dad for their unwavering support and guidance throughout the years. I thank my sisters, Pam and Michelle, who have proven to be great role models and I always will always look up to them. I thank my supervisor, Dr. Bart Hazes, for being a great mentor and friend, and for teaching me the skills I will need to be successful as a scientist. I thank others in the lab that have made this work possible, including Luke Price, Gerald Audette, Lisa Channon, Angela Brigley and Kirsty Dunlop. I acknowledge my project committee members, Dr. Mark Glover and Dr. Michele Barry, for their helpful advice and contributions to my project. Finally, I thank the rest of my friends and family who have supported me over the years; most importantly, the Thiessens, the Millers and the Worthingtons. Finally, I dedicate this thesis to my late Grandma, Christine Bacik, who was the kindest person I have ever met and will always be a great source of inspiration to me.

ABSTRACT

Poxviruses are large DNA viruses that replicate exclusively in the cytoplasm of host cells. To sustain genome replication independent of the host nucleus and cell cycle, most poxviruses encode genes involved in nucleotide metabolism. One such enzyme, ribonucleotide reductase (RNR), is required for the synthesis of deoxyribonucleotides through the reduction of ribonucleotides in all living cells and many viruses. Glutaredoxins (Grx) act as reducing agents for RNR in many prokaryotes and eukaryotes, including humans. The same relationship has been proposed for the Grx-1 and R1 proteins expressed by all orthopoxviruses, including vaccinia, variola, and ectromelia virus. To study structure-function relationships of the Grx family, and reveal potential viral adaptations, crystal structures of the ectromelia virus Grx-1, EVM053, were solved in the oxidized and reduced states. The structures demonstrated a large redox-induced conformational rearrangement of a tyrosine, Tyr21, near the active site. The movement of Tyr21 is a viral-specific adaptation that may alter enzyme redox potential or enhance substrate interactions. EVM053 also exhibits a novel *cis*-proline, Pro53, in a loop that has been shown to contribute to R1-binding in *E. coli* Grx-1. The *cis*-peptide bond of Pro53 may be required to promote electrostatic interactions between Lys52 and the C-terminal carboxylate of R1. Mutagenesis combined with functional analyses was used to further assess the importance of these residues for catalysis and substrate specificity. Dimethylarsenite was covalently attached to the active site cysteine, Cys23, in the reduced EVM053 structure, and this led to the discovery that both EVM053 and human Grx-1 have dimethylarsenate reductase activity. Methylation and reduction of arsenic metabolites is widely considered to be part of the detoxification

of arsenic in many mammals, including humans. Class omega glutathione-S transferases (GSTO), demonstrate several structural and functional properties similar to that of Grxs and also have been shown to act as reducing agents for methylated arsenic species. GSTO activity has been implicated as a factor that contributes to the progression of neurodegenerative diseases such as Alzheimer's disease. These results point toward a previously unknown role for Grx in the prevention or progression of such diseases. In conclusion, these structural and functional analyses generated new testable hypotheses regarding Grx substrate specificity, control of redox potential, and a putative physiological role in arsenic metabolism.

Table of Contents

List of Tables

List of Figures

List of Abbreviations

AD, Alzheimer's disease

AMPPNP, 5'-adenylylimido-diphosphate

APL, acute promyelocytic leukemia

AS3MT, arsenic methyltransferase

AsIII, arsenite

AsV, arsenate

ATO, arsenic trioxide

ATP, adenosine triphosphate

DHA, dehydroascorbate

DLS, dynamic light scattering

DMA-5/DMAV, dimethylarsenate

DMA-3/DMAIII, dimethylarsenite

dGMP, deoxyguanosine monophosphate

DNA, deoxyribonucleic acid

dNDP, deoxyribonucleotidediphosphate

dNTP, deoxyribonucleotidetriphosphate

dTMP, deoxythymidine monophosphate

dTDP, deoxythymidine diphosphate

dTTP, deoxythymidine triphosphate

DTT, dithiothreitol

dUMP, deoxyuridine monophosphate

dUMPNPP, 2'-deoxy-uridine-5'-(α,β)-imido triphosphate

dUTP, deoxyuridine triphosphate

dUTPase, deoxyuridine triphosphate nucleotidohydrolase

EIAV, equine infectious anemia virus

EVM, ectromelia virus strain Moscow

FIV, feline immunodeficiency virus

GAPDH, glyceraldehyde-3-phosphate dehydrogenase

Grx, glutaredoxin

GSH, reduced glutathione

GSSG, oxidized glutathione

GST, glutathione S-transferase

GSTO, glutathione S-transferase Class Omega

HGT, horizontal gene transfer

IMAC, immobilized metal affinity chromatography

LB, Luria-Bertani

MBP, maltose binding protein

MCV, molluscum contagiosum virus

MMA-5/MMAV, monomethylarsenate

MMA-3/MMAIII, monomethylarsenite

MPD, 2-methyl-2,4-pentanediol

NADPH, nicotinamide adenine dinucleotide phosphate

NDP, ribonucleotidediphosphate

NLS, nuclear localization signal

NMR, nuclear magnetic resonance

NTD, N-terminal domain

PD, Parkinson's disease

PCR, polymerase chain reaction

PEG, polyethylene glycol

PDI, protein disulfide isomerase

RMSD, root mean square deviation

RNR, ribonucleotide reductase

ROS, reactive oxygen species

SSB, single stranded DNA binding protein

TMA, trimethylarsenic

TMPK, thymidylate kinase

TK, thymidine kinase

Trx, thioredoxin

UDG, uracil DNA glycosylase

WT, wild type

CHAPTER I

GENERAL INTRODUCTION

1.1 Poxviruses

1.1.1 Background

Smallpox (variola virus) is believed to have killed more people than any other virus and smallpox disease epidemics have greatly affected the course of human history (Kawalek and Rudikoff, 2002). The smallpox disease was widespread in medieval Europe and very early cases are known from ancient China and Egypt (Li *et al.*, 2007). European settlers introduced the virus into the new world and smallpox outbreaks were not uncommon in major North American cities even as the twentieth century began, with mortality rates of up to 40% (Fenner, 2000). Fortunately, the poxvirus family also provided an effective solution for smallpox disease in the form of cowpox and later vaccinia virus. The procedure of vaccination first introduced by Edward Jenner in 1796 provided long-term immunity to the disease and the continued use of this procedure ultimately led to the eradication of smallpox disease in 1980 (Hawkes, 1979; Berche, 2001; Stone, 2002).

Although smallpox outbreaks are now considered a thing of the past, the threat of future poxvirus outbreaks remains. Stocks of variola virus are still being held in secure repositories both in the United States and Russia (Kawalek and Rudikoff, 2002; Mahy, 2003). While the stocks could be used to develop more effective vaccines or antiviral agents, the risk of misuse of these stocks for the purposes of bioterrorism remains a distinct possibility (Esposito *et al.*, 2006). Viruses closely related to variola virus such as vaccinia, monkeypox and ectromelia (mousepox), could also potentially

1

be engineered into a deadly strain of the virus that could be used as a highly effective bioterror weapon. Furthermore, monkeypox has already caused sporadic zoonotic infections in humans, with mortality rates of up to 25% (Meyer *et al.*, 2002; Di Giulio and Eckburg, 2004).

The consequences of a poxviral outbreak in a largely non-vaccinated population would be very serious since worldwide vaccination campaigns were suspended in 1976 and there are currently only a limited number of antiviral agents available to treat poxviral infections in humans (Sliva and Schnierle, 2007). The effectiveness and safety of the few antiviral agents that do exist to treat such infections is also in doubt (Whitley, 2003). For example, cidofovir, the only antiviral agent currently approved for use against orthopoxviruses, has been shown to be ineffective against many strains of poxviruses, and may not be sufficient in the case of an outbreak of an engineered strain of variola (Smee *et al.*, 2002; Quenelle *et al.*, 2003). Renal toxicity is also an adverse reaction associated with cidofovir (De Clercq, 2003). Many countries have been stockpiling smallpox vaccine, but vaccination is also problematic since it can cause adverse reactions in immunocompromised individuals and also due to practical considerations (Smee *et al.*, 2004). With the potential use of poxviruses as a bioterror weapon and threat of further poxviral zoonotic infections in humans, continued research of poxviruses is important to discover therapeutic targets and develop effective antiviral agents to combat the possibility of poxvirus outbreaks in an unprotected world population (Mahy, 2003; Whitley, 2003).

1.1.2 Poxvirus biology

Poxviruses are large double-stranded DNA viruses that, unlike most other DNA viruses, replicate exclusively in the cytoplasm of host cells **(Figure 1.1)**. The virus codes for genes that are transcribed and expressed at different time points in the viral lifecycle and these gene products are divided into three categories; early, intermediate and late genes (Moss and Salzman, 1968; Broyles, 2003). Expression of early genes is initiated immediately after cell entry, before virus core unpacking, and this requires the presence of a set of viral proteins that are encapsidated in the viral particle during the late stages of virus morphogenesis (Moss, 2001). For the most part the proteins contained within the capsid form the transcription machinery required for the transcription of early genes (Katsafanas and Moss, 2007). The synthesis of early proteins is required for virion core uncoating, host interactions, release of the viral DNA into the cytoplasm and DNA replication (Schramm and Locker, 2005). Most poxviruses also encode early genes that are required for nucleotide metabolism and orthopoxviruses encode the largest number of genes involved in the production of deoxyribonucleotides, the precursors of genomic DNA (see section 1.1.4).

DNA replication takes place in virosomes that are synthesized in part from the membranes of the endoplasmic reticulum and are formed following the expression of early gene products (Schramm and Locker, 2005). Without access to the host cell replication machinery, which is only present in host cell nuclei, poxviruses must express many of the proteins required for DNA replication. These genes are essential for genome replication and include the DNA polymerase, single-stranded DNA-binding protein (SSB), uracil DNA glycosylase (UDG), and a nucleic acid-independent

Poxviral lifecycle

Poxviral Entry

Viral core and virion associated proteins released into cytoplasm

Early gene transcription, expression, and formation of virosome

Virosome

Intermediate gene transcription and expression, DNA replication, late gene transcription

Virion assembly, incorporation of late gene products into virion

Intracellular mature virion production

Membrane wrapping

Transport via microtubules

Virion release

Figure 1.1. Poxviral lifecycle

nucleoside triphosphatase (DNA primase) (Moss, 2001). Intermediate genes are transcribed at the end of the early phase and because most of the intermediate gene products act as transcription factors for late genes, they trigger the start of the late phase of the viral lifecycle. One exception is SSB, which is expressed at both early and intermediate times in the viral life cycle (Rochester and Traktman, 1998). Many late gene products are structural proteins that form the viral core or are involved in virion assembly (Condit *et al.*, 2006). As noted above, many of the late gene products are incorporated into the virion during the assembly process.

The mechanism of poxviral entry and release from cells remains a controversial subject that is complicated by the existence of multiple forms of the viruses that differ by the presence or absence of additional outer membranes (Moss, 2006). The mature viruses maintain at least one outer membrane, but mature virions may undergo additional membrane wrapping through the Trans Golgi network (Schmelz *et al.*, 1994). The viruses then move along microtubules towards the periphery of the cell, the outer membrane of the wrapped virus fuses with the plasma membrane, and the virus is released from the cell through exocytosis (Moss and Ward, 2001; Smith and Law, 2004).

1.1.3 Poxvirus phylogeny

Poxviruses are believed to share a common origin with a group of other large DNA viruses that includes the asfarviruses, iridoviruses, phycodnaviruses and mimiviruses (Iyer *et al.*, 2001). These viruses share several orthologous genes that are not present in any other viral or cellular life forms, and complete at least part of their

life cycle in the cytoplasm of host cells (Iyer *et al.*, 2006). Although the origin, mechanism of divergence and phylogenetic relationship between these viruses remains poorly understood, it is believed that gene gain and gene loss has played an important role in the evolution of these viruses (see section 1.1.6).

The recent sequencing of many poxviral genomes, more than 50 and counting, has allowed extensive analysis of poxviral phylogeny (Lefkowitz *et al.*, 2006). The poxvirus family is divided into two major subfamilies, Entomopoxvirinae and Chordopoxvirinae, which infect insects and amniotes, respectively **(Figure 1.2)** (Gubser *et al.*, 2004). Chordopoxviruses are further divided into at least ten genera; Crocodilepox, Avipox, Molluscipox, Parapox, Orthopox, Yatapox, Leporipox, Deerpox, Capripox, and Suipox viruses (Bratke and McLysaght, 2008). Orthopoxviruses include many of the poxviruses that are highly pathogenic in mammals and are known to have genomes with a particularly high A+T nucleotide content. This genus includes variola, vaccinia, monkeypox and ectromelia virus. Ectromelia virus strain Moscow (EVM), the causative agent of mousepox, is often used to study poxvirus infections *in vivo*. The pathogenicity of EVM infection in mice strongly resembles the pathogenicity of human smallpox disease, although the progression of the disease is much faster in mice (Fenner, 2000; Sliva and Schnierle, 2007).

While infection by many of the poxvirus genera including orthopox and leporipox viruses results in acute and potentially lethal infections, infection by others, such as molluscipox and parapox viruses are mainly benign and confined to specific host tissues (Bugert and Darai, 2000). The molluscipoxvirus, *Molluscum contagiosum*
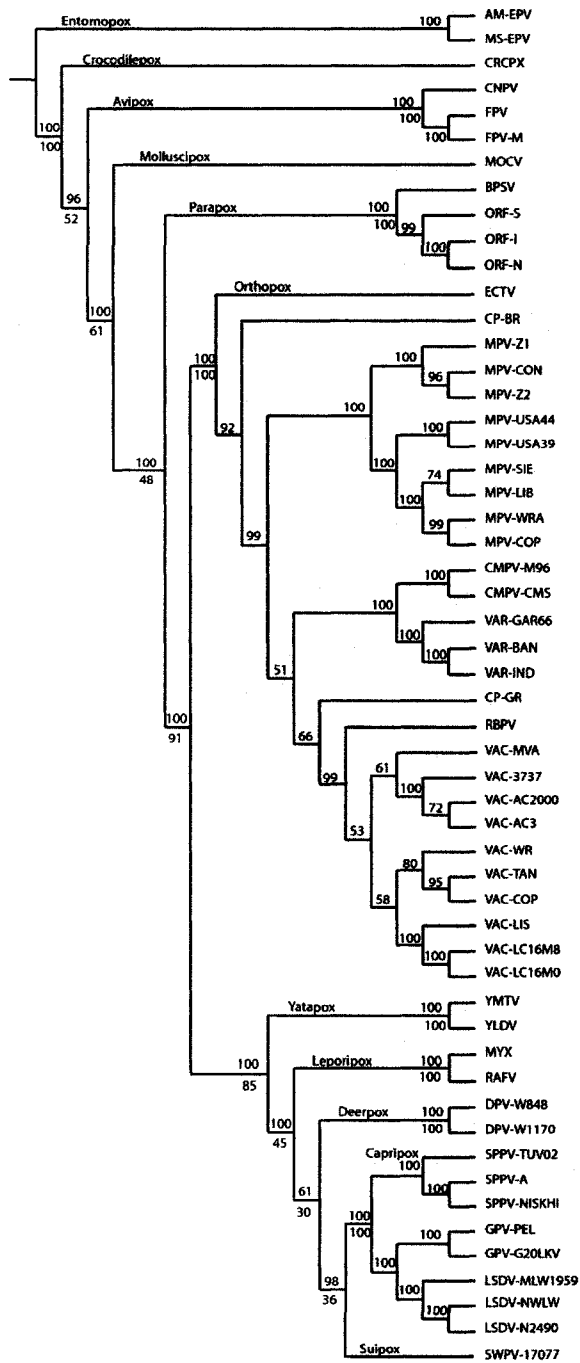
Figure 1.2. Poxviral phylogeny by maximum likelihood. Numbers above branches are bootstrap value percentages using a concatenated alignment of 33 strictly conserved proteins. Numbers below branches are the percentage of trees that supported the branch based on single protein alignments. Figure adapted from Bratke & McLysaght, 2008.

virus (MCV), is another virus with particular significance to humans since it replicates exclusively in the human epidermis, causing benign cutaneous neoplasms, and is a common sexually transmitted disease (Bugert and Darai, 1997).

1.1.4 Poxviral nucleotide metabolism

Given their large genomes and cytoplasmic site of replication, it is perhaps not surprising that many poxviruses encode multiple enzymes involved in nucleotide metabolism. Enzymes involved in the synthesis and metabolism of deoxyribonucleotide precursors in poxviruses include, ribonucleotide reductase (RNR) subunits R1 and R2, thymidine kinase (TK), thymidylate kinase (TMPK), and deoxyuridine triphosphate nucleotidohydrolase (dUTPase) (Hruby *et al.*, 1983; Slabaugh and Mathews, 1984; Tengelsen *et al.*, 1988; Johnson *et al.*, 1991; Broyles, 1993). These proteins demonstrate strong homology to corresponding host enzymes, suggesting they were acquired from host cells through an as yet undetermined mechanism of horizontal gene transfer (see section 1.1.6).

The presence or absence of enzymes involved in nucleotide metabolism varies amongst the poxviruses. It can be seen from **Table 1.1** that orthopoxviruses have the most complete arsenal of proteins involved in nucleotide metabolism, suggesting nucleotide biosynthesis is of more fundamental importance for these viruses. In fact, of the 100 genes located in the terminal regions of orthopoxviruses, only 12 are conserved amongst all orthopoxviruses, and include RNR R2 and dUTPase (Gubser *et al.*, 2004).

Unlike enzymes involved in DNA replication, enzymes involved in nucleotide

Gene product	Orthopox	Capripox	Leporipox	Suipox	Parapox	Yatapox	Avipox	Molluscum/crocodilepox	Entomopox
RNR R1	Present			Present					
RNR R2	Present	Present	Present	Present		Present	Present #		
Grx-1	Present								
dUTPase	Present	Present	Present	Present	Present *	Present	Present		Present+
TK	Present	Present	Present	Present			Present		Present+
TMPK	Present						Present #		
Deoxycitidine kinase							Present		
Thymidylate synthase									Present %

Table 1.1. Presence or absence of enzymes involved in nucleotide metabolism varies amongst poxviruses
* Present in Orf virus; # Present in Canarypox; + Present in Amsacta moorei entomopox ; % Present in Melanoplus sanguinipes entomopox

9

metabolism are not essential for viral replication *in vitro* (Moss, 2001). However, in dividing cells in tissue cultures, large pools of deoxyribonucleotides are generally present, making the need for the enzymes *in vitro*, redundant. A similar argument may explain why some poxviruses do not encode any enzymes involved in nucleotide metabolism. For example, MCV does not encode any of these enzymes, but this virus replicates slowly in rapidly dividing skin cells that are expected to contain a preponderance of nucleotide precursors (Bugert and Darai, 1997). Consequently, for this virus the host nucleotide metabolism enzymes are likely to be adequate to sustain its replication rate. Crocodilepox also does not encode enzymes involved in nucleotide metabolism, but conserves many genes that are shared only with MCV, suggesting a similar evolution for this virus (Afonso *et al.*, 2006). The absence of most nucleotide metabolism proteins in the entomopoxvirus, *Melanoplus sanguinipes* may also reflect the environment in which the virus replicates. This virus replicates in rapidly dividing midgut cells that are also expected to contain a high concentration of nucleotide precursors (Afonso *et al.*, 2006). Thus, the presence or absence of these enzymes appears to depend on the host environment in which the virus replicates.

Most eukaryotic organisms show upregulation of proteins involved in nucleotide metabolism only during the S phase of the cell cycle and accordingly the expression of mammalian enzymes involved in nucleotide metabolism has for the most part shown to be cell-cycle dependent **(Table 1.2)**. The requirement for poxviral expression of these proteins may thus also reflect the need for nucleotide biosynthesis in non-dividing cells. In addition, while enzymes required for nucleotide metabolism are not required for viral replication *in vitro*, evidence that the poxviral enzymes affect

Gene product	Mutation	Means of inoculation	In vivo effect on virulence	Mammalian homologue expression and activity	References
Vaccinia virus TK	Insertional inactivation	Intraperitoneal inoculation of mice	Doses as high as 10⁹ PFUs of TK– recombinants were insufficient to produce lethal effects in mice. Wt strains produced LD₅₀ at 10³ PFUs. Significantly lower production of vaccinia virus neutralizing antibody in mice infected with TK- strains.	Cell cycle-dependent expression. 10-20 fold increase in cytosolic human TK synthesis from G1 to S phase in cycling human cells.	Buller, et al., 1985; Kauffman, et al., 1991.
Ectromelia virus TK	Insertional inactivation	Intracranial inoculation of mice	LD₅₀ for intracranial route of inoculation 10³ fold higher in TK- than wt strains.	See above	Kochneva, et al., 1994.
Vaccinia virus RNR large subunit (R1)	Insertional inactivation	Intracranial inoculation of mice	Approximately 10-fold more RNR R1 deficient virus than wt virus required to produce LD₅₀ in mice.	Cell cycle-independent expression. Bovine R1 concentration remains constant and in excess throughout cell cycle in bovine kidney MDKB cells.	Child, et al., 1990; Engstrom, et al., 1985; Sikorska, et al., 1990.
Vaccinia virus RNR small subunit (R2)	180 bp deletion	Intracranial and intranasal inoculation of mice	LD₅₀ was reduced by approximately 10³ in mice infected with R2 deficient recombinant viruses compared to wt virus inoculation. Reduction in pock formation on skin for R2- strain.	Cell cycle-dependent expression. Active mouse R2 protein concentration increases (3-7 fold) when cells pass from G1 to S phase in mouse mammary tumour TA3 cells.	Lee, et al., 1992; Eriksson, et al., 1984.
Orf virus dUTPase	Complete deletion	Scarification on the inside of the hind leg	Reduced size of lesion that resolved more rapidly, when compared to wt virus.	Cell cycle-dependent expression. Human dUTPase expression occurs in late G1 phase in human cells. Level of dUTPase expression decreases substantially as cells progress into G2 phase.	Fleming, et al., 1995; Strahler, et al., 1993.
Thymidylate kinase	NA	NA	Not known	Cell cycle-dependent activity. Human TMPK enzymatic activity peaks at S phase of cell cycle.	Huang, et al., 1994.

Table 1.2. *In vivo* effects of poxviral mutations and mammalian regulation of enzymes involved in nucleotide metabolism.

virulence and dissemination of the virus suggest a significant role *in vivo* (**Table 1.2**). By constructing poxviral mutants with specific gene inactivations, it has been determined that several genes involved in nucleotide metabolism contribute to poxviral virulence (Buller *et al.*, 1985; Child *et al.*, 1990; Taylor *et al.*, 1991; Lee *et al.*, 1992; Kochneva *et al.*, 1994; Fleming *et al.*, 1995). Studies have demonstrated that TK null vaccinia virus and ectromelia virus mutants result in reduced virulence and dissemination as compared to wild-type viruses when injected into mice by various routes of inoculation. While inactivation of the RNR R1 subunit of vaccinia virus resulted in only a 10-fold reduction in virulence as measured by LD_{50}, inactivation of the R2 subunit resulted in a 1000-fold reduction of virulence in mice. Thus, the targeting of these enzymes by antiviral drugs could allow the host to more effectively clear the pathogen and result in reduced mortality rates. However, the strong sequence similarity between many of the poxviral and host enzymes dictates the need for functional and structural information in order to specifically target the poxviral enzyme without targeting the host enzyme.

There has been extensive functional characterization of enzymes involved in nucleotide metabolism and many of their structures have been solved. The following section is a summary of these analyses and discusses some of the potential poxviral-specific adaptations.

1.1.4.1 Ribonucleotide reductase (RNR)

RNR is an enzyme that is required for the synthesis of deoxyribonucleotides through the reduction of ribonucleotides in all living cells and many viruses. Three

classes of RNR have evolved from a common ancestor and each class utilizes a free radical mechanism to reduce ribonucleotide substrates (Stubbe, 1990; Reichard, 1997). All eukaryotes, many bacteria and all viruses that encode an RNR, including poxviruses, utilize class 1 RNR. Accordingly, the focus of this thesis will be on class 1 RNR. This enzyme is composed of two subunits, the larger R1 and the smaller R2, which in turn have been shown to form dimeric ($R1_2R2_2$), tetrameric ($R1_4R2_4$) and hexameric ($R1_6R2_6$) structures (see below).

The R1 subunit provides the binding sites for ribonucleotides and reduces these substrates through thiol redox chemistry of conserved cysteine residues (Stubbe, 1990). The active site cysteines receive their reducing power through a thiol cascade, with a C-terminal dithiol/disulfide that shuttles electrons to the dithiol/disulfide pair in the active site (Zhang et al., 2007). The R1 C-terminal disulfide is in turn reduced by either thioredoxin (Trx) or glutaredoxin (Grx, see next section).

The R2 subunit is an iron binding protein that is responsible for the generation of a tyrosyl radical. The radical is then thought be transported by an electron transfer chain to a third active site cysteine in R1, which is positioned next to the NDP substrate (Nordlund et al., 1990; Nordlund and Eklund, 1993). The cysteine radical is then believed to catalyze the first step in ribonucleotide reduction, the abstraction of the 3'-H from the substrate ribose moiety (Cerqueira et al., 2006). After this activation step, the substrate is reduced by the cysteines of the R1 active site dithiol.

RNR has a highly complex mechanism of not only catalysis, but also regulation. Fluctuations in cellular dNTP pools adjust not only the overall enzyme activity by complex allosteric regulation, but also substrate specificity (Larsson et al.,

13

2004). Despite extensive analysis of several RNRs, many questions regarding the allosteric regulation of RNR remain. While it is known that dATP inhibits enzyme activity and ATP promotes catalysis, the detailed mechanisms of how binding of either of these molecules regulates activity remains poorly understood. However, it is believed that protein-protein interactions of the R1 and R2 subunits are important for this regulation. Quaternary structure analysis of mammalian R1 has shown that ATP promotes formation of R1 in a hexameric form, whereas dATP stabilizes a tetrameric form (Kashlan and Cooperman, 2003). Furthermore, functional studies of *E. coli* R1 have shown that dATP may cause a tighter complex between R1 and R2, and thereby inhibit enzymatic activity (Kasrayan *et al.*, 2004). Elucidation of the detailed mechanism of how these complexes form or how they modulate RNR activity has been hampered by the lack of structures of this enzyme beyond the dimeric state or with bound ATP/dATP in the allosteric activity site.

Crystal structures of Class 1 R1 have been determined for *E. coli* (Eriksson *et al.*, 1997), and more recently for yeast (Xu *et al.*, 2006a; Xu *et al.*, 2006b). The *E. coli* structure was solved both with and without an ATP analogue, AMPPNP, in the allosteric activity site, but the structures did not demonstrate significant conformational changes at or near the ATP/dATP binding site. This lack of structural change was attributed to artefacts of how the protein complex was prepared and is not likely to be of physiological significance since only an ATP analogue was crystallized in the structures. While the crystal structures of the yeast R1 provided insight into regulation of substrate specificity, the results provided little information about potential mechanisms of allosteric regulation since none of the models were solved with either

14

ATP or dATP in the allosteric activity binding site, and the models were not solved beyond the dimeric state. Since R1 activity and quaternary structure depends on the binding of either dATP or ATP, structures of these two complexes would be of great benefit in order to determine the structural basis for RNR activation and inhibition.

The most extensive structural studies of R2 have been performed using the *E. coli* protein, although the structure has also been well characterized for the mouse (Kauppi *et al.*, 1996). Although the interface between R1 and R2 remains poorly defined, the final seven amino acid residues of the C-terminus of R2 have been shown to play an essential role for the binding of R2 to R1 in mice (Cosentino *et al.*, 1991; Yang *et al.*, 1990).

RNR is considered an important target for anticancer and antiviral agents since it is absolutely required for the *de novo* synthesis of DNA and thus is essential for DNA replication (Roy *et al.*, 2003a; Roy *et al.*, 2003b). A deoxycitidine analog, gemcitabine, is a potent inhibitor of human RNR R1 and is being used as an anticancer drug for various carcinomas including bladder, breast, lung and pancreatic cancer (Cerqueira *et al.*, 2007). Gemcitabine is falsely recognized by RNR as a substrate and leads to loss of enzymatic activity (Pereira *et al.* 2001; Xu *et al.*, 2006b). To date, no structures of mammalian or orthopoxviral R1 have been solved. Since these two enzymes share 76% identity, the solution of either structure could lead to the development of more effective anticancer or antiviral agents that target this enzyme.

1.1.4.2 Glutaredoxin (Grx)

Grxs are redox enzymes that have been shown to act as a reducing agent and

cofactor for the activity of RNR in many organisms from *E. coli* to humans (Holmgren, 1976; Padilla *et al.*, 1995; Fernandes and Holmgren, 2004). The fact that the RNR R1 subunit is a known substrate for many Grxs suggests that the viral Grx (O2L in vaccinia, EVM053 in ectromelia virus) may be the reducing agent for the viral RNR. However, there are arguments both for and against such a role. Experimental support comes from a study with knockout vaccinia viruses lacking either O2L or the viral RNR R1 subunit. In cells pretreated with α-amanitin, an inhibitor of host but not viral transcription, both recombinant viruses caused similar defects in nucleotide metabolism, suggesting that R1 and O2L participate in the same metabolic pathway (Rajagopal *et al.*, 1995). Bioinformatics also supports a functional link since O2L orthologs are only found in poxviruses that also encode the RNR R1 subunit. The arguments against a role for O2L as an RNR reducing factor arise from functional considerations. First, it appears likely that host Grx and Trx can reduce the viral RNR R1 subunit. Indeed, swinepox, the only non-orthopoxvirus with a RNR R1 gene, does not encode an O2L ortholog, suggesting it relies on the corresponding host enzyme. Second, O2L is expressed as a late gene, after DNA replication has started, in contrast to the early expression of all other viral genes that are involved in nucleotide metabolism (Moss, 2001). This exception may be explained by the fact that O2L is packaged in the virion and is thus introduced into cells upon infection. However, it is not clear why O2L would be needed earlier than the other enzymes involved in nucleotide metabolism and its packaging in the viral capsid may also point to additional roles in the very early stages after infection (see section 4.2.5).

O2L/EVM053 shares 45% sequence identity with human Grx-1 and in addition

to the sequence similarity, functional studies have shown that the viral Grx also shares the thioltransferase and dehydroascorbate reductase activities that are typical for this enzyme family (Ahn and Moss, 1992). The implication of Grxs in important redox-sensitive regulatory roles has placed new emphasis on the need to better understand catalysis and substrate specificity determinants for this class of proteins. The study of functional and structural similarities and differences between mammalian and poxviral Grxs can extend our understanding of adaptations that affect the role of this enzyme. A thorough understanding of their molecular mechanisms will greatly contribute to this field of research and is a major focus of this thesis. A more in depth background of Grxs and cellular redox regulation is presented in section 1.2

1.1.4.3 Thymidine kinase (TK)

TK is a key enzyme involved in the salvage pathway of nucleotide metabolism, catalyzing the phosphorylation of thymidine using ATP as the phosphate donor (Black and Hruby, 1990). The enzyme transfers the γ-phosphoryl moiety of ATP to deoxythymidine to produce deoxythymidine monophosphate (dTMP). Type I TKs form dimers that also have thymidylate kinase activity (the phosphorylation of dTMP to dTDP) and are mainly found in viruses such as Herpes simplex virus-1 and Varicella Zoster virus as well as in the mitochondria of eukaryotic cells. Type II TK (TKII) enzymes are found in poxviruses and the cytoplasm of eukaryotic cells (66% sequence identity) and are active as tetramers. Although a relatively small protein (177 amino acids in EVM), TKII must coordinate the binding of thymidine, dTDP, dTTP, ATP, and must also house regions that bring the four subunits of the protein together into the

functional tetramer. (Black and Hruby, 1992). Both dTDP and dTTP, which are generated at the end of the metabolic pathway, can act as feedback inhibitors of TK (Hruby, 1985).

Functional and biochemical characterization of mammalian and poxviral TK has very recently been complemented with crystallographic structures of both human cytosolic TK and vaccinia TK bound to dTTP (Birringer et al., 2005; El Omari et al., 2006). While the structures were overall very similar, a comparison of the active sites revealed subtle differences in the region required for thymidine binding. The vaccinia structure demonstrated a more open conformation in the active site and thus may be used to develop poxviral specific antiviral agents, since the site would allow for the binding of bulkier groups.

1.1.4.4 Thymidylate kinase (TMPK)

TMPK catalyses the phosphorylation of dTMP to dTDP using ATP as its preferred phosphoryl donor (Ostermann et al., 2000). Deoxythymidine diphosphate is then phosphorylated to dTTP by nucleoside diphosphate kinase. All orthopoxviruses encode a TMPK and the enzyme demonstrates 43% identity to human TMPK (Smith et al., 1989). Although there are no crystal structures of poxviral TMPK, crystal structures of human TMPK have been determined, both with and without the presence of several prodrugs (Ostermann et al., 2003). Orthopoxviral TMPK was shown to be active by its ability to complement a temperature-sensitive TMPK mutant of Saccharomyces cerevisiae at the restrictive temperature (Hughes et al., 1991). Interestingly, unlike most other TMPK enzymes, the viral enzyme has also been shown

to phosphorylate dUMP and dGMP, which could provide a basis for selective inhibitors that target the viral, but not the host TMPK (Topalis et al., 2005).

1.1.4.5 Deoxyuridine triphosphate nucleotidohydrolase (dUTPase)

dUTPase catalyses the hydrolysis of dUTP to dUMP and PPi in the presence of magnesium in order to reduce the number of dUTPs misincorporated into DNA (Caradonna and Muller-Weeks, 2001). dUMP produced by dUTPase is also a substrate for the eukaryotic thymidylate synthase, which methylates the substrate in order to produce dTMP (Persson et al., 2001). Uracil incorporation into DNA, either through deamination of cytosine or due to increased uracil content in nucleotide pools, can lead to mutagenic mispairs that are directly or indirectly genotoxic (Kavli et al., 2007; Sousa et al., 2007).

Human dUTPase exists as both nuclear and mitochondrial isoforms that are generated by the alternate use of 5' exons (Tinkelenberg et al., 2003). The enzyme is also present in most poxviruses, herpesviruses and some retroviruses and is viewed as an exceptional drug target to combat herpesvirus (Studebaker et al., 2001). With the knowledge that the dUTP/dTTP ratio is often high in non-dividing cells, the high A+T content of orthopoxvirus genomes suggests the role of dUTPase and UDG (see below) are very important to orthopoxviral propagation (Chen et al., 2002).

dUTPase forms a trimer in crystal structures of human (Mol et al., 1996), E. coli (Larsson et al., 1996), feline immunodeficiency virus (Prasad et al., 2000), equine infectious anemia virus (EIAV) (Dauter et al., 1999), and M. tuberculosis (Chan et al., 2004) dUTPases. Human dUTPase shows 65% sequence identity to orthopoxviral

dUTPases and vaccinia virus dUTPase crystal structures have recently been solved in complex with a non-hydrolyzable substrate analog (dUMPNPP), product (dUMP) and inhibitor (dUDP) (Samal *et al.*, 2007). Although the structures were overall quite similar, the most striking difference between the human and poxviral dUTPase was a much larger cavity between the three monomers that form the trimer in the poxviral enzyme. The cavity in the vaccinia dUTPase structure is the largest observed for all dUTPase structures and is almost twice as large as that for human dUTPase (1140 $Å^3$ for vaccinia dUTPase and 653 $Å^3$ for the human structure). This larger size is attributed to a greater abundance of positively and negatively charged residues in the interface region, while a greater relative abundance of hydrophobic residues are present in the much smaller channel area in EIAV and *E. coli* dUTPase structures (185 and 32 $Å^3$, respectively).

In eukaryotic dUTPases, the trimer is stabilized by nine residues (three from each monomer) and the replacement of one of these residues in the poxviral enzyme (Glu in humans, Gln in poxviral) promotes the binding of an anion (Cl$^-$), whereas for the human structure a positively charged metal ion (Mg$^+$) was observed at the structurally analogous position (Mol *et al.*, 1996). The larger size of this pocket in the poxviral structure and the stronger propensity to bind a negatively charged anion at this interface could potentially be used for the development of a poxviral specific antiviral that could exploit both of these factors by disrupting trimer assembly and thus abrogate catalytic activity.

1.1.5 Do orthopoxviruses form a replitase complex?

Enzymes involved in nucleotide metabolism have been shown to assemble into complexes known as dNTP synthetase complexes (Wheeler *et al.*, 1996). For example, T4 bacteriophage has been shown to assemble such a complex at the replication fork in infected *E. coli* cells and is composed of several enzymes of both viral and host origin involved in nucleotide synthesis including; T4 RNR, thymidylate synthase, NDP kinase, and *E. coli* adenylate kinase (Allen *et al.*, 1980; Chiu *et al.*, 1982; Kim *et al.*, 2005a). Similarly, proteins involved in T4 DNA replication also form complexes known as replisomes, and are composed of several proteins including; DNA polymerase, DNA primase and single-stranded DNA binding protein (gp32) (Ishmael *et al.*, 2003). Interestingly, several T4 dNTP-synthesizing enzymes have been shown to be present in T4 DNA-protein complexes (Wheeler *et al.*, 1996). Furthermore, experiments have demonstrated direct associations between gp32 and T4 RNR, thymidylate synthase and NDP kinase, suggesting dNTP synthetases and replisomes form even larger complexes (Kim *et al.*, 2005b). Similar complexes have been postulated to form in eukaryotic cells during the S-phase of the cell cycle and are known as replitases (Reddy and Fager, 1993; Murthy and Reddy, 2006).

It is perhaps not surprising that such complexes would form since the high local concentration of newly synthesized dNTPs would be most advantageous close to the site of DNA replication. A replitase complex has also been postulated to exist for poxviruses, as evidenced by protein-protein interactions of an enzyme involved in DNA replication, I3L SSB, and nucleotide metabolism, RNR R2 (see next section). However, relatively little is known about how a replitase complex could form at some

point during the poxviral lifecycle. The ability of replitases to form would seem to vary substantially amongst poxviruses due to the absence of enzymes involved in nucleotide metabolism in many poxviruses (Table 1.1), although it is possible that the viruses "hijack" the host orthologs in order to form the complex. As noted above, T4 dNTP synthetase complexes have been shown to incorporate host enzymes into these complexes, suggesting host enzymes could also be incorporated into a poxviral replitase. However, if replitase complexes were to have evolved in poxviruses, the orthopoxviruses are the most likely candidates to have evolved specific mechanisms to regulate the formation and function of such a complex, since they encode the largest number of proteins involved in deoxyribonucleotide production amongst all known poxviruses (Table 1.1). The following is a summary of proteins involved in poxviral DNA replication that may also participate in the formation of a replitase complex.

1.1.5.1 Single-stranded DNA binding protein (I3L)

I3L is an essential poxviral single stranded DNA binding protein that does not show recognizable homology to other DNA binding proteins (Rochester and Traktman, 1998). In addition to its strong affinity for ssDNA, I3L has also demonstrated DNA aggregating properties (Tseng *et al.*, 1999). I3L is expressed both at early and intermediate stages in the poxviral lifecycle and is localized to the virosome (Domi and Beaud, 2000). Although not directly involved in nucleotide metabolism, I3L has been shown to form an interaction with poxviral RNR R2. This association was demonstrated using anti-idiotypic anitbodies and is likely dependent on interactions of R2 with the acidic C-terminal region of I3L (Davis and Mathews, 1993). Another

potential function of I3L may thus be to recruit RNR to the virosome, and in analogy to T4 SSB, may play an important role in recruiting other enzymes involved in nucleotide metabolism to the replication fork.

1.1.5.2 Uracil DNA Glycosylase (UDG)

UDG is a ubiquitous enzyme that plays an important role in DNA repair since it removes uracil bases from DNA by hydrolyzing the glycosylic bond between uracil and the deoxyribose sugar (Caradonna and Muller-Weeks, 2001). Vaccinia virus UDG (vvUDG) demonstrates only 19% sequence identity to the corresponding human enzyme, suggesting this enzyme was not recently acquired through horizontal gene transfer. Other evidence for a more distant relationship of vvUDG comes from fundamental differences regarding the function of the enzyme. The poxviral enzyme shows stronger affinity for ssDNA but much lower excision efficiency than human UDG. Furthermore, $MgCl_2$ strongly inhibits vvUDG activity, but strongly enhances human UDG activity (Scaramozzino *et al.*, 2003).

Its role in removing misincorporated uracil from DNA suggests the enzyme functions to minimize deleterious mutations in orthopoxviruses (Ellison *et al.*, 1996). Indeed, mutations of this enzyme in the catalytic site resulted in decreased virulence when these virus mutants were administered in mice (De Silva and Moss, 2003). However, vvUDG also has a function that is essential for poxviral DNA replication that is independent of its uracil glycosylase function, since vaccinia can not replicate in the absence of vvUDG (Ellison *et al.*, 1996). The essential role for vvUDG in poxviral replication is in all probability related to its presence in the replication fork where it

23

forms an interaction with A20, a known processivity factor, and possibly other enzymes involved in DNA replication (Stanitsa et al., 2006).

Crystal structures of human UDG have been solved in complex with an inhibitor (Mol et al., 1995), and more recently the vaccinia structure was determined (Schormann et al., 2007). The vvUDG structure was observed to form a dimer in two crystal forms, and this dimeric assembly was also confirmed by dynamic light scattering (DLS) analysis. The dimeric form of the structure led the authors to propose a model for the interaction of vvUDG and the A20 protein.

1.1.5.3 Poxvirus DNA primase (D5)

DNA primase (also known as NTPase or D5) is a large protein (90 kDa) that is absolutely required for DNA replication in poxviruses (Evans et al., 1995). D5 homologs have been observed in most nucleo-cytoplasmic large DNA viruses and is thus considered an important ancestral protein of this virus family. However, D5 homologs have not been found in prokaryotes or eukaryotes and its functional role *in vivo* has remained elusive. *In vitro*, the protein has been shown to hydrolyse all eight common ribo- and deoxyribonucleotide triphosphates to their respective diphosphate forms (Evans et al., 1995). More recently, the enzyme was shown to synthesize oligoribonucleotides using single-stranded DNA as a template and thus the primary function of D5 is now believed to act as a primase (De Silva et al., 2007).

1.1.5.4 Implications for the formation of a poxviral replitase

D5 has been shown to interact with A20 (Boyle et al., 2007), and thus, the

activity of D5 may also be linked to the role of vvUDG. A20 has also been shown to interact with E9, the catalytic subunit of the polymerase, *in vivo* (Stanitsa *et al.*, 2006). The affinity of D5 and vvUDG for ssDNA, makes it interesting to speculate that these proteins may also interact with, or be in close proximity, to I3L SSB **(Figure 1.3)**. The known interaction of I3L SSB with orthopoxviral R2, further suggests the DNA replication complex could also form interactions with enzymes involved in nucleotide metabolism to form a replitase complex. With the knowledge that T4 SSB gp32 has been shown to be crucial for interactions between enzymes involved in dNTP synthesis and DNA replication (Kim *et al.*, 2005b), it is also interesting to speculate that poxviral SSB could also play a significant role in the formation of a poxviral replitase complex.

The story becomes less clear for poxviruses that do not encode R2 or other enzymes involved in nucleotide metabolism. These viruses could potentially use host R2, but this could be problematic since the host R2 is cell-cycle regulated, which would limit viral replication outside of the S phase of the cell cycle (Reddy and Fager, 1993; Murthy and Reddy, 2006).

1.1.6 Poxviral horizontal gene transfer (HGT): gene gain and gene loss

Although poxviruses have had an enormous impact on humanity, our knowledge of their origin and evolution remains poorly understood. What is clear is that gene gain and loss appears to have formed a major role in poxviral evolution and host range. It is estimated that as many as 50% of genes present in poxviruses have been acquired through horizontal gene transfer (HGT) (Hughes and Friedman, 2005).

Several genes involved in nucleotide metabolism are not found in all
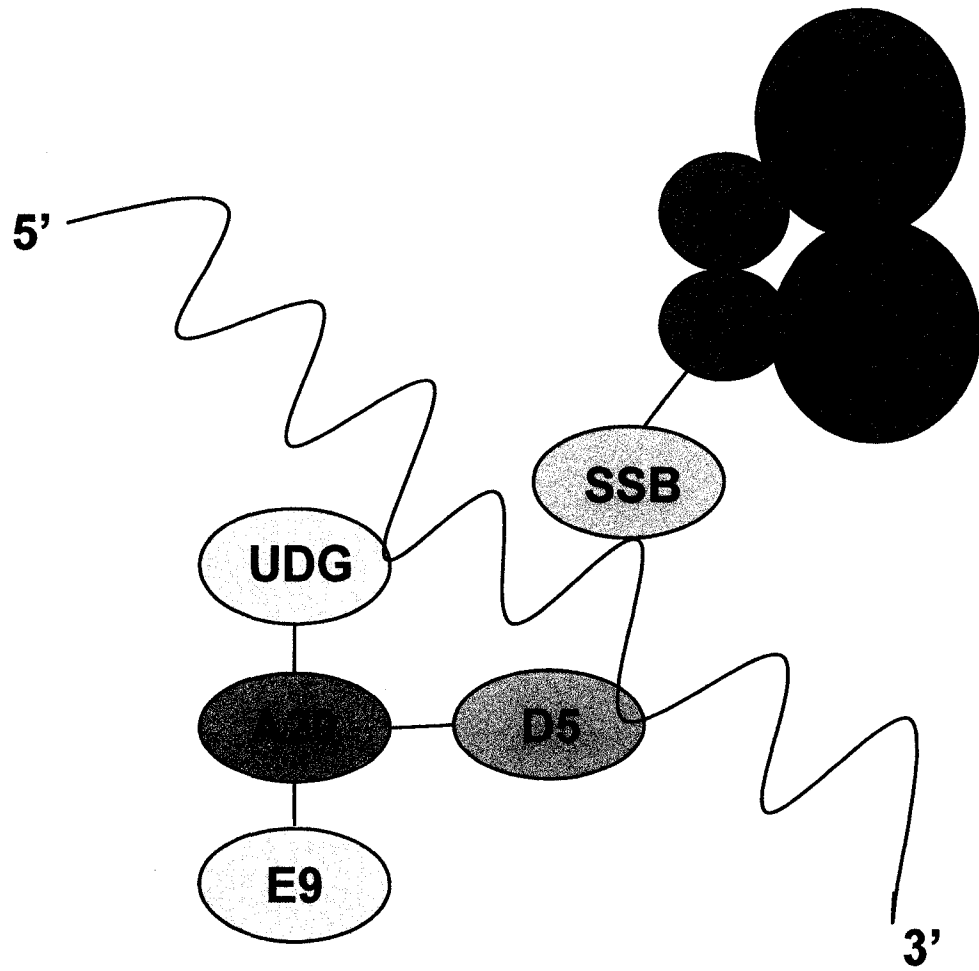
Figure 1.3. Schematic model of putative poxvirus replitase complex. The presence of single-stranded DNA may promote interactions of enzymes involved in nucleotide metabolism with enzymes involved in DNA replication.

poxviruses, but are commonly found in other related large cytoplasmic DNA viruses, which might suggest that these genes have been lost and gained, perhaps several times, in response to changes in the host cell environments in which the viruses propagate (Iyer *et al.*, 2006). Evidence for multiple HGT events in poxviruses has been inferred from an analysis of sequence similarity of poxviral genes to their host cell homologues, in combination with gene order comparisons (Bratke and McLysaght, 2008). For example, TK and RNR R2 from avipoxviruses and orthopoxviruses appear to have been acquired through independent HGT events since these enzymes show strong homology to their respective host cell homologue and are located at different regions of the genome, which otherwise show conservation of gene order (Bratke and McLysaght, 2008). Similar observations have been made for poxviral Interleukin-10, and a glutathione peroxidase that is found only in MCV and avipoxviruses (see section 1.2.5). The ability of poxviruses and other large DNA viruses to efficiently gain and lose genes allows these viruses to quickly adapt to new environments, and also may greatly affect viral pathogenesis.

Genes acquired through HGT have been observed in many parasitic life forms, both cellular and viral, and is a common mechanism for the transfer of genetic information between otherwise dissimilar organisms. In order to predict mechanisms of HGT in poxviruses, it is important to first consider that a large fraction of DNA acquired by eukaryotic organisms may have been through the reverse transcription of RNA sequences, and a relatively large segment of mammalian genomes is now being recognized as being of retroviral origin (Buzdin, 2007). For eukaryotic organisms, gene transfer could occur through infection of retroviruses, and the activity of the virally

encoded reverse transcriptase, together with the integrase. For this mechanism, the reverse transcriptase would catalyze the synthesis of dsDNA from cytosolic host cell mRNAs and the DNA would then be integrated into the host cell genome.

In the case of poxviruses, the mechanism of HGT necessitates the removal of introns (poxviruses do not contain introns in their genomes), and thus the mechanism of reverse transcription of mRNAs into DNA which are then recombined into the poxviral genome is also a plausible mechanism of HGT for poxviruses (Bugert and Darai, 2000). For poxviruses, this mechanism would seemingly require the simultaneous infection of a retrovirus and a poxvirus in the host. Although perhaps a seemingly infrequent event, on an evolutionary time scale such events might occur at a rate high enough to maintain a pertinent level of gene transfer. Another possible mechanism of HGT in poxviruses may be through a process of retrotransposition. This mechanism recently gained support from the finding of a retroposon known only in reptilian genomes, in a taterapoxvirus (Piskurek and Okada, 2007).

1.1.7 Poxvirus protein evolution

Genes that are hijacked by poxviruses from their host might be expected to show a faster rate of amino acid substitutions than host cell homologues due to the much shorter generation time of poxviruses compared to mammals. Positive selection may also be stronger for poxviral proteins acquired by HGT since the newly acquired protein would be expected to undergo adaptations that are specific to the poxviral lifecycle. An increased rate of positive selection may also occur in order to adapt to host cell immune responses or other changes in the host cell environment.

Orthopoxviruses are the most closely related of the poxviruses as far as overall genomic sequence conservation. The genus has a greater rate of gene acquisition than other poxviruses and has many genes that exhibit evidence of positive selection (McLysaght *et al.*, 2003). An enzyme that shows evidence of HGT, dUTPase, has also shown evidence of positive selection as evidenced by a high ratio of nonsynonymous/synonymous mutations (ω); for dUTPase ω = 5.68 (McLysaght *et al.*, 2003; Bratke and McLysaght, 2008). For this analysis, a ratio of ω > 1 is generally considered to be evidence of positive selection since synonymous mutations are expected to accumulate at a much greater rate than nonsynonymous mutations in the absence of adaptive evolution (Yang, 1997). The much greater volume of the channel at the trimeric interface in poxviral dUTPase and the highly significant results of the sequence analyses strongly support the hypothesis of strong positive selection for this protein.

The presence of dUTPase in all but a few poxviruses, the very high A+T content in many poxviral genomes, and the high dUTP/dTTP content in non-dividing cells, all suggest strong selective pressures for this enzyme to perform optimally. Perhaps more importantly, enzymes such as dUTPase must evade cellular regulation, or other factors that localize these enzymes to cellular organelles. Poxvirus homologues of cellular genes have also shown evidence for the evolution of viral specific adaptations through the loss of portions of the host encoded genes. To illustrate, sequence alignments of the protein coding sequences of poxviral and mammalian RNR R2, TK and dUTPase, have revealed several key differences. It can be seen from **Figure 1.4a** that the mammalian RNR R2 subunit has a longer N-terminal

```
EV R2        --------------------------------------------------------------
Mouse R2     MLSVRTPLATIADQQQLQLSPLKRLTLADKENTPPTLSSTRVLASKAARRIFQDSAELES


EV R2        ---------MEPILAPNPNRFVIFPIQYHDIWNMYKKAEASFWTVEEVDISKDINDWNKL
Mouse R2     KAPTNPSVEDEPLLRENPRRFVVFPIEYHDIWQMYKKAEASFWTAEEVDLSKDIQHWEAL
                     **:*   **.***:***:*****:***********.****:****:.*: *


EV R2        TPDEKYFIKHVLAFFAASDGIVNENLAERFCTEVQVTEARCFYGFQMAIENIHSEMYSLL
Mouse R2     KPDERHFISHVLAFFAASDGIVNENLVERFSQEVQVTEARCFYGFQIAMENIHSEMYSLL
             .***:;**.****************.***.  **************:*;**********


EV R2        IDTYVKDSNEKNYLFNAIETMPCVKKKADWAQKWIHDS-AGYGERLIAFAAVEGIFFSGS
Mouse R2     IDTYIKDPKEREYLFNAIETMPCVKKKADWALRWIGDKEATYGERVVAFAAVEGIFFSGS
             ****:**.:*:;******************* :**  *.  * ****:;*************


EV R2        FASIFWLKKRGLMPGLTFSNELISRDEGLHCDFACLMFKHLLYPPSEETVRSIITDAVSI
Mouse R2     FASIFWLKKRGLMPGLTFSNELISRDEGLHCDFACLMFKHLVHKPAEQRVREIITNAVRI
             ****************************************::  *:*: **.***:** *


EV R2        EQEFLTVALPVKLIGMNCEMMKTYIEFIADRLISELGFKKIYNVTNPFDFMENISLEGKT
Mouse R2     EQEFLTEALPVKLIGMNCTLMKQYIEFVADRLMLELGFNKIFRVENPFDFMENISLEGKT
             ****** *********** :** ****:****:  ****:**:.* **************


EV R2        NFFEKRVGEYQKMGVMS-QEDNHFSLDVDF
Mouse R2     NFFEKRVGEYQRMGVMSNSTENSFTLDADF
             ***********:*****  .  :* *:**.**
```

Figure 1.4a. Amino acid sequence alignment of EVM and mouse RNR R2. The mouse subunit has a longer N-terminal region and a KEN sequence motif (underlined) that has been shown to play a role in the cell cycle regulation of the enzyme. The motif is also absent in all other sequenced poxviruses.

```
HumanTK      MSCINLPTVLPGSPSKTRGQIQVILGPMFSGKSTELMRRVRRFQIAQYKCLVIKYAKDTR
VariolaTK    ---------------MNGGHIQLIIGPMFSGKSTELIRRVRRYQIAQYKCVTIKYSNDNR
             .  *:**:*:**********;*****:*******:.***::*.*


HumanTK      YSSSFCTHDRNTMEALPACLLRDVAQEALGVAVIGIDEGQFFPDIMEFCEAMANAGKTVI
VariolaTK    YGTGLWTHDKNNFEALEATKLCDVLEAITDFSVIGIDEGQFFPDIVEFCERMANEGKIVI
             *.:.: ***:*.:*** *   * **  :   ..:*************:**** *** ** **


HumanTK      VAALDGTFQRKPFGAILNLVPLAESVVKLTAVCMECFREAAYTKRLGTEKEVEVIGGADK
VariolaTK    VAALDGTFQRKPFNNILDLIPLSEMVVKLTAVCMKCFKEASFSKRLGTETKIEIIGGIDM
             *************. **:;**:* *********:**;**:;::******.;:*:*** *


HumanTK      YHSVCRLCYFKKASGQPAGPDNKENCPVPGKPGEAVAARKLFAPQQILQCSPAN
VariolaTK    YQSVCRKCYIDS--------------------------------------------
             *:**** **:..
```

Figure 1.4b. Amino acid sequence alignment of human and variola virus TK. The KEN sequence motif required for cell cycle regulation in human cells is also absent from the variola sequence and all other sequenced poxviruses.

```
dUTPaseN    --------------------------------------------------------------
dUTPaseM    MTPLCPRPALCYHFLTSLLRSAMQNARGTAEGRSRGTLRARPAPRPPAAQHGIPRPLSSA
dUTPaseV    ------------------------------------------------------------


dUTPaseN    --------------------------------MPCSEETPAISPSKRARPAEVGGMQLRFARLS
dUTPaseM    GRLSQGCRGASTVGAAGWKGELPKAGGSPAPGPETPAISPSKRARPAEVGGMQLRFARLS
dUTPaseV    -------------------------------------------MFNMNINSPVRFVKET
                                                      .  :**.:  :


dUTPaseN    EHATAPTRGSARAAGYDLYSAYDYTIPPMEKAVVKTDIQIALPSGCYGRVAPRSGLAAKH
dUTPaseM    EHATAPTRGSARAAGYDLYSAYDYTIPPMEKAVVKTDIQIALPSGCYGRVAPRSGLAAKH
dUTPaseV    NRAKSPTRQSPYAAGYDLYSAYDYTIPPGERQLIKTDISMSMPKFCYGRIAPRSGLSLKG
            ::*.:*** *. *************** *: :**** .::.*. ****:******: *


dUTPaseN    FIDVGAGVIDEDYRGNVGVVLFNFGKEKFEVKKGDRIAQLICERIFYPEIEEVQALDDTE
dUTPaseM    FIDVGAGVIDEDYRGNVGVVLFNFGKEKFEVKKGDRIAQLICERIFYPEIEEVQALDDTE
dUTPaseV    -IDIGGGVIDEDYRGNIGVILINNGKYTFNVNTGDRIAQLIYQRIYYPELKEVQSLDSTD
             **:*.**********:**:*:* ** .*:*:.******** :**:***::***:**.*:


dUTPaseN    RGSGGFGSTGKN
dUTPaseM    RGSGGFGSTGKN
dUTPaseV    RGDQGFGSTGLR
            **. ****** .
```

Figure 1.4c. Amino acid sequence alignment of human nuclear (dUTPaseN), mitochondrial (dUTPaseM) and variola virus (dUTPaseV) dUTPases. The 69 residue N-terminal region required for mitochondrial localization (dUTPaseM) and seven residue nuclear localisation signal (underlined) are absent from the variola sequence and all other poxviruses.

region than the poxvirus counterpart. Interestingly, this region has been shown to regulate mouse R2, through a KEN sequence motif that targets the protein for degradation (Chabes *et al.*, 2003). Furthermore, this motif is also absent in poxviral TK **(Figure 1.4b)**, and the mammalian C-terminal region has also been shown to be required for cell cycle regulation of this enzyme in human cells (Kauffman and Kelly, 1991; Kauffman *et al.*, 1991). In addition, the N-terminal regions thought to be required for human dUTPase mitochondrial and nuclear localization (Ladner and Caradonna, 1997; Tinkelenberg *et al.*, 2003) are absent from the poxvirus sequences **(Figure 1.4c)**. The apparent loss of regulatory or localization signals in the poxviral enzymes demonstrates that despite strong sequence identity, these enzymes have evolved other characteristics that make them distinct from their eukaryotic counterparts. The study of poxviral genes involved in nucleotide metabolism demands further functional and structural analysis in order to reveal other poxviral specific adaptations and to exploit these characteristics for the development of antiviral therapies.

1.2 Thiol-thiolate redox reactions

1.2.1 Maintenance of the cellular redox balance through thiol chemistry

The cytoplasm is an environment where many redox reactions continuously produce and consume reducing equivalents. The redox state of the cell affects these reactions and an unbalanced redox potential has significant impact on cellular and molecular functions. Severe oxidative stress can arrest cell cycle progression and

induce apoptotic cell death (Kwon *et al.*, 2003). In particular, highly oxidizing compounds such as peroxides, nitric oxide, free radicals, and other reactive oxygen species (ROS) must be effectively neutralized in order to prevent considerable harm to the cell. Cells must also continuously balance the rates of oxidizing and reducing reactions even during basal conditions in order to regulate protein function in either a positive or negative manner. Accordingly, the functions of many proteins and other thiol-containing molecules are governed through the transport and distribution of reducing equivalents to and from these molecules. In addition to the complex interplay of protein thiols with other protein or non-protein thiols, thiol containing molecules have also been shown to act as reducing agents for other biologically important redox sensitive compounds such as dehydroascorbate (DHA) (Washburn and Wells, 1999).

1.2.2 Glutathione and Glutathionylation

The most abundant low molecular mass thiols *in vivo* are free cysteine and GSH. GSH is a relatively ubiquitous molecule that is synthesized from cysteine, glycine and glutamate to form a tripeptide (L-γ-glutamyl-cysteinylglycine) that acts as the cellular "redox buffer" and is present in millimolar concentrations in the cell (~0.2-10mM) (Dalle-Donne *et al.*, 2007). Indeed, the ratio of reduced (GSH) to oxidized (GSSG) is an indicator of the cellular redox state, and a normal intracellular physiological ratio for GSH:GSSG is ~100 (Klatt and Lamas, 2000). In addition to its relatively high intracellular concentration, GSH has a strongly negative redox potential (-240 mV) **(Figure 1.5)**, making the molecule a highly effective reducing agent (Schafer and Buettner, 2001). GSH participates in enzymatic reactions but it can also

33
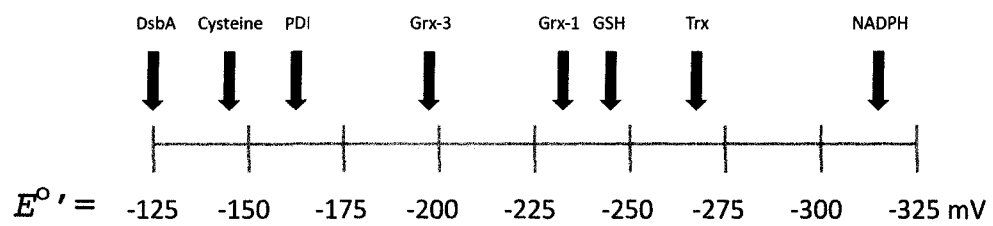
Figure 1.5. Standard state redox potentials of thioredoxin fold oxidoreductases and other cellular redox molecules.

act directly as an antioxidant to quench ROS (Parke and Sapota, 1996). Free cysteine shows a much less negative redox potential compared to GSH (-145 mV) and is more abundant in the extracellular space, and is thus often found in the oxidized conformation as a cystine or as a mixed disulfide (Jones et al., 2004).

In addition to the oxidation of two GSH to GSSG, GSH can also react with other thiol groups to give mixed disulfides. In particular, the addition of GS- to protein cysteines (glutathionylation), has emerged as an important post-translation modification system that responds to the cellular redox state (Dalle-Donne et al., 2007). Glutathionylation is a transient modification that can directly affect enzyme activity by modifying catalytic or regulatory cysteines, alter protein-protein interactions, or protect sensitive cysteine residues from ROS during oxidative bursts followed by de-protection after the cell returns to a normal redox state (Casadei et al., 2008). This offers reversible oxidation to protein cysteines, which otherwise could be irreversible, since oxidation often leads to protein denaturation or misfolding and irregular covalent aggregations. Glutathionylation and deglutathionylation of proteins thus acts not only as a mechanism of modulating redox status of proteins, but also acts as a post-translational modification to activate or deactivate protein function, similar to the processes of phosphorylation or ubiquitination (Filomeni et al., 2005).

Examples of protein targets for glutathionylation reactions include nuclear factor 1 and protein tyrosine phosphatases, which are inhibited by glutathionylation, although the inhibition can be subsequently reversed by Grx through this enzymes deglutathionylating activity (see next section) (Bandyopadhyay et al., 1998; Barrett et al., 1999). This type of regulation is also seen amongst viral proteins. For example,

HIV-protease is inhibited by glutathionylation, but this can also be reversed by Grx (Davis *et al.*, 1997). The full impact of glutathionylation is only just emerging with proteomics methods starting to reveal the targets and consequences of glutathionylation.

1.2.3 Thioredoxin-fold oxidoreductases

Trxs and Grxs form a structurally and functionally related family of small redox proteins that play important roles in the reduction of protein disulfides, mixed disulfides, and other redox reactions (Fernandes and Holmgren, 2004). These proteins share a common fold consisting of a central five-stranded β-sheet surrounded by 3-4 α-helices (Martin, 1995). Catalysis by Trx-fold enzymes relies on two catalytic cysteine residues (CXXC) that cycle between reduced (dithiol) and oxidized (disulfide) states, and are located at the N-terminus of an α-helix (Mossner *et al.*, 1998).

Mechanistically, thiol reactions typically proceed via nucleophilic attack and require deprotonation of the thiol to a negatively charged thiolate to occur efficiently. Since thiol groups commonly have a pKa of about 8 to 9, only a small fraction of thiols are in the thiolate form at a cytoplasmic pH of around 7.4. However, cysteines with reduced pKa are frequently found in the active sites of enzymes, where the protein environment can lower the pKa of the thiol to stimulate the formation of the thiolate and thus increase nucleophilicity **(Figure 1.6a)**. Factors that decrease the pKa of the nucleophilic thiolate will thus have a significant effect on the rate of thiol-displacement reactions, and are mainly due to electron withdrawing effects such as that of an α-helix

a)

$$R\text{-}SH \overset{pKa}{\rightleftharpoons} R\text{-}S_n^- + H^+$$

b)

$$R\text{-}S_n^- + \underset{R}{S}\text{=}S_{lg}\text{-}R \rightleftharpoons \left[\overset{\delta^- \; \delta^- \; \delta^-}{\underset{R}{R\text{-}S_n \cdots S \cdots S_{lg}R}} \right] \rightleftharpoons R\text{-}S_n\text{=}\underset{R}{S} + {}^-S_{lg}\text{-}R$$
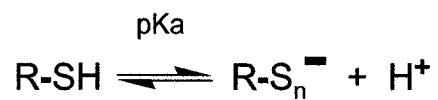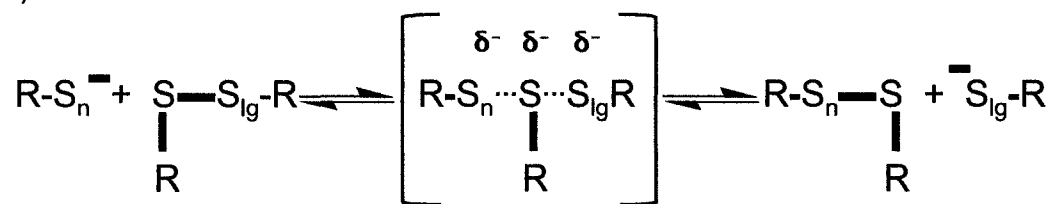
Figure 1.6. a) Factors that decrease thiol pKa will enhance thiolate formation at physiological pH and increase its nucleophilicity (S_n); b) During S_N2 thiol displacement reactions, a nucleophilic thiolate attacks a disulfide resulting in a negatively charged transition state, and the leaving group thiol (S_{lg}), is released in the reduced state. The thiol that leaves generally has the lower pKa.

dipole, close proximity of the thiol to a positively charged amino acid, or other factors that stabilize the thiolate anion (Gilbert, 1984). However, the same factors that lower the pKa of the thiol, may also cause it to become a better leaving group, by means of the higher stabilization of the thiolate form over the thiol form. Accordingly, when a thiolate attacks a disulfide bond, the thiol with the lowest pKa is favoured as the leaving group **(Figure 1.6b)** (Gilbert, 1995).

NADPH is formed directly during catalytic reactions, primarily the pentosephosphate pathway, and can stably store two electrons with a very low redox potential (-315 mV) **(Figure 1.5)**. These electrons are used directly to drive many reductive reactions in an enzyme-catalysed manner. Trxs (CGPC catalytic motif) and Grxs (CPYC catalytic motif) receive their reducing power from the cellular NADPH pool in slightly different ways. Trx-reductase directly couples the two-electron oxidation of NADPH to the two-electron reduction of Trx. In contrast, Grxs are typically reduced by two molecules of reduced GSH (GSH), which are concomitantly oxidized to GSSG. NADPH then reduces GSSG back to two GSH molecules in a reaction catalyzed by GSH-reductase.

Whereas Trx requires both active site cysteines to catalyze reduction reactions, Grxs can catalyze many reactions with only a single cysteine and monothiol Grxs form a special subclass that conserve only one catalytic cysteine. In the monothiol reaction, the intra-molecular nucleophilic attack by the second active site cysteine is replaced with an inter-molecular attack by GSH or other external thiol (Shenton *et al.*, 2002). This liberates the mixed disulfide reaction intermediate and restores the enzyme to its reduced state.

Trxs have a very low redox potential (-270 mV for Escherichia coli Trx), which makes them efficient catalysts for the reduction of disulfides in other proteins (Krause *et al.*, 1991). Grxs have a higher redox potential (-198 to -233 mV) and they reduce general protein disulfides with lower efficiency (Aslund *et al.*, 1997; Jung and Thomas, 1996). However, Grxs have been described as reducing agents for a few specific targets that rely on disulfide formation and reduction during catalysis. Examples include RNR and arsenate reductase (Holmgren, 1976; Mukhopadhyay and Rosen, 2002). Grxs are also known to effectively reduce mixed disulfides between GSH and thiols of protein cysteine residues (Gravina and Mieyal, 1993). Interestingly, recent research has shown that Grxs also can have efficient glutathionylation activity and the role of some Grxs as either a reducing or oxidizing agent may depend on the redox status of its environment (Beer *et al.*, 2004; Xiao *et al.*, 2005).

Another Trx-fold oxidoreductase, protein disufide isomerase (PDI, CGHC catalytic motif), has been shown to catalyze net protein reduction in the presence of reducing agents and net oxidation in the presence of a disulfide, although its higher redox potential (-145 to -175mV) makes it a relatively more efficient catalyst of protein disulfide bond formation (Freedman *et al.*, 1984; Lundstrom and Holmgren, 1993; Dalle-Donne *et al.*, 2007). PDI is known to play a role in oxidative protein folding in the lumen of the endoplasmic reticulum (Noiva and Lennarz, 1992). Finally, *E. coli* periplasmic protein disulfide oxidase (DsbA, CPHC catalytic motif), demonstrates a redox potential of -125 mV, which makes it the most oxidizing of all known Trx-fold oxidoreductases (Zapun *et al.*, 1993).

1.2.4 Human glutaredoxins

Three Grxs are known to exist in humans, Grx-1 is primarily cytoplasmic, Grx-2 is localized to the mitochondria and nucleus, while Grx-5 has not been well characterized and is a monothiol Grx with a CGFS consensus sequence (Lundberg *et al.*, 2001; Sagemark *et al.*, 2007). Mammalian Grx-1 is most similar to poxviral Grx-1 in structure, function and sequence, but also conserves several cysteine residues not present in poxviral Grx-1, that have been proposed to play a regulatory role (Fernandes and Holmgren, 2004). Grx-2 differs from most Grxs in that it has a CSYC active site motif and can be reduced by Trx-reductase in addition to GSH. Grx-2 has also been shown to contain a second disulfide that apparently enhances protein stability. The redox potentials of human Grx-1 and Grx-2 are very similar at -232 and -221 mV, respectively (Sagemark *et al.*, 2007).

In the mitochondria as much as 70% of protein cysteines are gluathionylated, and perhaps not surprisingly Grx-2 has shown to have stronger affinity for GSH-protein mixed disulfides than Grx-1 and thus may play a more prominent role in reversible glutathionylation reactions during periods of oxidative stress (Beer *et al.*, 2004; Johansson *et al.*, 2004). The ability of Grx-2 to accept reducing equivalents from Trx-reductase could also be beneficial in times of severe oxidative stress when GSH levels become very low due to efflux, oxidation to GSSG or the abundant formation of GSH-protein mixed disulfides. The direct reduction of Grx by Trx-reductase could thus act to restore the redox balance during such situations. Since human Grx-2 is present in the mitochondria and nucleus it is not expected to play a direct role in poxviral biology. However, its ability to function in more oxidizing environments and catalyze oxidation

and glutathionylation of thiol containing proteins demonstrates an evolution that could have implications for poxviral Grx-1, which also must function in the potentially more oxidizing environment of the virosome, and this will be more thoroughly discussed in chapter 3.

1.2.5 Poxviral redox proteins

In addition to the vertebrate-like Grx-1 encoded by orthopoxviruses already discussed, all poxviruses conserve another Grx-like gene (G4L in vaccinia, EVM065 in ectromelia) that is involved in the maturation of viral capsid proteins (White *et al.*, 2002). Although G4L demonstrates some properties that are common to other Grxs such as DHA reductase and thioltransferase activity, the protein shows only weak homology to other Grxs in the first 40 residues (~25% identity) and less thereafter (Gvakharia, 1996). Furthermore, while most Grxs demonstrate a conserved CPYC catalytic motif, G4L conserves a CSIC motif, which also suggests the protein has evolved novel functions that diverge from most other Grxs. G4L is known to be involved in disulfide bond formation along with two other proteins E10 and A2.5, which form a thiol-disulfide interchange pathway that is absolutely required for virus formation (Senkevich *et al.*, 2002).

In eukaryotic cells, disulfide bond formation is generally catalyzed in the endoplasmic reticulum, which offers some protection against the reducing environment of the cytoplasm. The formation of disulfide bonds by poxviruses must thus have evolved mechanisms to ensure disulfide bond formation in the cytoplasm, although the redox status of the virosome may offer some protection from reducing agents. The

structure of G4L was recently solved and shed some light on how the poxviral proteins may efficiently catalyze this oxidizing reaction (Su *et al.*, 2006). The structure shows similarities to other Trx-fold proteins, but also has a finger-like projection that could act to block substrate binding sites seen in other Grx structures. This region becomes even less accessible when the protein forms a dimer, which may impede any reducing agents from entering the active site, and thus the protein could be maintained in the oxidized state even when in strongly reducing conditions.

Glutathione peroxidase is another redox protein that is encoded by avipoxviruses and MCV. The MCV enzyme demonstrates 84% sequence identity to the human homologue and both enzymes are selenoproteins (Moss *et al.*, 2000). The viral enzyme was shown to protect human keratinocytes against UV or hydrogen peroxide induced apoptosis, suggesting important roles as an antioxidant and antiapoptotic protein in the viral lifecycle (Shisler *et al.*, 1998).

1.3 Thesis outline and objectives

Protein crystallography provides crucial information regarding protein function, mechanism of catalysis, and insights into interactions with substrates, inhibitors or other proteins. This knowledge is increasingly utilized by pharmaceutical companies for the purposes of structure-based drug design and structure determination is the most direct method for revealing how drugs interact with target proteins. The development and use of drugs that target enzymes involved in nucleotide metabolism has proven to be an effective strategy in regards to both antiviral and chemotherapeutic agents. One major obstacle for the development of drugs that target poxviral enzymes involved in

nucleotide metabolism, is that these enzymes show strong homology to the corresponding mammalian enzymes. However, structural information can be used to exploit differences between the host and viral protein structures and assist in the development of drugs that specifically target the viral enzymes. One of the goals of this study was thus to structurally characterize poxviral proteins using X-ray crystallography and to compare these structures to already determined mammalian or related structures in order to derive viral specific adaptations.

Poxvirus research is also valuable since it has significant impact on our understanding of cell biology in general and antiviral mechanisms in particular. The widespread occurrence of poxviruses in nature, as well as the immunological response to infection by these viruses, suggests a co-evolution of poxviruses with many vertebrate lineages. Since many poxviral proteins show strong sequence identity to host proteins, by studying these poxviral proteins, we also learn much about their host counterparts. Thus, the study of poxviruses is not only required to develop effective antivirals, but also has a much bigger scope in regards to host-pathogen interactions, the transfer of genetic information amongst very diverse life forms, and the evolution of both viruses and eukaryotic organisms.

One important outcome of structural biology is that once structures are determined, new structure-based hypotheses are often generated, and can lead to discoveries that may not have been found through other techniques of protein characterization. Another goal of this project was to follow up on these structural findings with functional analyses, in order to better understand the molecular mechanisms of enzyme function in general.

In the first phase of this project, a broad range of dNTP metabolism or associated poxviral genes were targeted. Cloning, expression, purification and crystallization methods and results of this phase are provided in chapter 2. EVM Grx-1 (EVM053) was then selected from these targets for further structural study and the crystal structures of this enzyme in the reduced, oxidized and dimethylarsenylated states are described in chapter 3. Comparisons of these structures to mammalian, *E. coli* and other related Grx structures led to structure-based hypotheses that were further probed by biochemical studies which are reported in chapter 4. The unanticipated observation of a dimethylarsenylated active site cysteine in one of the EVM053 structures, resulted in the discovery that Grxs can act as dimethylarsenate reductases. Biochemical characterization of this activity and its potential physiological relevance is presented in Chapter 5.

2.1 Protein production and crystallization

2.1.1 Cloning

Primers were developed using the computer program OligoAnalyzer 3.0 (Integrated DNA technologies) **(Table 2.1)**. Purified genomic EVM DNA was kindly provided by Dr. Michele Barry. Target genes were PCR amplified using Pfx polymerase (Invitrogen) or Phusion DNA polymerase (Finnzymes). A DNA vector and cloning procedure that was developed in the laboratory of Dr. Bart Hazes known as COMPASS was used for cloning. The COMPASS method uses overlap extension PCR to create expression vectors by fusing linear DNA fragments to a host module fragment derived from a pET-Blue2 plasmid (Novagen). The host module is about 2300 nucleotides in length and contains all the regions necessary for recombinant gene expression in *E. coli* cells **(Figure 2.1a)**. Regions 5' to 3' include; a translation terminator, a hairpin transcription termination loop, an ampicillin resistance selection marker *(bla)*, an origin of replication, the T7 promoter, a ribosome binding site and a translation initiation site.

The COMPASS system facilitates the fusion of target proteins to N- or C-terminal fusion tags, by their incorporation into the host module via an additional PCR amplification reaction **(Figure 2.1b)**. The fusion of maltose binding protein (MBP) or a hexahistidine tag to the target protein facilitated the purification process and in the case

Protein	Primer name	Primer sequence
EVM026	EVM026_for	CAC CAT CAC CAC CAT CAT ATG
	EVM026_rev	CTG TCA GAC CAA GTT TAC TCG GCG CGC CCA CCC TTT TA
EVM028	EVM028_for	ATG GAA CCG ATC CTT GCA
	EVM028_rev	CTG TCA GAC CAA GTT TAG TGT GCG AAA GTA AGG AGA CA
EVM053	EVM053_for	ATG GCC GAG GAA TTT GTA CA
	EVM053_rev	CTG TCA GAC CAA GTT TAC GGA TAC ATG AAC ATG TCG C
	Tyr21>Ala_for	<u>GCT</u> ACA TGT CCT TTT TGT AGA AAC GCA CTG G
	Tyr21>Ala_rev	CTT GAC AAA AAT TGT CAC TTT GTT ATT GGC CAA CC
	Tyr21>Trp_for	<u>TGG</u> ACA TGT CCT TTT TGT AGA AAC G
	Tyr21>Trp_rev	CTT GAC AAA AAT TGT CAC TTT GTT ATT GGC
	Cys26>Ser_for	<u>AGT</u> AGA AAC GCA CTG GAT ATT CTA AAT AAG TTT AGT
	Cys26>Ser_rev	AAA AGG ACA TGT ATA CTT GAC AAA AAT TGT CAC
	Pro53>Ala_for	<u>GCC</u> GAA AAT GAA TTG CGC GAC T
	Pro53>Ala_rev	TTT AAA TTC TTT AAT ATC GAC AAT TTC ATA CGC TCC TC
EVM056	EVM056_for	ATG AGT AAG GTA ATC AAG AAG AGA GTT GA
	EVM056_rev	CTG TCA GAC CAA GTT TAG TCT GTC AAA TCA TCT TCC GGA G
EVM057	EVM057_for	ATG TTT GTC GTT AAA CGA AAT GGA T
	EVM057_rev	CTG TCA GAC CAA GTT TAG CAC AAG TCT GTA GAG AAT CGC
	R1_primer1_for	ATG GAG GAT TTA TTC AAC TAT GTT AAT CCT
	R1_primer2_for	ATG TTA ATG CGT GTC GCG GTA G
	R1_primer3_for	ATG TCT AGC TGT TTT CTA CTT AAC ATG ATG GAT G
	R1_primer4_for	TAA ACA AAA ACA TTT TTA TTC TCA AAT GAG ATA AAG TG
	R1_primer1_rev	TTG GTG ACG ACT AGT TCC CGC
	R1_primer2_rev	ATA ATT TTC TCT CGG TTA AAA CTC TAA GGA G
EVM065	EVM065_for	ATG AAG AAC GTA CTG ATT ATT TTC GG
	EVM065_rev	CTG TCA GAC CAA GTT TAG GCG TAT ACA ACG TCG CAT
EVM078	EVM078_for	ATG AAC GGT GGA CAT ATT CAG TTG
	EVM078_rev	CTG TCA GAC CAA GTT TAC TCG CGA CCT CAT TTG CAC TT
EVM093	EVM093_for	ATG AAC TCG GTA ACT GTG TCG C
	EVM093_rev	CTG TCA GAC CAA GTT TAA TGC CGA TGG GAC ACC TA T
EVM094	EVM094_for	ATG GAT GCG GAT ATT AGA GGT AAT G
	EVM094_rev	CTG TCA GAC CAA GTT TAT GGA AGC TAC CAA GGC GA
EVM147	EVM147_for	ATG ACC TAT ATA TTT ATT TTC AGT TTT ATT ATA CGC
	EVM147_rev	CTG TCA GAC CAA GTT TATAT GCA TAT CGT ACA CGT ATC CG

Table 2.1. Primer DNA sequences used for production of recombinant EVM full length and truncated protein constructs. Mutated codon is underlined for primers used to generate point mutations. All primers were designed using OligoAnalyzer 3.0 (Integrated DNA technologies).

a)

| 5' TAA | *bla* | ori | T7 | RBS | ATG 3' |

b)

Host module

Target module
C-terminal targets   N-terminal targets

Fusion module
N-terminal fusions   C-terminal fusions

PCR

ligation

N-terminal fusion   C-terminal fusion   Target with no fusion
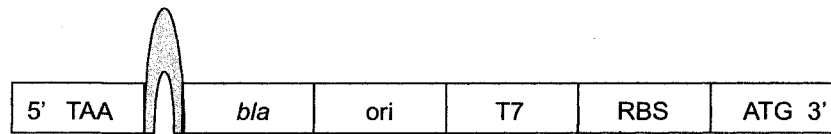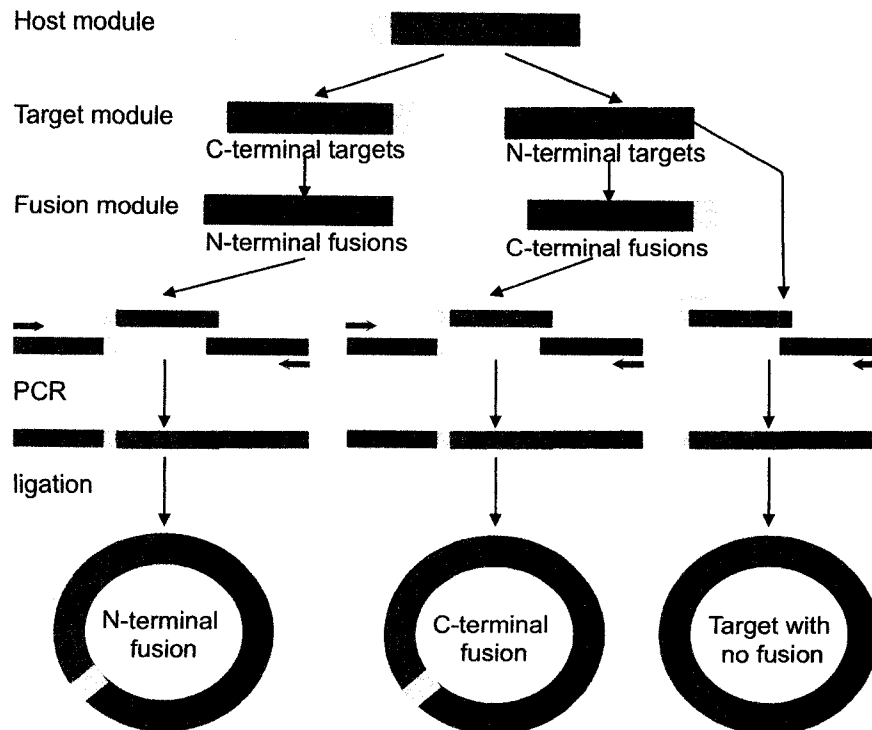
Figure 2.1. a. COMPASS Host module construct. Cyan region represents hairpin transcription termination loop. *Bla* is an ampicillin resistance selection marker. Other regions include; an origin of replication (ori), the T7 promoter and a ribosome binding site (RBS).

b. COMPASS cloning of N-terminal fusion, C-terminal fusion, and native proteins. A host fragment (red) is combined with DNA-fragments from the target (green) and, optionally, fusion (modules). The fusion module contains subsets for N-terminal and C-terminal fusions that differ in their overlap sequence (olive or purple). The user PCR amplifies their target gene with one of the two primers adding an overlap sequence, olive or purple, as indicated. PCR on the mix of fragments with primers to the outside fragments both amplifies and anneals the fragment which, after ligation, gives the vector of choice.

47

of dUTPase, resulted in increased solubility of the protein (**see appendix**). MBP is known to be a highly soluble protein and has been shown to improve solubility of other proteins when co-expressed as a fusion protein (Kapust and Waugh, 1999).

For N-terminal hexahistidine tagging of gene targets (non-cleavable), a reverse primer complimentary to both the 3' region of the target gene and 5' region of the host module was used to incorporate the target gene at the 5' end of the host module in a first round of PCR amplification. The forward primer was developed starting directly at the translation initiation site (ATG). A primer encoding 6 histidines and an overhang complimentary to 3' end of host module was then incorporated in a second round of PCR amplification with the same forward primer. N-terminal tagged MBP fused recombinant gene products were constructed using similar techniques. Full-length amplification products were gel purified using a QIAquick gel extraction kit (Qiagen). Host modules containing the recombinant gene products were then phosphorylated using T4 kinase, purified and ligated using T4 DNA ligase (Invitrogen).

The resulting expression vector was initially transformed by electroporation into *E. coli* DH5α cells. To briefly describe this procedure, electrocompotent cells were incubated with the expression vector on ice for 10 min and then transferred to pre-chilled electrocells (0.2 cm gap). Cells were electroporated for 5 msec at 2.5 kV, 25 μF, 200 Ω. 1 mL SOC medium (0.5% Yeast Extract, 2% Tryptone, 10 mM NaCl, 2.5 mM KCl, 10 mM $MgCl_2$, 10 mM $MgSO_4$, 20 mM Glucose) was immediately added to electrocells following electroporation and material was then transferred into sterile 1.5 ml tubes and incubated for 1 hour on a shaker at 310 K, 225 rpm.

Transformants were subsequently plated onto LB (Luria-Bertani) plates containing 50 µg ml⁻¹ carbenicillin and incubated overnight at 310 K. Colonies were picked and plasmids purified using a QIAprep Spin Miniprep Kit (Qiagen). Plasmid DNA was then transformed into *E. coli* expression cells, BL-21 AI, by electroporation. Transformants were again plated and harvested from plates containing selective media following incubation at 310 K. Colonies were frozen at -80° C in aliquots of LB broth containing 10% glycerol until required for expression.

2.1.2 Expression and purification

A minimum of 2 L and up to 30 L of *E. coli* cell culture was grown up to obtain sufficient protein for crystallization trials. To briefly describe this procedure, protein expression from recombinant cells (cryostocked frozen colonies) was started by a 1:100 dilution of an overnight BL21AI culture into (LB) broth containing 50 µg ml⁻¹ carbenicillin. Cells were cultured at 310 K with shaking until an absorbance of OD_{600} = 0.5-0.8 was reached. Protein expression was induced by adding arabinose to 0.05% or IPTG 0.05 mM followed by an incubation period at 310 K. The optimal incubation time was determined by monitoring culture samples at multiple time points for relative expression and solubility characteristics. When problems were encountered with low expression levels or insolubility, several of the target proteins were also expressed at lower temperatures (277-303 K) or lower concentrations of inducing agent. Cultures were centrifuged at 4000*g* for 20 min and the cell pellets were resuspended in buffer (generally 10 mM Tris pH 7.4-8.0, 500 mM sodium chloride). The resuspended cells

were sonicated and cell debris removed by centrifugation at 9000g for 30 min at 277 K. The supernatant was filtered using a .45 μm filter disk (Millipore) prior to purification.

Following expression in *E. coli* cells, recombinant proteins were purified at 4° C or room temperature on an Akta purifier liquid chromatography system (Amersham Pharmacia). All purification protocols started with affinity chromatography, followed by ion exchange chromatography and, in some cases, a final size exclusion chromatography step was used.

For the his$_6$-tagged proteins, the first purification step was immobilized metal affinity chromatography (IMAC) (HiTrap, GE Healthcare). The sample was loaded in a buffer with high salt present (500 mM NaCl) to avoid non-specific ion exchange effects with the nickel column due to the positive charge of the nickel, and the salt was then removed during a wash step. The reduction of the salt concentration from 500 mM to 50 mM during the wash step facilitated the use of a second purification step using ion exchange chromatography and also prevented precipitation of proteins that are not stable in high salt concentrations (i.e. RNR R2, **see appendix**). For the wash step 5-50 mM imidazole was generally present in the buffer while a gradient of 50-500 mM imidazole was used to elute the protein target.

For proteins fused to MBP, the protein was first purified on an amylose affinity column, using maltose for elution. Cleavage of MBP from the target protein was performed using the protease, rhinovirus 3C protease, also known as PreScission Protease (GE Healthcare) at a concentration of approximately 1 unit/100 μg protein for 16h at 4° C.

For a second purification step, ion exchange columns were most often used, and generally resulted in highly pure protein. Ion exchange chromatography separates molecules based on their intrinsic charge and increasing concentrations of NaCl or other salts are used to elute the protein target in the case of either anion or cation exchange column chromatography. A gradient of 50-1000 mM NaCl was generally used to elute target proteins using this procedure.

Size exclusion chromatography (SuperDex 75 Prep Grade Column, GE Healthcare) was also used in cases where following affinity and ion exchange chromatography, the protein was still not adequately pure for crystallization trials, or when there was evidence of protein polydispersity or varying oligomerization status (see next section).

For SDS-PAGE analysis, 5-20 µg of protein sample was mixed 5:1 with sample buffer (10% w/v SDS, 10mM DTT, 20 % v/v glycerol, 0.2 M Tris-HCl, pH 6.8, 0.05% w/v bromophenolblue). Samples were heated by boiling for 5 min before loading onto 15% acrylamide gels, and run for 40-50 min at 200 V in running buffer (25 mM Tris-HCl, 200 mM glycine, 0.1% (w/v) SDS). Protein bands were visualized using Coomasie blue staining solution and protein weight was estimated using Precision Plus Protein standards (Bio-Rad Life Sciences). SDS-PAGE analysis of expression and purification of four poxviral proteins involved in nucleotide metabolism is demonstrated in **Figure 2.2.** Proteins were concentrated using membrane centrifugal filter devices (Millipore). BCA assays or amino acid analysis (Alberta Peptide Institute) were performed to determine protein concentration prior to crystallization trials.
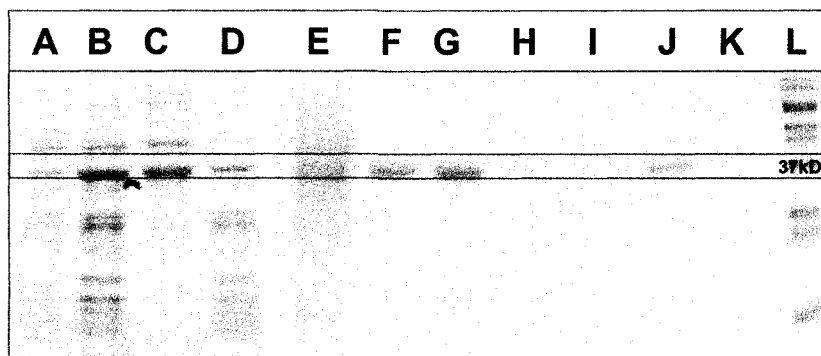
Figure 2.2a. SDS-PAGE of EVM028 gene product expression and purification.
Expected molecular weight is 37.2 kD. a) t=0 expression; b) t=3 h; c) soluble fraction; d)
insoluble fraction; e) Ni column flow-through; f-g) Ni column elute; h-k) Anion exchange
column elute; l) Protein standards ladder.
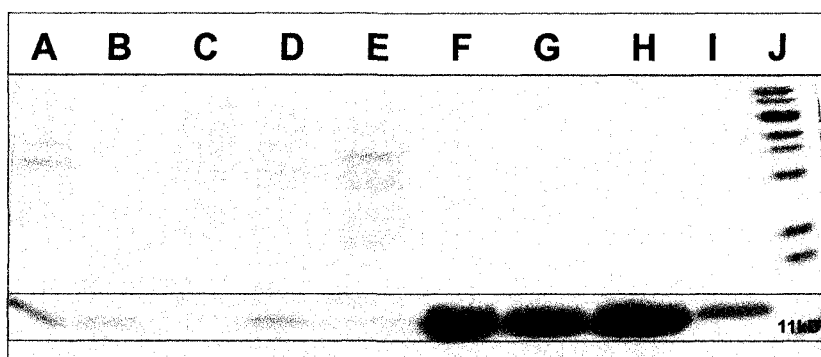
Figure 2.2b. SDS-PAGE of EVM053 gene product expression and purification.
Expected molecular weight is 13.2 kD. a) Soluble fraction; b) insoluble fraction c) t=0
expression; d) t=3 h; e) Ni column flow-through; f) Ni column elute; g-i) Anion exchange
column elute; j) Protein standards ladder.
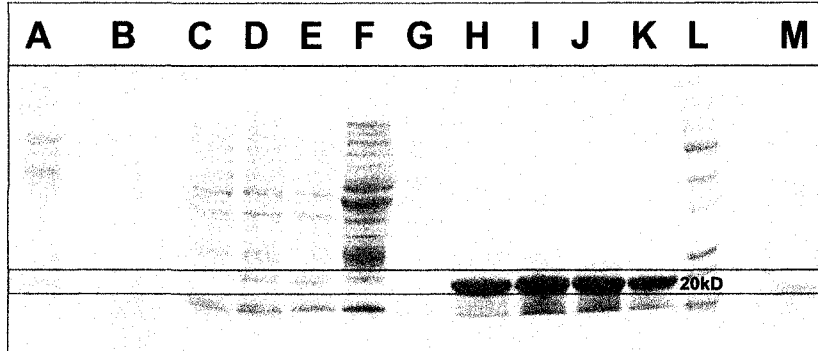
Figure 2.2c. SDS-PAGE of EVM078 gene product expression and purification.
Expected molecular weight is 20.1 kD. a) Soluble fraction; b) insoluble fraction; c) t=0
expression; d) t=2 h; e) t=3 h; f) Ni column flow-through; g) Ni column wash; h-k) Ni column
elute; l) Protein standards ladder; m) Anion exchange column elute.
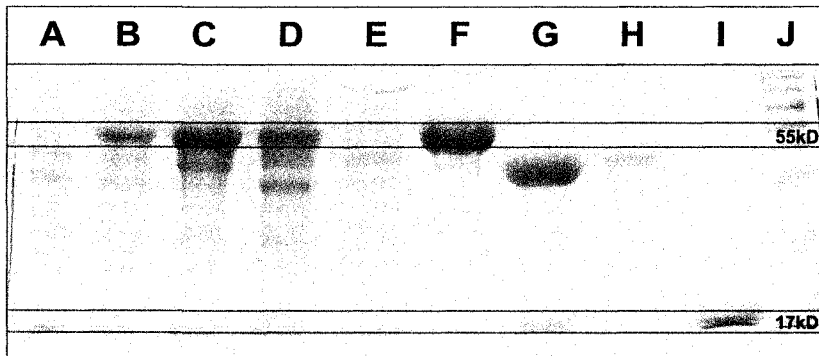
Figure 2.2d. SDS-PAGE of MBP/EVM026 gene product expression and purification.
Expected molecular weights of MBP/EVM026 and EVM026 are 60.2 kD and 17.2 kD,
respectively. a) t=0 expression; b) t= 3 h; c) soluble fraction; d) insoluble fraction; e) Amylose
affinity column flow-through; f) Amylose affinity column elute; g) Cleavage of MBP/EVM026
fusion protein following elution from amylose affinity column (t=20 h); h) Cation exchange
column flow-through; i) Cation exchange column elute; j) Protein standards ladder.

2.1.3 Light scattering analysis

Static and dynamic light scattering analysis gives information on the molecular mass and hydrodynamic radius of particles in solution (Wilson, 2003). For protein samples this gives important information regarding the protein's quaternary structure in solution. The analysis also indicates if the sample contains a homogenous population of one fixed size (monodispersed) or a heterogeneous collection of protein aggregates (polydispersed). Monodispersed protein samples tend to be more amenable for crystallization (Derewenda, 2004) and thus several of the proteins, once purified, were analyzed for this characteristic. For a typical analysis, 100 μg of protein in 10 mM Tris buffer supplemented with 150 mM NaCl was loaded onto a Superose 6 or 12 size exclusion column (GE Healthcare), with the eluent analyzed by an in-line multi-angle light scattering detector (DAWN EOS with QELS analyzer, Wyatt Technology).

2.1.4 Crystallization

After the production of adequate amounts of purified protein, crystallization is the second and often largest hurdle in obtaining a crystal structure. This is mainly because the physical processes required to grow protein crystals are complex, highly unpredictable and vary dramatically for different proteins. Broad crystallization screens of various chemical environments are often used to explore the most important variables that may induce and promote crystal growth. Variables that can affect the formation and growth of protein crystals include; pH, temperature, type and concentration of precipitant (salt, PEG, ammonium sulfate, MPD, and many others), or additives. The

54

protein sample itself is also a major determinant and protein purity, concentration and polydispersity affect crystallization potential. Certain information regarding protein cofactors or substrates, or conditions in which homologous proteins have crystallized, can also provide valuable clues as to what conditions the target protein might crystallize in.

The most commonly used method to grow crystals is the vapour diffusion method. In this method, drops of protein (commonly 0.1 - 8 µl) are suspended above wells containing the various screen reagents. The protein must be at a high concentration (generally 10 - 20 mg/ml for initial screens) and is mixed, typically at a 1:1 ratio, with the well solution. The reagents within the drop and the reservoir then equilibrate through vapor diffusion, which concentrates the precipitating agents and the protein within the drop, until conditions that initiate crystal nucleation may be achieved.

For the first round of crystallization screens, a Honeybee X32 crystallization robot (Genomic Solutions) was used. Robotic experiments were created in 96-well Greiner crystallization plates where up to 3 crystallization drops are equilibrated against a reservoir with precipitant solution. The crystallization drop was typically formed by mixing 100 or 200 nl of protein sample with an equal volume of precipitant solution, with 50 µL of precipitant solution being placed in the reservoir. Plates were sealed and incubated at room temperature to allow the more concentrated precipitant solution to absorb water from the drops by vapor diffusion. Plates were regularly observed by microscope to search for crystals or microcrystals.

The crystallization robot greatly facilitates and accelerates screening processes while reducing the requirement for large amounts of protein. Using the robot, only 200 μl of a protein sample is enough to run approximately 1000-2000 unique vapor diffusion crystallization experiments. Many of the reagent solutions used to set up these experiments are obtained from commercially available kits (Emerald BioSystems, Hampton Research) or were locally developed (Hazes crystallization screens). Using the crystallization robot allowed greater flexibility to set up experiments at various protein concentrations, or in the presence of substrates, inhibitors or other additives. This was quite advantageous for the I3L set-ups (**see appendix**) where extensive additive screens and oligos of various lengths were used.

Following initial screening on the crystallization robot, promising crystallization conditions were optimized to obtain diffraction quality crystals. This would be done by systematically altering pH levels and changing concentrations of precipitants, additives, or other factors that could influence the crystallization process. Other proven methods such as seeding and the dilution method (Dunlop and Hazes, 2003), were also utilized in attempts to optimize the growth of crystals.

2.2 Mutagenesis

For point mutations of EVM053 (ectromelia virus Grx-1) and truncations of EVM057 (ectromelia virus RNR R1), the Phusion Site-Directed Mutagenesis Kit (Finnzymes) was used in conjunction with the COMPASS system. For the point mutations the vector was amplified using phosphorylated primers containing the

nucleotide substitution at the 5' end. These recombinant vectors were also initially transformed into *E. coli* DH5α cells by electroporation, and then into BL21AI cells prior to expression. Point mutations were verified by DNA sequencing at the Molecular Biology Services Unit at the University of Alberta. All wild type and mutant EVM053 enzymes were shown to be active using L-cystine, DMA-5 or DHA as a substrate (see next section).

2.3 Functional analyses

2.3.1 NADPH-coupled activity assay

NADPH-coupled Grx activity assays were carried out essentially as described (Ahn and Moss, 1992). Briefly, a 100 µl reaction mixture contained 100 mM Tris (pH 6.8 for the arsenic reductase assays) or sodium phosphate (pH 7.5 for the L-cystine and R1 peptide assays), 0.5 mM EDTA, 0.35 mM NADPH, 1 mM GSH, 0.2 units GSH reductase (Sigma) and appropriate dilutions of purified EVM053 or the mutant preparations, unless otherwise indicated. Human Grx-1 was obtained from American Diagnostica. The oxidized EVM057 R1 C-terminal decapeptides were synthesized at the Alberta peptide institute and were N-terminal acetylated (Ac-DSEICTSCSG). Reactions were monitored spectrophotometrically at 340 nm for 2-3 min starting 30 s after addition of substrate at the indicated concentrations at room temperature. Absorption decrease was linear during this time period. For the pH profile studies of Grx catalyzed arsenic reduction, 100 mM of sodium acetate was used for pH 3.6 - 5.2, MES pH 5.6 - 6.6, Tris pH 6.8 - 8.8, CHES pH 9.0-10.5. These reactions were monitored for 2 min

following the addition of 50 mM AsV, MMA-5 or DMA-5. Reaction rates were corrected for the spontaneous rate in absence of enzyme and the result expressed as the formation of μmoles of NADP+/min/mg of enzyme. All results were analyzed using a minimum of two replicates with Graphpad 5.0 (Graphpad Software Inc.). Kinetic values were determined using non-linear regression.

2.3.2 DHA reductase activity assay

The DHA reductase assays were carried out essentially as described (Stahl *et al.*, 1983). A 100 μl reaction mixture contained 100 mM MES buffer pH 6.8, 0.5 mM EDTA, 1 mM GSH, 2 mM DHA and appropriate dilutions of EVM053, human Grx-1 or EVM053 point mutant enzymes. Enzyme preparations were also pre-incubated for 10 min in the presence of either 1mM GSH and 1 mM GSSG, or 1 mM GSH and 0.1 mM GSSG (see section 4.2.3). These reactions were monitored for 2 min at 265 nm 30 s after the addition of 2 mM DHA at room temperature. Absorption increase was linear during this time period. Reaction rates were corrected for the spontaneous rate in absence of enzyme and the result expressed as μmoles ascorbic acid formed/min/mg of enzyme. All results were analyzed using a minimum of two replicates with Graphpad 5.0 (Graphpad Software Inc.).

2.3.3 Tryptophan fluorescence-based activity assay

For the tryptophan fluorescence-based analysis, a stock solution of 0.45 μM Y21W in a buffer consisting of 10 mM Tris pH 7.0 and 50 mM NaCl, was pre-incubated overnight with 1 μM TCEP, GSSG, DHA, or 10 μM DTT. Changes in Y21W fluorescence in the presence of oxidizing (DHA, GSSG) or reducing agents (DTT, TCEP) was monitored using an excitation of 274 nm and an emission spectrum of 315-400 nm using a QM-4/2005 spectrofluorometer (Photon Technology International). For the fluorescence-based reductase assay, 4.5 μM Y21W was pre-incubated with 50 μM TCEP for 1 hour at room temperature and then thoroughly buffer exchanged using Amicon ultra centrifugal filter devices (Millipore) into buffer without reducing agent present. The reaction was initiated by the addition of 1 μM DHA or 10 μM DMA-5 to 0.45 μM Y21W reduced protein preparation. Fluorescence was then measured using an excitation wavelength of 274 nm and an emission of 338 nm at 15 second intervals over 2 min. Graphs for tryptophan fluorescence-based analyses were generated using Graphpad 5.0 (Graphpad Software Inc.).

CHAPTER III

POXVIRAL GLUTAREDOXIN STRUCTURE

3.1 Introduction

Glutaredoxins are oxidoreductases that belong to a family of structurally and functionally related proteins that include Trx, DsbA and PDI (see section 1.2.3). The catalytic sites of these enzymes typically conserve a CXXC motif that is required for redox reactions involving protein thiols and other redox sensitive molecules. The N-terminal active site cysteine for these proteins exhibits a lower pKa than free cysteine (8.7) of 6.3-7.5 for *Trx*s (Forman-Kay *et al.*, 1992; Dyson *et al.*, 1997) 3.5-5.0 for Grxs (Mieyal *et al.*, 1991; Foloppe and Nilsson, 2004), and 3.2-3.5 for *E. coli* DsbA and eukaryotic PDI (Nelson and Creighton, 1994; Darby and Creighton, 1995). This surface accessible cysteine is deprotonated to a thiolate under most physiological conditions and reactivity is enhanced both due to increased nucleophilicity and enhanced ability to act as a leaving group (see section 1.2.3). The second cysteine of the active site occupies a more buried location, has been shown to have a more basic pKa than free cysteine and is much less reactive than the N-terminal cysteine (Nelson and Creighton, 1994).

In addition to their prominent role in deglutathionylation reactions, Grxs act as powerful reducing agents for the large subunit of ribonucleotide reductase (R1) in many prokaryotes and eukaryotes, including humans (Padilla *et al.*, 1995). *E. coli* Grx-1 has a ten fold lower *Km* for RNR than Trx and evidence has shown that Grx is the major

reducing agent for RNR *in vivo* (Holmgren, 1979; Kren *et al.*, 1988). The same relationship has been proposed for the Grx-1 and R1 proteins expressed by all orthopoxviruses, including vaccinia, variola, and ectromelia virus (see section 1.1.4.2), which demonstrate 45% and 78% sequence identity to human Grx-1 and R1 respectively.

Unlike all other enzymes involved in poxviral nucleotide biosynthesis, Grx-1 is expressed late in the viral lifecycle, following initiation of DNA replication. A relatively large number of copies of the enzyme have been shown to associate with the virion, suggesting Grx-1 brought into the cell upon entry, may be adequate to support RNR activity (Ahn and Moss, 1992). However, since Grxs are involved in many redox reactions, the poxviral Grx-1 may also have different roles during early and late times in the poxviral life-cycle (Ahn and Moss, 1992; Fernandes and Holmgren., 2004).

Although the role of orthopoxviral Grxs remains controversial, a comparison of the poxviral Grx-1 to other Grx structures could reveal adaptations that reflect different functional needs of these viral enzymes. Several Grx structures have been determined using NMR and X-ray crystallographic techniques. Grxs with homology to the orthopoxviral Grx-1 include the crystal structures of oxidized pig liver Grx-1 and glutathionylated human Grx-2, and NMR structures of human Grx-1 in the reduced and glutathionylated states (Katti *et al.*, 1995; Johansson *et al.*, 2007; Sun *et al.*, 1998; Yang *et al.*, 1998). NMR structures of *E. coli* Grx-1 and Grx-3 have also been determined in oxidized, reduced, and glutathione mixed disulfide conformations (Sodano *et al.*, 1991; Bushweller *et al.*, 1994; Xia *et al.*, 1992; Nordstrand *et al.*, 1999; Nordstrand *et al.*, 2000). Furthermore, a structure of an *E. Coli* Grx-1 with the C-terminus of RNR-R1

bound to the active site has been determined (Berardi and Bushweller, 1999). Common to these Grx structures are the central core of four β-sheets surrounded by α-helices, a cis-proline residue near the active site, and a conserved GSH binding groove. A crystal structure of poxviral Grx-2 has also been solved (Su et al., 2006), but this structure does not appear to conserve a GSH binding site and likely represents a unique Grx-like oxidoreductase that plays a more significant role in disulfide bond formation (White et al., 2002).

To study structure-function relationships of the vertebrate Grx-1 family, and reveal potential viral adaptations, the crystal structures of the ectromelia virus Grx, EVM053, were solved to 1.8 Å in both the reduced and oxidized conformations. This is the first high resolution Grx crystal structure determined in both oxidation states. A detailed analysis of the implications of these structures, in addition to functional assays (see chapter 4), provided new insights into the enzyme's substrate specificity and the role of the enzyme in the orthopoxviral lifecycle. Comparisons of EVM053 with structures of mammalian, E. coli, and T4 bacteriophage Grxs demonstrated unique features including the first observation of a large redox-linked structural rearrangement, a novel cis-proline residue, and dimethylarsenylation of Cys23. These observations generated new testable hypotheses about substrate specificity, control of redox potential, and a putative physiological role in arsenic metabolism.

3.2 Results
3.2.1 Model completeness and quality

EVM053 crystallizes in space group $C222_1$, with two molecules in the asymmetric unit (referred to as chains A and B). Diffraction data to 1.8 Å were obtained for both the reduced and oxidized structures and final R values are $R_{cryst} = 18.3\%$, $R_{free} = 20.8\%$ for the reduced structure and $R_{cryst} = 18.0\%$ and $R_{free} = 21.9\%$ for the oxidized structure. For each protein model all native residues were built except the C-terminal cysteine residue for which no clear density was observed. At the N-terminus, several residues from the His$_6$-tag demonstrated interpretable electron density. In both chains of the oxidized and reduced structures, electron density for the residue immediately preceding the N-terminal methionine of the native protein indicated that the histidine had been mutated into a glutamine, and this was confirmed by sequencing. Two histidines preceding the glutamine were built in the A chain of both structures, while one extra histidine was built for the B chains. Throughout this section, residue numbers refer to the native EVM053 sequence, unless otherwise specified. Due to lack of electron density, the side-chain atoms beyond the C^β position could not be modeled for Lys49 in any of the structures. The side-chains of Arg27 and Arg40 showed disorder in some but not all structures. The following residues have been modeled with dual side-chain conformations: oxidized chain A, Glu4; oxidized chain B, Gln63, Ser84, Ser100; reduced chain A, Cys23; reduced chain B, Arg58.

3.2.2 Overall structure of EVM053

As expected, the overall structure of EVM053 conforms to the Grx fold, with a core of four β-strands flanked by five α-helices **(Figure 3.1)**. The active site cysteine
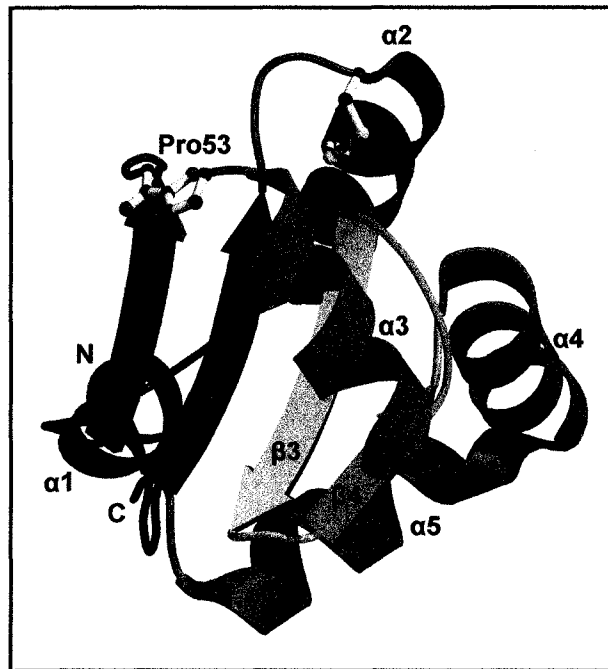
Figure 3.1. Cartoon representation of EVM053 in the oxidized conformation. Helices are shown as coils and strands as arrows. The disulfide bond formed by the active site cysteines is shown in orange and the *cis* Pro53 is drawn in ball-and-stick format.

pair is located in the loop connecting the first β-strand to the second α-helix and the cysteines form a CPFC sequence motif. This is identical to the active site motif in pig Grx-1 and very similar to the CPYC motif in other vertebrate Grx-1 sequences (Fernandes and Holmgren, 2004). The first cysteine, Cys23, is exposed to solvent whereas the second cysteine, Cys26, adopts a more buried location in the first turn of the second α-helix. A proline at position 71 forms a cis-peptide bond in EVM053 and all other Grxs and Trxs of known structure (Nordstrand et al., 1999). This cis-proline induces a sharp turn in the main chain at the start of β-strand 3 and it positions the proline side-chain atoms directly beside the active site cysteines. Interestingly, EVM053 contains a second cis-proline, Pro53, at the start of the third α-helix **(Figure 3.1)**. This proline is conserved in all orthopoxvirus orthologs but is not present in any other known Grx. The corresponding region in E. coli Grx-1 has been shown to interact with the RNR R1 C-terminal peptide, suggesting a potential role for cis-Pro53 in substrate binding (Berardi and Bushweller, 1999) (see section 3.2.7).

The two EVM053 monomers per asymmetric unit form two types of dimers, one related by non-crystallographic two-fold symmetry (585 Å^2 buried surface), the other by the crystallographic two-fold along the x-axis (840 Å^2 buried surface). However, Superose 6 size exclusion chromatography with real-time analysis of the eluent by static and dynamic light scattering (Dawn EOS/QELS, Wyatt Inc.) yielded an estimated molecular mass of 14.8 kDa (13272 Da predicted monomer mass) and a polydispersity factor of 1.0 **(see Figure 2.3)**. This confirms that, like other known Grx-1 enzymes, EVM053 is a monomer in solution.

3.2.3 EVM053 active site structure

The A and B chains of oxidized EVM053 adopt an active site structure that is very similar to the conformation reported for oxidized pig Grx-1 (Katti *et al.*, 1995) **(Table 3.1)**. The disulfide bond length refined to 2.07 and 2.10 Å for the A and B chains, respectively. This is slightly longer than the ideal value of 2.03 Å, but similar to the 2.08 Å in oxidized pig Grx-1. Electron density for the active site disulfide bond is shown in **Figure 3.2a**. The active site structure of reduced EVM053 differs for the A and B chains. In chain A, the Cys23 side-chain displays two alternate conformations with occupancies that refined to 0.57 and 0.43 for rotamers A and B, respectively **(Figure 3.2b)**. Rotamer A corresponds to the conformation observed in other reduced Grx structures and is also similar to the conformation of Cys23 in the B chain. Rotamer A places the Cys23 sulfur atom at 3.27 Å from the sulfur of Cys26, which is too close for a normal non-bonded interaction. Short sulfur-sulfur distances have been reported for disulfides that have been disrupted by radiation damage (Burmeister, 2000). However, the same type of damage does not occur in reduced disulfides. In addition, other common features of radiation damage such as an increase in unit cell volume or decarboxylation of glutamic and aspartic residues were not observed. Furthermore, the X-ray dose during data collection was similar to that used for the oxidized structure for which no signs of radiation damage were observed. A more likely interpretation is that the short sulfur-sulfur distance represents a thiol-thiolate hydrogen bond. Thiol-thiolate hydrogen bonds have been observed in several structures with sulfur-sulfur distances of 3.0 to 3.5 Å and the existence of a thiol-thiolate hydrogen bond in Grxs has been proposed previously (Guddat *et al.*, 1998; Lennon *et al.*, 1999; Conway *et al.*, 2002;

Model[1]	Oxidized EVM053		Reduced EVM053			Pig Grx-1
	Chain A	Chain B	Chain A^A	Chain A^B	Chain B	Oxidized
23S$^\gamma$-26S$^\gamma$ [Å]	2.10	2.07	3.27	5.69	3.82	2.08
23S$^\gamma$-25N [Å]	4.48	4.38	3.86	5.13	3.41	4.20
23S$^\gamma$-26N [Å]	3.32	3.25	3.41	5.77	3.62	3.34
23 Chi1 [°]	150.0	166.2	169.7	-129.8	171.8	167.8

[1] Chain A and chain B represent the two EVM053 monomers that are present in the asymmetric unit of the crystals. Superscript A and B indicate the alternate side-chain conformations of Cys23 in the A chain model of the reduced crystals.

Table 3.1. EVM053 active site geometry.
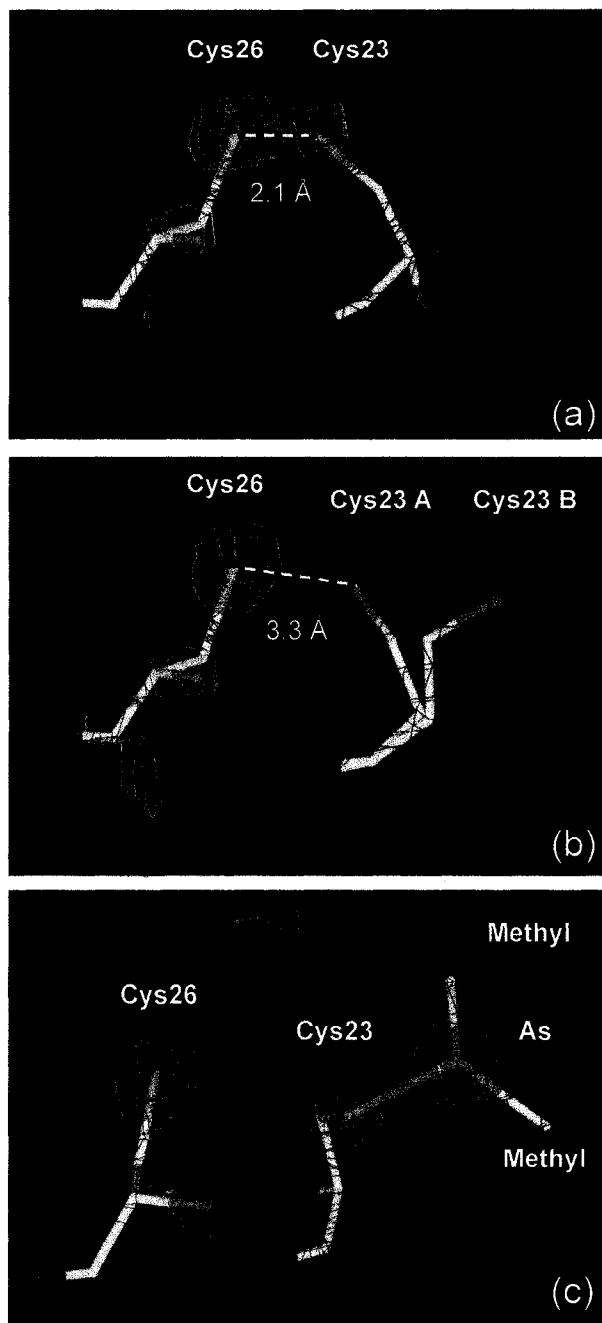
Figure 3.2. Electron density (2|Fobs| - |Fcalc|) for the active site of EVM053 in the (a) oxidized; (b) reduced; (c) dimethylarsenylated states. The disulfide bond in the oxidized structure and the proposed hydrogen bond in the reduced structure are indicated by dashed lines.

Nordstrand *et al.*, 1999). In the B rotamer, the Cys23 sulfur atom points away from the active site and the distance between the active site sulfur atoms is 5.69 Å (see section 3.3.1).

Electron density for chain B supports only one side-chain conformation for Cys23 with a distance of 3.82 Å between the two sulfur atoms in the active site. In this chain, additional electron density indicates that Cys23 has been covalently modified, and the density features are consistent with the addition of dimethylarsenite (DMA-3) **(Figure 3.2c)**. Cacodylate (dimethylarsenate, DMA-5) was used as the crystallization buffer and DTT as a reducing agent. DTT is known to reduce cacodylate and the resulting DMA-3 can form stable adducts with cysteine (Maignan *et al.*, 1998). The modeling of the extra density as DMA-3 is further supported by the fact that the arsenic density peak is larger than the density for the sulfur atom, as expected for a higher atomic number element. Moreover, the center of the extra density is located 2.4 Å from the Cys23 sulfur, too far for a disulfide bond and very similar to sulfur-arsenic bond lengths observed in other structures (Maignan *et al.*, 1998). Finally, two methyl groups expected for DMA-3 are clearly visible in the density **(Figure 3.2c)**. Arsenylation is not complete and the DMA-3 occupancy refined to 0.58.

3.2.4 Redox-state induced structural changes

Comparison of the reduced and oxidized EVM053 structures revealed a dramatic structural rearrangement of Tyr21 near the active site **(Figure 3.3)**. This residue flips around, causing the main-chain C^{α} atom to move by 1.6 and 1.8 Å, while the side-chain
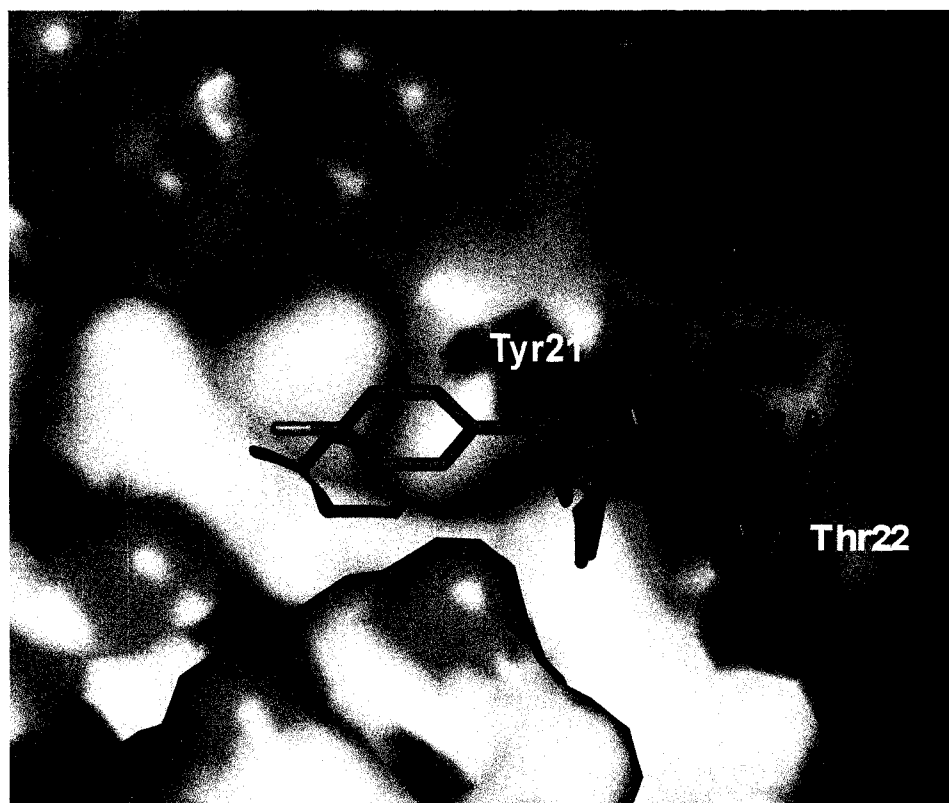
Figure 3.3. Structural changes due to redox state. Side-chain conformations of Tyr21 and Thr22 in the reduced (cyan) and oxidized (green) B chain states are shown. Equivalent structural changes exist in the A chain models. The molecular surface representation of the reduced B chain is shown to demonstrate that Tyr21 is stabilized by interactions with a hydrophobic pocket formed by residues Val19, Ile30 and Ile45. In the oxidized state Tyr21 is exposed to solvent. Oxygen, nitrogen, and carbon atom surfaces are rendered in red, blue, and grey, respectively.

hydroxyl moves 10.7 and 11.2 Å in the A and B chains, respectively. In the reduced conformation, the side-chain of Tyr21 is packed onto a strongly hydrophobic pocket at the surface of the protein formed by residues Val19, Leu30 and Ile45. In contrast, in the oxidized state the tyrosine side-chain is solvent exposed. All orthopox EVM053 orthologs conserve either a tyrosine or phenylalanine at this position, consistent with a functional role for an aromatic residue. This is not the case for mammalian Grx-1, where the equivalent residue is a proline. Reduction of the active site disulfide also triggers a change in Thr22, with the main-chain oxygen moving towards the solvent, while the side-chain swivels around the C^{α}-C^{β} bond to avoid steric hindrance. As a result, Lys20 in the B chain forms a hydrogen bond with the Thr22 side-chain hydroxyl in the reduced state, instead of the hydrogen bond with the main-chain oxygen of Thr22 in the oxidized state **(see right-hand side of Figure 3.4)**. Interestingly, the redox-induced change of Thr22 in EVM053 is also observed when comparing the structures of oxidized pig and reduced human Grx-1.

3.2.5 Structural flexibility in the GSH-binding loop

A comparison of the A and B chains showed structural differences in residues 68-70 that were observed in both the oxidized and reduced states **(left-hand side of Figure 3.4)**. Although these differences appear to be due to crystal packing effects, they suggest structural flexibility of this region, which is of interest since Thr69 and Val70 are highly conserved residues that have been shown to contribute to GSH binding in published Grx-GSH complex structures (Nordstrand *et al.*, 1999; Yang *et al.*, 1998;

71
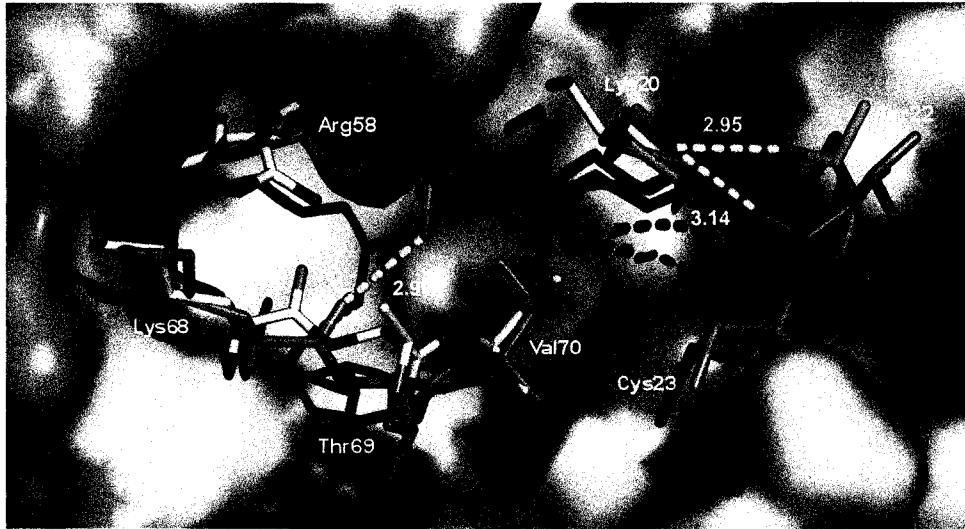
Figure 3.4. Structural changes in the GSH-binding loop and potential structural cross-talk with Thr22. Side-chains demonstrating alternate conformations are shown in yellow (oxidized A), green (oxidized B), and cyan (reduced B). The side-chain of Arg58 adopts a more buried side-chain conformation in chain B that is stabilized by a hydrogen bond to the main-chain carbonyl oxygen of Lys68. The Lys20 side-chain moves closer to the active site in chain B, likely due to electrostatic repulsion by Arg58. Thr22 forms different hydrogen bonds with the B chain conformation of Lys20 depending on the oxidation state. Hydrogen bonds are indicated by yellow dashed lines with atomic distances in angstroms.

Bushweller *et al.*, 1994; Johansson *et al.*, 2007). In the A chain, Thr69 is tilted towards the active site, which would interfere with GSH binding. In chain B, the GSH-binding loop corresponds more closely to that observed for other Grxs, including structures in complex with bound GSH (see below).

The deviating conformation of the residue 68-70 loop in the A chain may be related to the presence of an arginine at position 58, a residue that is strictly conserved as a glutamine in all vertebrate Grx-1 and Grx-2 sequences. Structures of GSH in complex with human Grx-1 (Yang *et al.*, 1998) and human Grx-2 (Johansson *et al.*, 2007) show that the conserved glutamine forms a hydrogen bonding network with the strictly conserved Lys20 (Lys34 in Grx-2), the C-terminal carboxylate of GSH, and the main-chain carbonyl oxygen of residue 68 (Arg79 in Grx-2; see next section). The Arg58 side-chain of EVM053 cannot make an equivalent hydrogen bond with Lys20. In contrast, electrostatic repulsion will drive the two positively charged residues apart. In chain A, this electrostatic repulsion is avoided by a more exposed conformation of Arg58 that places its positive side-chain far from Lys20 (yellow model in **Figure 3.4**). In this conformation, the main-chain carbonyl oxygen of residue 68 is not stabilized by a hydrogen bond, which may affect the position of Thr69. In the oxidized B chain, Arg58 adopts a conformation more similar to that of the conserved glutamine, including the stabilizing hydrogen bond to the main-chain carbonyl oxygen of residue 68 (green model in **Figure 3.4**). In this case the electrostatic repulsion causes an alternate conformation of the Lys20 side-chain, which places its positive charge closer to the active site and within hydrogen bonding distance of Thr22.

3.2.6 Model for the EVM053-SG complex

GSH binding to EVM053 was modeled based on the human Grx-2-GSH crystal structure (Johansson *et al.*, 2007), which shows clear electron density for the bound glutathione with favourable interactions between the GSH γ-glutamyl backbone carboxylate and the N-terminal end of α-helix 4. In the Grx-2-GSH model, the distance between the thiols of the nucleophilic active site cysteine and GSH is 2.83 Å, suggesting that GSH is bound as a non-covalent complex and likely forms a thiol-thiolate hydrogen bond. **Figures 3.5a** and **3.5b** show the experimental Grx-2-GSH complex structure and the EVM053 B chain with a model of bound GSH. To make the EVM053-GSH model, the Grx-2-GSH structure was superimposed onto the reduced EVM053 B chain by optimizing the fit between all main-chain atoms of residues 20 to 26, 68 to 70, and 82 to 84 of EVM053 and the corresponding atoms of Grx-2 (52 atoms matched with an RMSD of 0.38 Å). The program SSBOND was used to create a stereochemically optimal mixed disulfide bond (Hazes and Dijkstra, 1988). Interestingly, four residues that contribute to GSH-binding in Grx-2 (Lys34, Gln69, Thr80 and Thr95) have different conformations in the corresponding residues of the EVM053 A and B chains (Lys20, Arg58, Thr69 and Ser84). There is a steric conflict between the GSH-glycine and Thr69 in the GSH-binding loop of the A chain. A conformational change of this loop towards a more Grx-2-like conformation is needed to accommodate GSH and such a rearrangement is actually observed in the B chain. Residues Lys20 and Ser84 will most likely also adopt Grx-2-like conformations upon GSH binding. We predict that Arg58 will adopt the exposed conformation shown in pink in **Figure 3.5b**. This
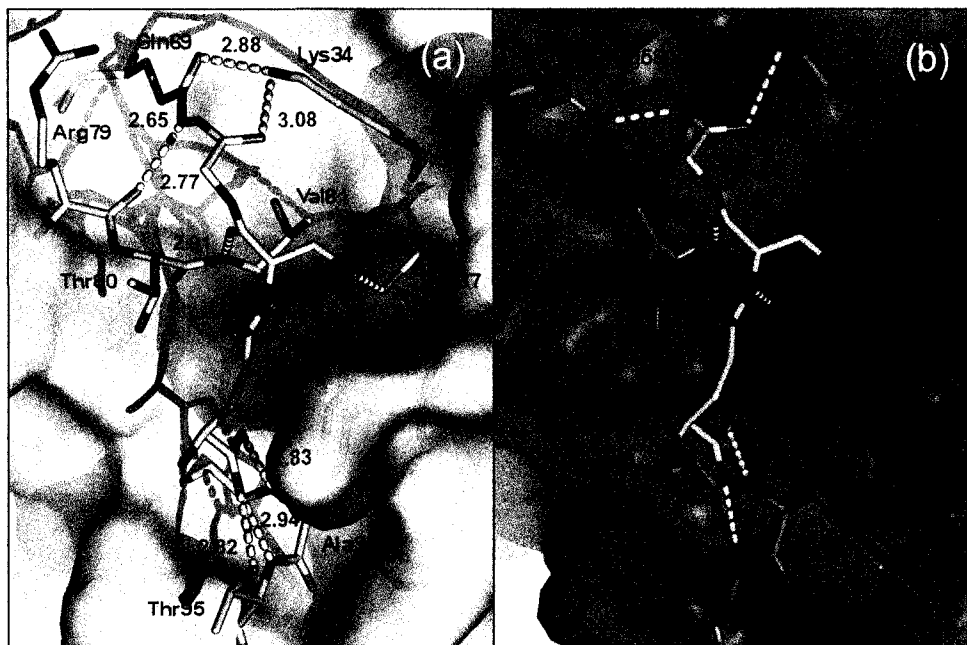
Figure 3.5. GSH binding to Grx-2 and EVM053. GSH is shown in yellow and residues involved in GSH-binding are drawn in stick format. Proposed hydrogen bonds are indicated by dashed lines and atomic distances are given in angstroms. (a) Experimental crystal structure of the Grx-2-GSH complex. The distance of 2.83 Å between the thiols of the nucleophilic active site cysteine and GSH suggests that GSH is bound as a non-covalent complex in this structure. (b) Computer model of the reduced EVM053 B chain (cyan molecular surface representation) with GSH positioned based on the Grx-2-GSH complex structure. This complex was modeled as a covalent mixed-disulfide intermediate, which is indicated by a solid orange bond. Positions of the GSH-binding residues are shown for both the A (pink) and B (cyan) chain conformations. For EVM053 in the GSH-bound state, it is predicted that Thr69 adopts the B chain conformation, while Arg58 and Lys20 adopt the A chain conformation. Although the side-chain terminus of Ser84 is too far to form a hydrogen bond with GSH in either conformation, a small rotation of this side-chain could allow a hydrogen bond once GSH is bound.

conformation can make a salt-bridge interaction with the GSH-glycine carboxylate and avoids an electrostatic conflict with Lys20.

3.2.7 Implications for the binding of R1

The NMR structure of *E. coli* Grx-1 in complex with a peptide representing the C-terminal 25 residues of *E. coli* RNR R1 has been determined (Berardi and Bushweller, 1999). This structure represents the covalent intermediate of disulfide reduction by Grx with a mixed disulfide between Cys11 of the enzyme and Cys759 of the peptide (Cys14 and Cys754 were mutated to serine to obtain a stable complex). Only the C-terminal ten residues of the peptide were well-ordered and electrostatic complementarity between the anionic peptide and cationic peptide-binding groove, including four salt bridges, was proposed to be a major determinant of binding. However, R1 and Grx-1 sequences from mammals and orthopoxviruses do not appear to conserve these salt bridges, with the possible exception of a salt bridge to the C-terminal carboxylate of the peptide. In *E. coli*, the R1 C-terminal residues that follow the reactive cysteine (Lys760-Ile761) extend towards the loop following the second β-strand of Grx-1, and the C-terminal carboxylate makes a salt bridge with Arg39 at the start of the loop **(Figure 3.6a)**. In orthopoxviruses the R1 sequence terminates in a Ser-Gly dipeptide, and Lys49 of EVM053 is structurally equivalent to Arg39 of *E. coli* Grx-1 **(Figure 3.6a-b)**. In the EVM053 structure the side chain of Lys49 is disordered beyond the C^β atom but its position is compatible with a role in R1-peptide binding. Mammalian Grx-1 sequences do not conserve a basic residue that corresponds to Arg39 of *E. coli* Grx-1.
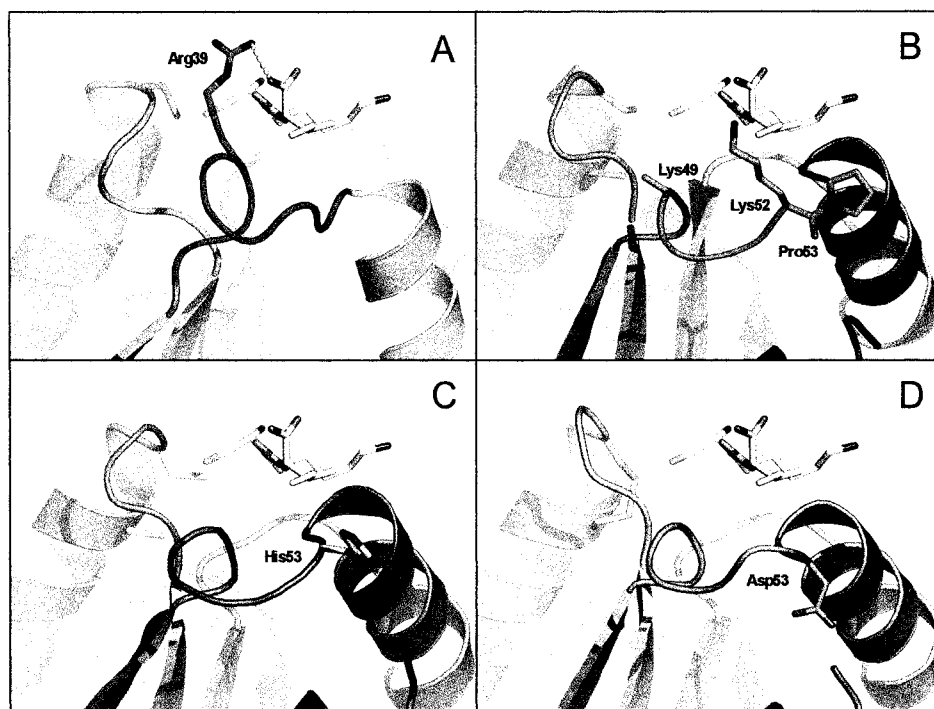
Figure 3.6. Proposed role of the Grx β2-α3 loop in binding of the R1 peptide substrate. Functionally important residues in the β2-α3 loop and the active site cysteines are shown in stick format. (a) Experimental NMR model of *E. coli* Grx-1 in complex with the R1 peptide for which the C-terminal three residues (Cys-Lys-Ile) are shown in yellow. A salt bridge between Arg39 and the C-terminal carboxylate of R1 is demonstrated by a dashed line. Panels (b), (c), and (d) show the EVM053, human Grx-1, and pig Grx-1 structures in the same orientation as the *E. coli* Grx-1 model. The anticipated location for the Cys-Ser-Gly tripeptide of orthopoxviral R1 and the Cys-Gly-Ser tripeptide of mammalian R1 is indicated by the superimposed R1 tripeptide from the *E. coli* Grx-1-mixed disulfide structure. The Lys49 side-chain in EVM053 could not be modeled beyond the $C^β$ position, and only the $C^α$-$C^β$ bond is shown to indicate its location.

Figures 3.6b-d show the loop between β-strand 2 and α-helix 3 in EVM053, human Grx-1 and pig Grx-1, respectively. The predicted location of the R1-peptide is indicated by the Cys-Lys-Ile tripeptide that has been positioned based on the *E. coli* Grx-1-R1 complex structure. Interestingly, this loop is the region where the main-chain conformation of EVM053 deviates most from the human and pig Grx-1 structures. This deviation is due to the *cis*-peptide bond formed by Pro53, which tilts Lys52 more towards the C-terminus of the R1-peptide. Upon R1-peptide binding, Lys52 could adopt a conformation that stabilizes the negative carboxy terminus of the peptide. In human Grx-1, His53 is the only basic residue in the loop region that could form a salt bridge with the R1-peptide carboxy terminus, although it would require some conformational rearrangements. In contrast, pig Grx-1 has no basic residues in the loop and Asp53 is not compatible with a role in R1 peptide binding.

3.3 Discussion

This work demonstrates a high level of structural conservation between EVM053 and the Grx-1 of humans and pig. Based on the sequence and structural similarities, the EVM053 structures can be used to complement the limited available knowledge for the orthologous mammalian enzymes. In particular, these structures represent the first example where high-resolution crystal structures of both the reduced and oxidized states of a Grx have been determined. At the same time, the stable integration of a host enzyme into the orthopoxvirus genome makes it likely that the viral enzyme has acquired virus-specific adaptations. These structural studies aim to increase the

78

understanding of Grxs in general and delineate the features that may be virus-specific adaptations.

3.3.1 Cysteine-activation by thiolate stabilization

Efficient nucleophilic attack by the active site cysteine requires that the thiol is deprotonated to the thiolate state. To facilitate this, thioredoxin-fold enzymes stabilize the thiolate form as evidenced by a depressed pKa value. Stabilization of the thiolate also affects the equilibrium between oxidized and reduced states, with greater stabilization favouring the reduced state and thus increasing the redox potential. Compared to Trxs, Grxs have a lower pKa and, as expected, a higher redox potential. For Grxs, multiple factors are suspected to contribute to thiolate stabilization, including nearby positively charged residues, hydrogen bonding between the thiolate and main-chain amide nitrogen atoms at the start of α-helix 2, hydrogen bonding between the thiolate and the thiol of the second active site cysteine, and influences of the dipole moment of α-helix 2 (Katti *et al.*, 1995; Nordstrand *et al.*, 1999; Eklund *et al.*, 1992; Sun *et al.*, 1998; Foloppe and Nilsson, 2004; Foloppe and Nilsson, 2007).

In the EVM053 structures, positively charged residues in the vicinity of the active site (Lys20, Arg27, Arg58) are not close enough to form effective electrostatic interactions with the thiolate anion. Lys20 could adopt a conformation that brings it in contact with the thiolate and this has been proposed for human Grx-1 based on computational models (Jao *et al.*, 2006). However, when these authors replaced the

lysine by glutamine or leucine there was essentially no effect on the pKa value, which argues against a significant role for Lys20 in lowering the pKa.

The EVM053 structures support the proposed thiolate stabilization by the helix-dipole, hydrogen bonding to the amide nitrogen atoms of Phe25 and Cys26, and the formation of a thiol-thiolate hydrogen bond **(Table 3.1)**. Stabilization by hydrogen bonds has also been supported by molecular dynamics simulations of pig Grx, which demonstrated a direct correlation between the number of hydrogen bonds formed by the active site thiolate and the pKa value for this residue (Foloppe and Nilsson, 2007).

The importance of the thiol-thiolate hydrogen bond regarding Grx catalytic activity and its effects on thiol pKa are less clear. Mutating Cys26 to a serine results in a 194% increase in activity for pig Grx-1 when dehydroascorbate is used as a substrate (Washburn and Wells, 1999) and similar results have been obtained for EVM053 (see section 4.2.3). These results may be explained by the formation of a more polar hydrogen bond interaction between Cys23 and the Ser26 hydroxyl, perhaps resulting in a more nucleophilic thiolate. However, the effects of mutating this residue to a serine have shown contrasting effects on thiol pKa, showing an increase in human pKa by 0.6 units and a decrease in pig pKa Grx by 0.3 units (Jao *et al.*, 2006; Foloppe and Nilsson, 2007). Other experiments have shown that mutating Cys26 to an alanine in the pig Grx resulted in an increase in pKa of 0.9 units and a loss of 91% of its activity, suggesting a hydrogen bond between Cys23 and either Cys26 or Ser26 (mutant) is critical for enzyme activity (Yang and Wells, 1991).

In many cases non-catalytic structural disulfide bonds are stabilized in the oxidized state since they provide stability to protein structures and are reciprocally stabilized by their position in the folded protein (Zapun *et al.*, 1993). Structural disulfides thus often have very negative redox potentials. For example a structural disulfide in human Grx-2 has shown to have a redox potential of -317 mV and remains in the oxidized state in all but the most reducing of conditions (Sagemark *et al.*, 2007a). Conversely, proteins like DsbA, maintain a reversible disulfide that is stabilized in the reduced conformation and has been shown to be 10^3 to 10^4 times more reactive than structural disulfides (Zapun *et al.*, 1993). DsbA demonstrates the highest redox potential and is the strongest oxidizing agent of all known thioredoxin-fold proteins (Wunderlich and Glockshuber, 1993). These proteins conserve a CPHC active site motif and also demonstrate a low pKa of the active site cysteine of 3.2-3.5 (Nelson and Creighton, 1994). Crystal structures of DsbA have been solved in the reduced and oxidized conformation and demonstrated that the reduced conformation is stabilized by hydrogen bonds with the main chain amides of the histidine and cysteine residues, as well as a thiol-thiolate hydrogen bond (Guddat *et al.*, 1998). In addition, the thiolate forms a salt bridge with the side chain of the histidine residue in the active site loop, providing more stabilization to the reduced form. The oxidizing eukaryotic PDI similarly conserves a histidine at this position (CGHC active site motif), also accounting for the higher redox potential and oxidizing nature of this protein.

Thioredoxins are the most reducing of thioredoxin-fold proteins and conserve the active site motif CGPC. Thioredoxin fold proteins form thiol-thiolate bonds in some but not all crystal structures (Guddat *et al.*, 1998), but more importantly, the presence of a

proline before the second cysteine does not allow for a hydrogen bond with the main chain amide for this residue. Thus, although Grx, Trx, DsbA and PDI conserve similar active site structures, differences in function due to varying redox potentials can be explained almost entirely by the relative ability of the N-terminal active site cysteine to form hydrogen bonds.

The observation of dual side chain conformations for Cys23 in chain A of reduced EVM053 is in all probability an artefact of the crystal-mounting conditions. The crystals were grown in mother liquor with a pH of 5.2 but to obtain the reduced structure 50 mM of GSH in its free acid form was added. Subsequent measurements show that this reduces the pH to 3.6, which is close to the pKa value for other Grxs. Accordingly, Cys23 may have been partially protonated such that the short sulfur-sulfur conformation represents a thiol-thiolate hydrogen bond and the other conformation represents a non-physiological thiol form of Cys23. It seems plausible that crystal packing interactions, in particular Asp93 and the negative helix dipole moment of α-helix 4 in a neighbouring monomer, make Cys23 in the A chain more sensitive to protonation by raising the pKa of this residue. This could also explain the preferential arsenylation of Cys23 in the B chain (see chapter 5).

3.3.2 GSH binding to glutaredoxin

Oxidized Grx reacts with GSH to form a Grx-SG mixed disulfide, and reduced Grx forms the same mixed disulfide when it reacts with GSSG or a variety of glutathione mixed disulfides (RSSG), including glutathionylated proteins. Specificity

for glutathione-containing substrates has been demonstrated in several studies and K_m

values for RSSG substrates in the low micromolar to low millimolar range have been

reported (Gravina and Mieyal, 1993; Srinivasan *et al.*, 1997; Rabenstein and Millis,

1995; Johansson *et al.*, 2004).

Three published NMR structures and a crystallographic structure have addressed

the structural basis for GSH binding to human Grx-1, *E. coli* Grx-1, *E. coli* Grx-3 and

human Grx-2 (Yang *et al.*, 1998; Bushweller *et al.*, 1994; Nordstrand *et al.*, 1999;

Johansson *et al.*, 2007). In the human Grx-2-GSH complex crystal structure, the GSH-

cysteine binding mode is very similar to that of the *E. coli* Grx-3 complex, but the γ-

glutamyl moiety adopts a different conformation that results in highly favourable

interactions between the γ-glutamyl carboxylate and the dipole of α-helix 4. Hydrogen

bonds are formed with two main-chain nitrogens at the start of that helix (residues 94

and 95) and the side chain hydroxyl of Thr95 **(Figure 3.5a)**. In EVM053 and all

orthopoxviral orthologs Ser84 is structurally and functionally equivalent to Thr95 of

human Grx-2. Accordingly, the EVM053-SG mixed disulfide model was built based on

the human Grx-2-GSH complex structure.

Thiol-disulfide interchange reactions involve an S_N2 transition state, which

favours an in-line attack of the sulfur-sulfur bond by a thiolate nucleophile (Whitesides

et al., 1983). In agreement, the thiols of Cys26, Cys23, and GSH are approximately co-

linear (152°). To make GSH a better nucleophile, one would further expect Grx to

stabilize the thiolate form of GSH. This is the case for glutathione S-transferases where

interactions with serine, tyrosine, or arginine residues lower the pKa of bound GSH

(Armstrong, 1997). For Grxs, the highly conserved Lys20 (Arg8 in *E. coli* Grx-1) could

in principle stabilize a GSH-thiolate anion but in Grx-SG complex structures this lysine forms a salt bridge with the GSH-glycine carboxylate. Although Lys20 may play an important role in stabilizing interactions with small molecule substrates such as DHA, the binding to the GSH-glycine carboxylate places the lysine side chain far from the active site when GSH is bound. However, the GSH sulfur is approximately in-line with the axis of α-helix 2 and the helix dipole may thus assist thiolate formation. γ-Glutamylcysteine is a much better substrate for Grx than cysteinylglycine, which agrees with the observation that the γ-glutamyl moiety makes more extensive interactions with the protein than the glycine moiety (Srinivasan *et al.*, 1997; Rabenstein and Millis, 1995). However, Grx still favours GSH over γ-glutamylcysteine, indicating that the glycine residue does contribute to activity (Gravina and Mieyal, 1993). This may be due to enhanced affinity through the salt-bridges formed between Grx and the GSH-glycine carboxylate or due to destabilization of the thiolate form of γ-glutamylcysteine resulting from the closer proximity of the negatively charged terminal carboxylate to the GSH sulfur atom.

The two EVM053 monomers show different conformations of the GSH-binding loop. The A chain conformation precludes GSH binding due to steric hindrance by Thr69. In the B chain, Thr69 has moved partially towards the position observed in the human Grx-2-GSH complex structure. At this moment it is not clear if the GSH-loop conformation in the A chain represents a functionally relevant conformation. This deserves further research because the Lys20 and Arg58 residues can potentially couple the oxidation state of the active site, as sensed by the Lys20 and Thr22 interaction, to

occupation of the GSH-binding site, as sensed by the Arg58 interaction with the main-chain carbonyl oxygen of residue 68 (**Figure 3.4**).

3.3.3 Ribonucleotide reductase binding to EVM053

Glutaredoxins from both mammals and *E. coli* have varying abilities to act as cofactors of RNR (Nordstrand *et al.*, 1999; Lycksell *et al.*, 1994). For example, Grx-3 of *E. coli* shows only 5% activity as a reductant of RNR compared to Grx-1 (Berardi and Bushweller, 1999). For mammals, Grx-1 from human and calf can support RNR activity, whereas the closely related enzymes from pig and rabbit can not (Hopper *et al.*, 1989; Padilla *et al.*, 1995). To explain the different R1 specificity of human and calf Grx-1 compared to the pig and rabbit enzyme I looked for residues in the peptide-binding groove that are not conserved between these species. The only sequence difference that correlates with specificity is in the $\alpha2$-$\beta3$ loop where pig and rabbit have an aspartate at position 53, compared to asparagine and histidine for bovine and human Grx-1, respectively. In the *E. coli* Grx-1-R1 complex structure this loop adopts a different conformation than in the native enzyme, which allows residue Arg39 to make a salt bridge with the C-terminal carboxylate of the peptide (Berardi and Bushweller, 1999). His53 in human Grx-1 could make a similar favourable electrostatic interaction, whereas Asn53 in bovine Grx-1 could stabilize the C-terminus by hydrogen bonding. In contrast, Asp53 in pig and rabbit Grx-1 cannot interact favourably with the C-terminal carboxylate of the peptide (**Figure 3.6**).

The orthopoxvirus Grx-1 sequences have acquired two basic residues in this loop that are not found in mammalian Grx-1 and that may stabilize R1 peptide binding. Lys49 is structurally equivalent to Arg39 of *E. coli* Grx-1. The second basic residue, Lys52, does not correspond to a basic residue in other Grxs but it is again close enough to form a salt-bridge with the R1 peptide C-terminus. The observation that Pro53 adopts the less common *cis*-proline conformation in EVM053 is likely also relevant for function because the *cis*-peptide bond tilts Lys52 towards the R1 peptide. Mutagenesis studies of Pro53 were thus needed to confirm a role in peptide binding for this residue (see section 4.2.4).

In the *E. Coli* R1-Grx-1 mixed disulfide, Tyr13 and Tyr72 were determined to be in close proximity to the N-terminal Cys of the peptide (mutated to a Ser in the structure) (Berardi and Bushweller, 1999). The structurally analogous position of Tyr13 in EVM053 is Phe25, and the residue maintains very similar spatial orientation. Tyr83 in EVM053 and Tyr72 of *E. coli* Grx-1 are also in very similar spatial orientations. The N-terminal Cys of R1 could potentially be "sandwiched" between Tyr83 and Phe25 and thus prevent the back-reaction (reoxidation of the peptide substrate). Interestingly, the analogous residue of Tyr83 is a Cys in pig and human Grx-1 as well as *E. coli* Grx-3, and this residue has been proposed to play a regulatory role in these enzymes (Nordstrand *et al.*, 1999). The conservation of a tyrosine residue at this location in EVM053 and *E. coli* Grx-1 and a Cys in mammalian and *E. coli* Grx-3, and the close proximity to the conserved Y/F of the CPY/FC motif, suggests this residue may form important interactions involved in peptide substrate binding, regulation or catalysis.

3.3.4 Redox-correlated conformational changes

The natural Grx catalytic cycle has three clear structural states of the active site; fully oxidized, glutathione mixed disulfide, and fully reduced. Comparison of oxidized and reduced T4 bacteriophage Grx showed increased flexibility in the active site loop for the latter, but no clear conformational changes (Wang *et al.*, 2004). For human and *E. coli* Grx-1, comparison of structures for the GSH mixed disulfide complex and the reduced state also did not show significant differences beyond changes in the active site itself. In contrast, the high-resolution NMR structures for the oxidized and GSH mixed disulfide states of *E. coli* Grx-3, showed a shift in the position of α-helix 1 and a concerted movement in the side chain rotamers of Tyr13 and Asp66 (Nordstrand *et al.*, 2000). This change moves Tyr13 from a highly solvent-exposed conformation in the oxidized state to a more buried conformation in the glutathionylated complex. The authors argue that the partially buried position of Tyr13 would specifically stabilize the mixed disulfide state and thus increase substrate affinity. A comparison between oxidized and reduced EVM053 structures demonstrated a large conformational change of another tyrosine, Tyr21 **(Figure 3.3)**, that is close to the active site and could also potentially play a role in stabilizing interactions with GSH (see section 4.2.3).

The structural rearrangement of Tyr21, which moves the aromatic side chain from a fully solvent–exposed conformation in the oxidized state, to a hydrophobic pocket in the reduced state, could also be expected to raise the redox potential of EVM053, by stabilizing the reduced form of the enzyme, and may also significantly affect the function of this enzyme (see next section).

Another, and not necessarily mutually exclusive hypothesis, is that the oxidation-state dependent conformation of Tyr21 signals the redox state of the enzyme. For instance, in the reduced state the conformation of Tyr21 may facilitate interaction between EVM053 and substrates that need to be reduced. Similar redox state-dependent binding has been described for *E. coli* Trx, for which only the reduced state binds to T7 bacteriophage polymerase (Doublie *et al.*, 1998). Although Tyr21 appears to be too far from the substrate binding groove to directly interact with the R1 C-terminal peptide or GSH, it remains a distinct possibility that this residue, and the strongly hydrophobic pocket that becomes exposed upon oxidation, may be required for interactions with other potential binding partners.

3.3.5 Redox stress during poxvirus genome replication

The Tyr21 conformational change mentioned above could be an adaptation to raise the redox potential of EVM053. This may be directly relevant for poxviruses because they replicate their genomes in small membrane-encapsidated vesicles referred to as virosomes (Schramm and Locker, 2005). To create thousands of genome copies, each ~200,000 bp long, in the period of about a day requires a high rate of dNTP production. The rate-limiting step in dNTP production is the reduction of NDP to dNDP by RNR in a process that consumes two GSH and produces one GSSG for each dNDP produced (Elledge *et al.*, 1992). Interestingly, RNR has been reported to be recruited to virosomes where its high activity could be expected to raise the local GSSG/GSH ratio (Davis, 1992). In a more oxidizing environment a higher redox potential for the viral

Grx might be needed to catalyze glutathionylation of protein thiols to ensure that proteins within the virosome are not irreversibly oxidized, and this will be discussed more thoroughly in chapter 4. A related adaptation may be the loss of three non-catalytic cysteine residues that are conserved in most mammalian Grx-1 enzymes (Cys8, Cys79, and Cys83 in human Grx-1), which have been proposed to play a redox-sensitive regulatory role (Sun *et al.*, 1998). Cys8 and Cys79 are surface exposed and oxidation of Cys8 has been shown to decrease the lifetime of human Grx-1 due to disulfide-linked aggregate formation (Padilla *et al.*, 1996). Cys83 is located in the substrate-binding groove at the N-terminal end of α-helix 4 where chemical modification of its thiol is likely to block access to the substrate-binding groove. In addition, the helix dipole can reduce the pKa of Cys83 making it more sensitive to oxidation by reactive oxygen species or glutathionylation (Sun *et al.*, 1998). Mutation of the cysteines could thus be a poxviral adaptation to avoid inhibition in an oxidizing environment. This model predicts that all poxviruses will experience redox stress during genome replication, yet only the orthopoxviruses express a Grx-1 ortholog. Although it is possible that other poxviruses have evolved alternative adaptations, it is tempting to speculate that the Grx-1 ortholog is needed by orthopoxviruses because they have the highest known rate of genome replication (Balassu and Robinson, 1987).

3.3.6 Summary of glutaredoxin structural analysis

The high-resolution crystal structures of oxidized and reduced EVM053 show close resemblance to Grx-1 structures from human and pig in both tertiary structure and

active site geometry. However, there are discrete differences that may reflect evolutionary adaptations to the viral life cycle. Most importantly, a redox-correlated structural change in the loop preceding the active site that greatly affects the conformation and solvent accessibility of Tyr21 was observed. This change is not seen in a comparison of reduced human Grx-1 with oxidized pig Grx-1. Moreover, all orthopoxviruses conserve an aromatic residue at this position, whereas mammalian Grx-1 orthologs conserve a proline. This suggests the rearrangement of Tyr21 is a virus-specific adaptation, possibly affecting substrate specificity or redox potential. In contrast, the redox-correlated conformational change of Thr22 is observed for both orthopoxviral and mammalian Grx-1. Since Thr22 can form hydrogen bonds with the side-chain of the highly conserved Lys20, the redox-induced conformational change may play a mechanistic role in catalysis by both the poxviral and mammalian enzymes. A second orthopox-specific feature is the conservation of a proline at position 53. In EVM053 this proline adopts an energetically strained *cis*-peptide conformation, which changes the conformation of the loop following the second β-strand. In *E. coli* Grx-1 this loop interacts with the bound C-terminal peptide of the RNR-R1 subunit. It was proposed that this loop is also important for RNR reduction by mammalian and orthopoxviral Grx-1. As a third viral adaptation, the replacement of three non-catalytic cysteine residues that are conserved in many mammalian Grx-1 sequences could prevent enzyme inhibition in oxidizing environments. Both the Tyr21 conformational change and the cysteine replacements may be adaptations to an oxidative environment in virosomes that results from high RNR activity.

CHAPTER IV

POXVIRAL GLUTAREDOXIN FUNCTION

4.1 Introduction

The EVM053 structural analyses generated several new structure-based hypotheses regarding poxviral specific adaptations of this enzyme. Perhaps the two most interesting structural features discovered from these analyses were the redox-correlated structural change of Tyr21 and the observation of a second *cis*-proline (Pro53) residue in the loop region required for interactions with the RNR R1 C-terminus. However, while the crystallographic evidence for the structural shifts of Tyr21 was strong, it was not completely clear if the shift of Tyr21 was an artefact of crystallization or if this would also occur in solution. Similarly, the significance of the *cis*-pro 53 residue would have to be further analyzed through mutagenesis and enzyme kinetic studies to determine what impact this residue has on potential interactions with peptide substrates. Thus, in order to follow up on and more thoroughly evaluate the structural findings, functional analyses of both wild type and EVM053 mutants were performed in order to further assess the potential biological significance of these findings.

Several EVM053 mutants were constructed, expressed and purified. These included two different point mutations of the Tyr21 residue to alanine and tryptophan (Y21A, Y21W) and mutation of the *cis*-Pro53 to an alanine (P53A). Mutation of the active site cysteine (Cys26), to a serine (C26S), was also performed in order to determine the effects of this mutation on catalytic activity in the presence of various substrates. Although this residue is not required for many Grx catalyzed reactions, its presence or absence has shown to dramatically effect rates of catalytic activity and

mutation of this residue can provide information about catalytic mechanisms.

The mutants demonstrated similar expression and solubility characteristics as wild type EVM053, and all of the mutants were shown to be active, indicating that none of the residues mutated were required for activity (see below). The results of the functional characterization of wild type and mutant EVM053 enzymes are presented in the following sections.

4.2 Results & Discussion

4.2.1 Redox correlated rearrangement of Tyr21

The structural analysis of EVM053 in the reduced and oxidized conformations demonstrated a redox-correlated rearrangement of Tyr21. However, since the pH in the reduced crystallographic structure was much more acidic than in the oxidized structure (3.6 compared to 5.2), it was not completely clear if this structural rearrangement may be due to a change in pH, rather than redox status. Thus, further evidence was required to determine whether this structural rearrangement occurs in a more biologically relevant environment.

Tyrosine residues emit only weak fluorescence signals, but conversely, tryptophan residues have a wavelength absorption maximum at 280 nm and an emission peak at 338 nm that is strongly influenced by the polarity of the local environment (Vivian and Callis, 2001). The fluorescence emission is expected to be more intense if the residue is in a hydrophobic environment than a hydrophilic environment. Although Tyr and Trp residues demonstrate very different fluorescence emission properties, the

two residues are similar in that they are bulky aromatic residues that have been shown to undergo structural rearrangements to modulate protein function and these residues, along with phenylalanine, are sometimes mechanistically utilized for this function (Holmgren, 1972; Krauth-Siegel *et al.*,1998; Vivian and Callis, 2001). The relative hydrophobicity of these residues differs with tryptophan being the most and tyrosine the least hydrophobic.

It was hypothesized that in the reduced conformation fluorescence emission of a Y21W mutant would be more intense, since the residue would reside in a hydrophobic pocket, than in the oxidized conformation where it is fully exposed to the aqueous environment. To test this, the Y21W mutant was incubated with known reducing (TCEP, DTT) and oxidizing agents (GSSG, DHA) and fluorescence emission was measured over a 315-400 nm wavelength scan **(Figure 4.1)**. From these analyses it is clear that the reduction of Y21W results in an increased fluorescence emission at the expected wavelength. The results demonstrate that the change in conformation is not dependent on the intrinsic nature of the redox agents since the results were almost identical for either of the two reducing or oxidizing agents. More importantly, these results strongly support the structural findings and demonstrate that the redox induced conformational change of this residue happens in solution at pH 7.0, and is therefore likely to occur *in vivo*.

4.2.2 Glutaredoxin tryptophan fluorescence based activity assay

The two most commonly used activity assays to monitor Grx activity are the NADPH-coupled assay and the DHA reductase assay **(Figure 4.2)**. While, the NADPH-
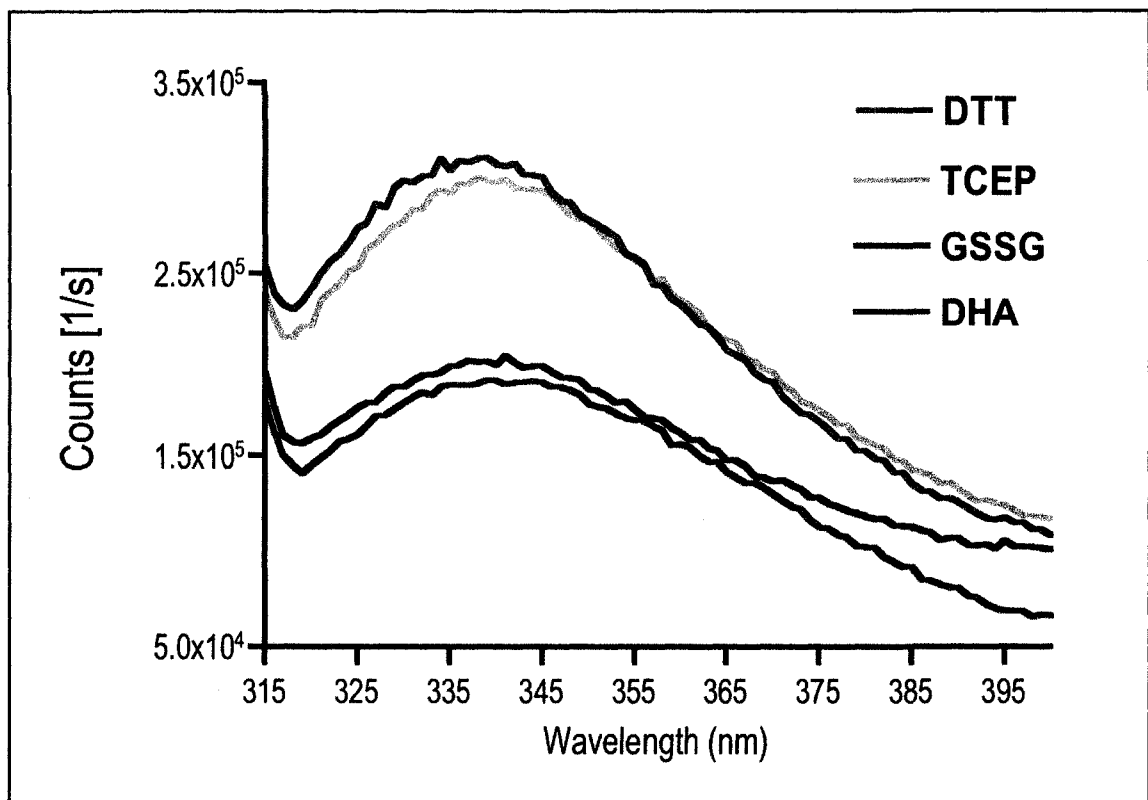
Figure 4.1. Fluorescence analysis of the Y21W mutant incubated in the presence of reducing (DTT, TCEP) or oxidizing reagents (GSSG, DHA), demonstrates a significant change in fluorescence emission at or near 338nm.

a)
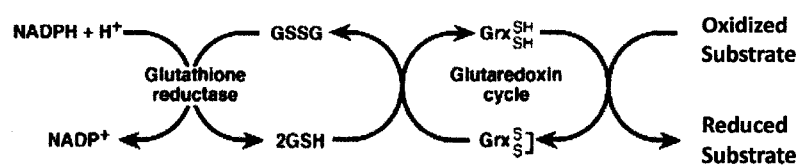
b)
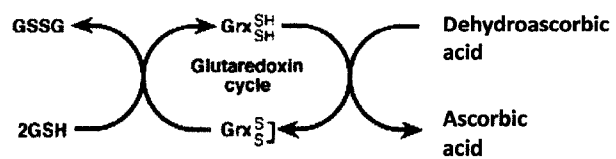
Figure 4.2. General reaction schemes for (a) NADPH-coupled and (b) DHA reductase activity assays. For clarity only the dithiol mechanism of reduction is shown.

coupled assay indirectly monitors Grx activity through the reduction of NADPH to NADP and subsequent decrease in absorbance at 340 nm, the DHA reductase assay directly monitors the reduction of DHA and concomitant production of ascorbic acid through an increase of absorbance at 265nm. The NADPH-based assay is commonly used to analyze Grx kinetics since it can be used for many oxidized Grx substrates. An important exception is GSSG which cannot be present in the reaction as it will be rapidly reduced by GSH-reductase. In addition, enzyme inhibition studies are complicated by the presence of GSH-reductase, since it is not clear whether potential inhibitors target Grx or the GSH-reductase. For the DHA reductase assay, the rate of Grx activity is directly coupled to product formation and does not require the presence of a second enzyme. However, this assay also has its limitations, the most evident being that since the change in absorbance intensity is directly dependent on the redox status of the substrate, only DHA can be used as a substrate in these reactions.

The fluorescence signal of Y21W provides the means for an alternate assay that directly detects the formation of the Grx intramolecular disulfide bond. Like the NADPH-coupled assay, this property can be used with any oxidized substrate including GSSG. The mutant enzyme preparation was preincubated with TCEP and then buffer exchanged into a buffer without any redox agents present. The enzyme was then measured for fluorescence intensity emission following the addition of substrates. **Figure 4.3** shows the results of these assays using either 1 μM DHA or 10 μM DMA-5 (the implications of DMA-5 as a substrate for Grx will be discussed thoroughly in chapter 5) as substrates in the presence of 0.45 μM reduced Y21W protein preparation. Fluorescence was measured using an excitation wavelength of 274 nm and an emission

DHA

DMAV
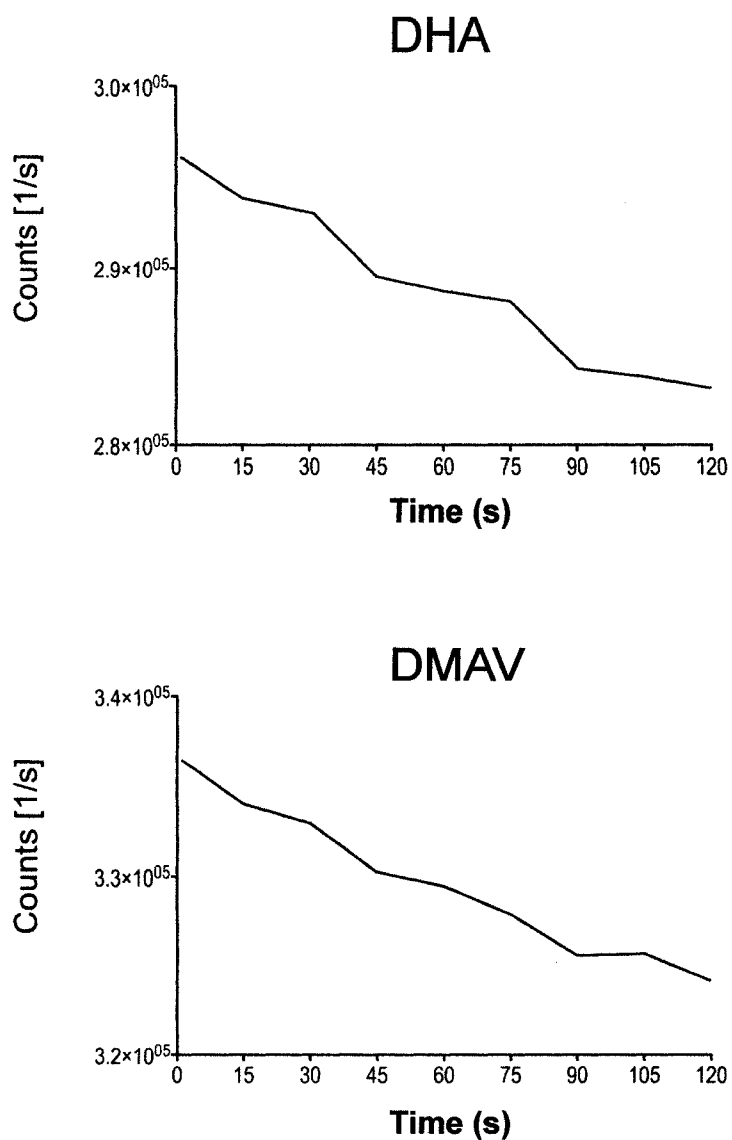
Figure 4.3. Tryptophan fluorescence based Grx activity assay. The Y21W mutant was pre-incubated with TCEP for 1 hour. The TCEP was removed by buffer exchange and the sample was then monitored for fluorescence emission following the addition of DHA or DMAV. The decrease in absorption demonstrates the reduction of either substrates by Grx can proceed through a dithiol mechanism and does not require the presence of GSH.

of 338 nm at 15 second intervals over 2 min. The results show that measurements of fluorescence change over time can be used to detect Grx activity by directly monitoring enzyme oxidation.

The fluorescence-based assay differs from both the NADPH-coupled and DHA assay in that enzyme turnover is not required for the determination of enzyme activity, since the assay directly measures the conversion of the enzyme from the reduced to oxidized state. This has many implications for the determination of Grx enzymatic mechanisms. For example, the assay can be used to directly measure whether the reaction may proceed through a dithiol mechanism since only the dithiol mechanism is possible using this assay. Furthermore, in both the DHA reductase and NADPH-coupled assay the presence of other reducing agents, generally GSH, are required for the reaction assay, whereas for the tryptophan-based assay GSH is not present, and thus the assay can be used to determine whether GSH is required for the reaction. In addition, the assay may also be used to test whether Grx can oxidize substrates.

The tryptophan fluorescence based assay thus demonstrated that the reduction of DHA by Y21W can proceed through a dithiol mechanism and does not require the presence of GSH, which also supports earlier findings for pig Grx-1 catalyzed DHA reduction (Washburn and Wells, 1999). Although the fluorescence based method is not likely to be applicable to Grxs in general, as it depends on the redox-correlated rearrangement of the tryptophan residue, the Y21W EVM053 mutant provides an interesting tool that may be exploited in future studies.

4.2.3 Functional role of Tyrosine21

The redox potential of enzymes depends on the relative stability of their oxidized and reduced states. Redox enzymes that are stabilized in the reduced state tend to be better oxidizing agents whereas the reverse is true for enzymes that have greater stability in the oxidized state (Guddat *et al.*, 1998). However, for an enzyme such as EVM053, the proposed greater stabilization of the reduced form could potentially be used as a mechanism to ensure that, in a more oxidizing environment, the active site will remain in the reduced state, and thus maintain a function as a reducing agent. Conversely, under oxidizing conditions the function of EVM053 may itself become that of an oxidizing agent either through the catalysis of disulfide bond formation of protein thiols or, more likely, through glutathionylation of protein thiols. The oxidation of protein thiols may be used as a mechanism to protect protein thiols from becoming irreversibly oxidized.

To test the role of Tyr21 in catalysis and its affect on sensitivity to the GSH:GSSG redox couple, the Y21W, Y21A, C26S mutants, as well as the wild type EVM053 and human Grx-1 enzymes, were tested for their abilities to reduce DHA with various ratios of GSH:GSSG present. While it was expected that the Y21W mutant would be more greatly stabilized in the reduced conformation, the removal of the aromatic side chain in the Y21A mutant was constructed in order to remove the proposed stabilizing effects of the hydrophobic side chain. The results are presented in **(Figure 4.4)**. The rate of DHA reduction in the presence of 1mM GSH demonstrates the ability of the enzymes to reduce this compound is in the order Y21A>C26S>EVM053>Human Grx-1>Y21W, with Y21A being the most effective reducing agent. The C26S mutant demonstrated a two-fold faster rate of
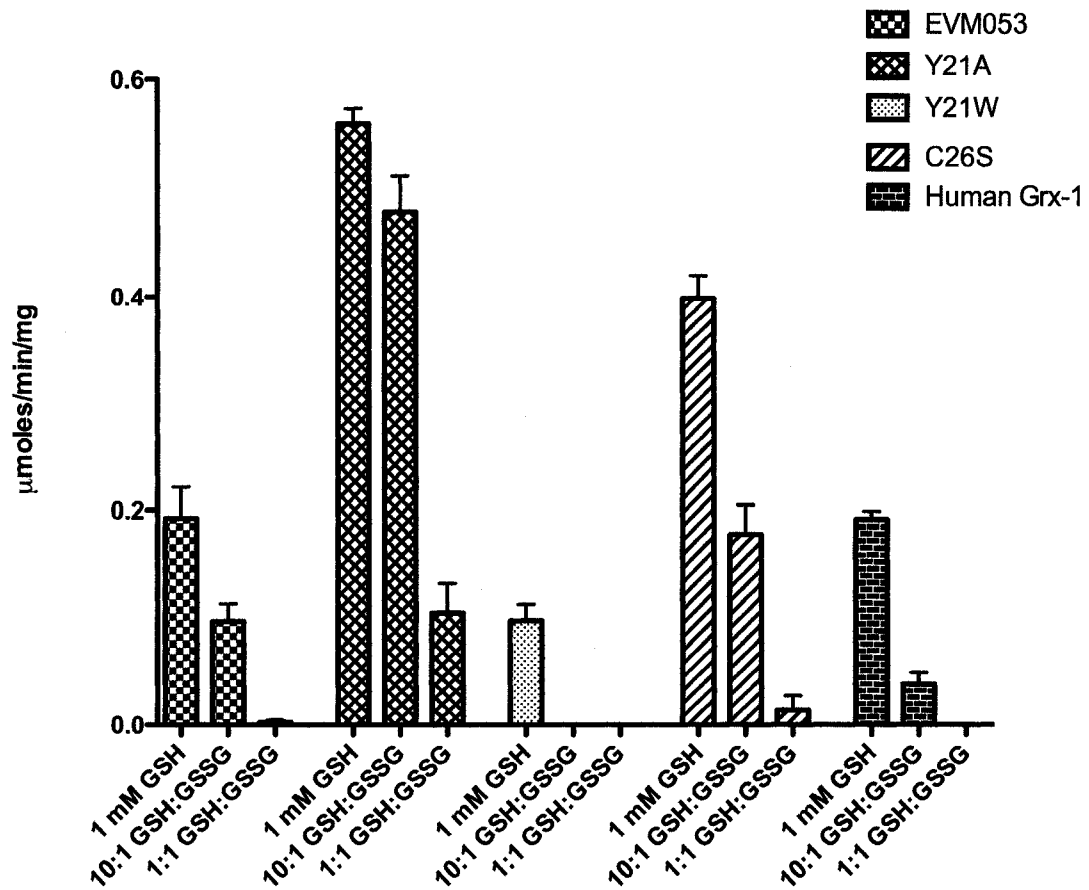
Figure 4.4. Rate of Grx catalyzed DHA reduction in the presence of 1mM GSH, 1 mM GSH and 0.1 mM GSSG or 1mM GSH and 1 mM GSSG. A 100 µl reaction mixture contained 2 mM DHA and appropriate dilutions of EVM053, human Grx-1 or EVM053 point mutant enzymes. These reactions were monitored for 2 minutes at 265nm, starting 30 seconds after the addition of DHA. Reaction rates were corrected for the spontaneous rate in the absence of enzyme.

average activity (206%) than wt EVM053, and similar results were obtained previously

for pig Grx-1 Y21A>C26S>EVM053≈Human Grx-1>Y21W, with Y21A being the most

effective reducing agent. The C26S mutant demonstrated a two-fold faster rate of

average activity (206%) than wt EVM053, and similar results were obtained previously

for pig Grx-1 (Washburn and Wells, 1999). The faster rate of DHA reduction for C26S

may be due to a more polar hydrogen bond interaction between Cys23 and the Ser26

hydroxyl (see section 3.3.1). Alternatively, the faster reaction rate for C26S may be

simply due to the fact that two GSH molecules are required to reduce the intramolecular

disulfide bond, while only one molecule is required to reduce the mixed disulfide, and

thus an additional step is required for the dithiol mechanism **(Figure 4.5)**. The rate of

activity for human Grx-1 in the presence of 1 mM GSH was very similar to that of

EVM053 **(Figure 4.4)**.

When the enzymes were pre-incubated for 10 minutes with a GSH:GSSG ratio

of 10:1 (1mM GSH, 0.1 mM GSSG) prior to the addition of DHA, the Y21A mutant

also showed the strongest relative activity with an average of 86% of the activity

compared to when no GSSG was present. The Y21W mutant did not demonstrate any

measurable activity under these conditions. The EVM053, C26S and human Grx-1

enzymes demonstrated only 51, 45 and 20% activity, respectively, compared to the same

enzyme with no GSSG present. The higher activity of EVM053 and C26S than human

Grx-1 may be due to the presence of several non-catalytic cysteines in human Grx-1 that

have been proposed to play a regulatory role (Sagemark et al., 2007) and are not present

in poxviral Grx-1. When the enzymes were pre-incubated with a 1:1 ratio of GSH:GSSG

(1 mM GSH, 1 mM GSSG) the Y21A mutant demonstrated an average 19% activity
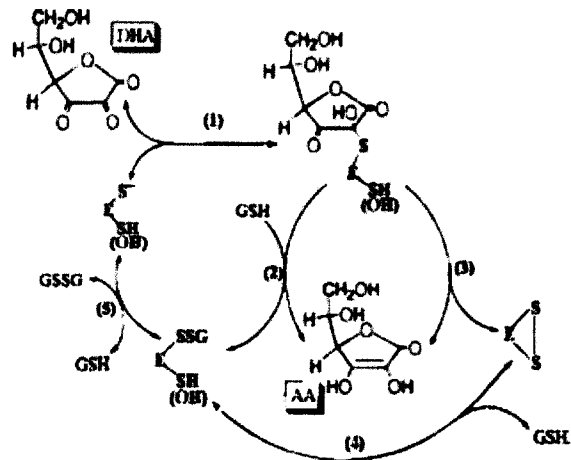
Figure 4.5. Proposed mechanism of Grx catalyzed DHA reduction. 1) Nucleophilic attack of Cys23 on DHA; 2) GSH provides second reducing equivalent in monothiol mechanism; 3) Cys26 provides second reducing equivalent in dithiol mechanism; 4) Intramolecular disulfide bond is broken by GSH; 5) Grx-SG mixed disulfide is reduced by GSH. Figure adapted from Washburn & Wells, 1999.

102

compared to conditions without GSSG present, while the other enzymes showed little to no activity.

These results indicate that the mutation of Tyr21 strongly affects EVM053 catalysis. In order to consider possible explanations for these results, one must first consider how Grx in a redox buffer composed of GSH:GSSG will adopt either a reduced, oxidized or mixed disulfide state. The accumulation of any of these three states is intrinsically dependent on enzyme redox potential and the ratio of GSH:GSSG present. EVM053 showed much less activity in the presence of a 10:1 ratio of GSH:GSSG than the Y21A mutant and Y21W was inactive as a DHA reductase in this redox buffer. Thus, for the Y21A mutant, it appears a relatively higher amount of the reduced form of the enzyme accumulates since it results in the highest rate of DHA reduction in the presence of GSSG. Accordingly, only the Y21A mutant demonstrated significant activity at an equimolar ratio of GSH:GSSG **(Figure 4.4)**.

Another possible effect of the mutations on catalytic activity could involve alterations in the active site. While Tyr21 of EVM053 is not positioned close enough for direct interactions with GSH or GSSG, the movement may place the active site cysteine in the optimal orientation for interactions with this molecule. Thiol-disulfide interchange reactions involve an S_N2 transition state, which favours an in-line attack of the sulfur-sulfur bond by a thiolate nucleophile (Bach *et al.*, 2008). In the modeled glutathionylated EVM053 structure, the thiols of Cys26, Cys23, and GSH demonstrate an angle of 152°. The Y21A and Y21W mutations may effect the positioning of Cys23 in such a way that this angle becomes more linear in the case of Y21A (i.e. greater than 152°) and less linear in the case of Y21W (i.e. less than 152°). This could explain the

faster rate of DHA reduction observed for Y21A compared to the Y21W and EVM053 enzymes, even when no GSSG is present.

The lower rate of activity of Y21W and EVM053 than Y21A could in theory also be due to a greater accumulation of the intramolecular disulfide bond. If the formation of an intramolecular disulfide bond led to the lower rate of activity, then EVM053 would be expected to show less relative activity than the C26S mutant in the presence of GSSG, since the latter can not form an intramolecular disulfide bond. However, the formation of the intramolecular disulfide bond does not appear to be strongly dependent on the ratio of GSH:GSSG since similar rates of activity were observed for C26S and EVM053 in the presence of a 10:1 ratio of GSH:GSSG (45 and 51% and activity, respectively, compared to the same enzyme with 1 mM GSH present). Instead the movement of Tyr21 may drive a relatively higher rate of formation of Grx-GSH mixed disulfides in the presence of GSSG, but not the intramolecular disulfide. This is perhaps not surprising since the structural analysis suggested that in the oxidized structure, Tyr21 is thermodynamically the least stable. The presence of Tyr21 and its dramatic response to redox environments may thus have evolved to enhance active site glutathionylation.

While the initial structural analysis suggested that the structural change of Tyr21 enhanced the stabilization of the reduced form over the oxidized form of the protein, from this kinetic analysis it appears the movement of this residue also enhances the formation of Grx-SG mixed disulfides, as seen from the lower relative DHA reductase activity of Y21W and EVM053 compared to Y21A in the presence of GSSG. The proposed stronger propensity of poxviral Grx to form mixed disulfides may have evolved to enhance the ability of this enzyme to catalyze reversible glutathionylation

reactions. Similar results have been obtained for *E. coli* Grx-3, which also demonstrates a shift of a tyrosine residue to a more stable conformation when glutathionylated, and stronger activity as a deglutathionylating agent than *E. coli* Grx-1 and other Grxs (Nordstrand *et al.*, 1999).

Although Grx is normally characterized as a reducing agent, human Grx-2 has been shown to catalyze both disulfide bond formation and glutathionylation of mitochondrial membrane proteins (Beer *et al.*, 2004). Furthermore, *E. coli* Grx-1 has also been shown to have significant oxidase activity in the presence of GSSG and has in fact been shown to be a stronger oxidizing agent than PDI (30-fold), which is somewhat surprising given the higher redox potential of PDI (Xiao *et al.*, 2005). The stronger oxidase activity of Grx is likely related to its enhanced ability to utilize glutathione to oxidize protein thiols under oxidizing conditions. This is supported by the observation that PDI requires both active site cysteines to catalyze disulfide bond formation while Grx requires only the N-terminal cysteine (Xiao *et al.*, 2005). With this knowledge, Tyr21 in poxviral Grx-1 could act to enhance glutathionylation reactions, either to assist in the folding of late proteins or to protect proteins from becoming irreversibly damaged through oxygenation or nitrosylation by ROS.

In one model, the glutathionylating activity could be used to protect late proteins that are packaged into the virion from irreversible oxidation after the virus exits the host cell into the harshly oxidizing extracellular environment. The incorporation of Grx into the virion would then allow the enzyme to also assist in de-protection of the virion encapsidated proteins through its deglutathionylating activity, once the virus re-enters the more reducing cytoplasmic environment upon infection. Additionally, this model

does not preclude a significant role for poxviral Grx-1 as a reducing agent for RNR, since the deglutathionylating activity would only be beneficial immediately following infection.

Finally, the redox correlated structural rearrangement of Tyr21 may also be used as a mechanism to enhance substrate interactions with an as yet unidentified cofactor or substrate. A similar role for tyrosine residues has been demonstrated for GSH-reductase catalysis, and two tyrosines, Tyr 114 and Tyr197 in this enzyme have also shown to undergo dramatic rearrangements in response to substrate binding (Pai and Schulz, 1983; Pai et al., 1988; Krauth-Siegel et al., 1998). While Tyr 114 rotates and translates about 1 Å in response to GSSG binding, the rearrangement of Tyr197 due to the binding of NADPH is similar to that seen in EVM053 Tyr21, with the OH group moving by 6.4 Å (Pai et al., 1988). The movement of Tyr197 of GSH-reductase has been proposed to act as a gate mechanism whereby binding of NADPH causes the residue to move and thus provide a more open pocket for the incoming nicotinamide (Krauth-Siegel et al., 1998). The proximity of Tyr21 to the active site of EVM053 and a strongly hydrophobic pocket highlights the possibility for a similar role in substrate binding for this residue.

4.2.4 Functional role of EVM053 *cis*-proline 53

The *E. coli* Grx-R1 mixed disulfide crystal structure revealed that R1 peptide binding was promoted through electrostatic interactions of the negatively charged R1 C-terminus and the positively charged Arg39 residue in the loop region following the second β-strand. While the mammalian Grx-1 structures do not conserve a basic residue

that corresponds to Arg39 of *E. coli* Grx-1, the corresponding region of EVM053 shows at least two residues, Lys49 and Lys52, which could potentially support this interaction. Furthermore, the presence of a *cis*-proline at position 53 suggested this residue may play an important structural role to promote R1 binding, since it could affect the positioning of the adjacent Lys52 residue (see section 3.2.7).

In order to further analyze the role of *cis*-Pro53 in the R1 disulfide bond reduction reaction, a peptide decamer corresponding to the final ten residues of the EVM057 R1 C-terminus was synthesized with the cysteines in the oxidized conformation, and used as a substrate in the standard Grx NADPH-coupled assay with EVM053 or a P53A mutant as the enzyme. The enzyme kinetics for these reactions are demonstrated in **Figure 4.6a-b**.

The P53A mutation did not completely obliterate catalysis, but the *Km* for the R1 substrate was greatly increased (2.3 mM) compared to the wild type enzyme *Km* (0.49 mM), suggesting affinity for the substrate is decreased when Pro53 is mutated to alanine. To confirm that the P53A mutation did not affect catalysis of disulfides in general, L-cystine was also tested as a substrate under identical conditions as the peptide. L-cystine is too small to interact with the putative R1 binding loop region, but the disulfide bond is chemically similar to that in the peptide. When L-cystine was used as a substrate, the kinetics for EVM053 and P53A were much more similar than for the peptide analysis, further demonstrating the enhancement of substrate specificity due to *cis*-Pro53 **(Figure 4.6c-d)**. Functional analysis of the P53A mutant coupled with structural data thus provided strong evidence that the *cis*-Pro 53 residue evolved in poxviral Grx-1 to promote binding interactions with the R1 C-terminus.
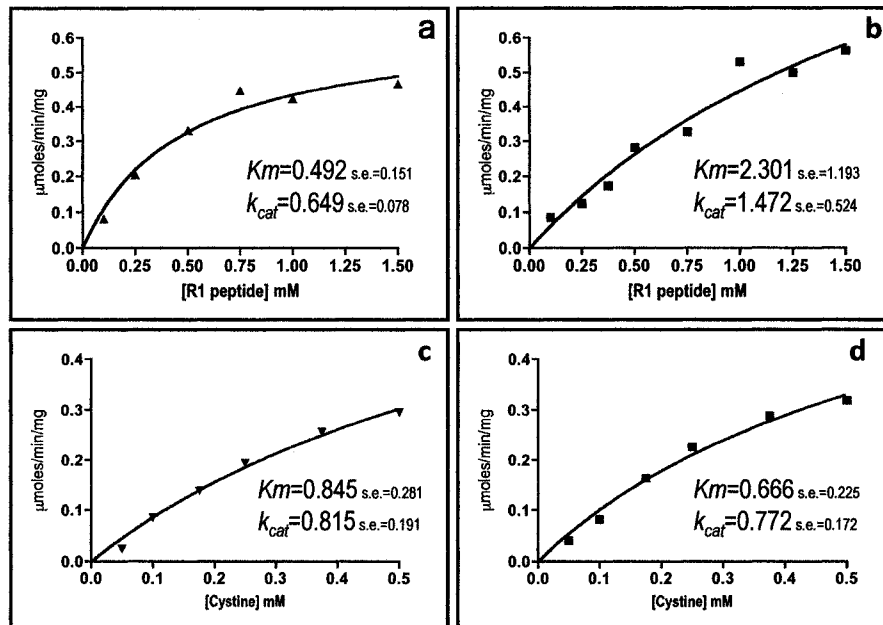
Figure 4.6 Kinetic analysis of the reduction of an RNR R1 peptide by EVM053 (a) and P53A (b). The results demonstrate a much lower *Km* value for the peptide for EVM053 than P53A. When cystine is used as the substrate, the kinetics are much more similar for the EVM053 (c) and P53A enzymes (d).

These findings support other results for *E. coli* Grx-1, which was reported as the main reducing agent for R1 *in vivo* (Holmgren, 1976), and also uses the loop between α-helix 3 and β-strand 2 to assist in the binding of the R1 C-terminal peptide (Berardi and Bushweller, 1999). The ability of Grxs to inhibit or promote interactions with peptide substrates thus appears to be driven through the substitution of residues in a loop region that does not play a direct role in catalysis. Future mutagenic experiments of this loop region will provide further insight into the molecular details of enzyme-substrate interactions.

CHAPTER V

GLUTAREDOXIN CATALYZED ARSENIC REDUCTION

5.1 Arsenic metabolism

5.1.1 Background

Arsenic and arsenic containing compounds are widely present in the environment, showing a high rate of occurrence in the air, drinking water and food sources (Singh et al., 2007). Exposure to this highly toxic and carcinogenic compound is exacerbated in regions near coal refineries, metal smelters, and from arsenic rich ground water sources such as those found in Bangladesh (Mukherjee et al., 2006). In living organisms, arsenic exists as trivalent (AsIII) or pentavalent (AsV) forms, and both inorganic and organic forms (mono- or di-methylated) are common (Messens and Silver, 2006). Arsenic is a potent carcinogen and exposure has been documented to cause several types of cancers of the skin, lung, liver, bladder and colon as well as blackfoot disease (Bates et al., 1992; Tseng, 1977). The carcinogenic effects of arsenic on DNA including, inhibition of DNA repair, deletion mutations and chromosomal alterations, can be ascribed to several molecular effects of arsenic. In its pentavalent state, arsenate closely resembles phosphate and can substitute for phosphate in many biochemical reactions (Rossman, 1981; Andrew et al., 2006). Arsenate compounds also act as strong oxidizing agents that lead to production of ROS and the depletion of GSH levels (Chou and Dang, 2005; Flora et al., 2007; Han et al., 2008). Furthermore, trivalent arsenicals are known to bind and inhibit the activity of many enzymes involved in maintaining cellular redox status including; GSH reductase, GSH peroxidase, Glutathione S-transferase (GST), and mammalian Trx-reductase, and can thus lead to aberrant protein

function and cellular redox status (Chouchane and Snow, 2001; Lu *et al.*, 2007).

All known organisms have evolved mechanisms to detoxify arsenic and the reduction of the compound from the pentavalent to trivalent form is a general feature of this process (Rosen, 2002). This reduction is invariably dependent on the thiol/disulfide redox systems within cells and all arsenate reductase enzymes characterized are dependent on thiol chemistry for this reaction (see section 5.2) (Messens and Silver, 2006). The need for arsenate reduction may be somewhat surprising considering the trivalent form is thought to be more toxic and reactive than the pentavalent form since it more readily binds to cysteine residues and thus inhibits protein function in addition to the depletion of GSH (Han *et al.*, 2008). One possible explanation for the evolution of arsenate reduction may be due to changes in the global atmosphere over time. Since the atmosphere was originally anaerobic, most environmental arsenic compounds existed in the reduced state. Upon introduction of the aerobic atmosphere, environmental compounds such as arsenic became increasingly oxidized. Since a pathway to eliminate the trivalent form of this compound likely already existed in bacteria, the reduction of arsenate may thus have evolved in order to make use of an already existing pathway of arsenite metabolism and secretion.

5.1.2 Arsenic metabolism in mammals

The metabolism of arsenic in mammals is a much less understood process than in bacteria and yeast, and is also a much more complex process due to methylation reactions that are seemingly involved in the metabolism of arsenic in most old world mammalian species, including humans (Wildfang *et al.*, 2001). The conservation of

arsenic reductase activities in mammals is also thought to assist in arsenic detoxification and excretion, since reduction is a prerequisite for the methylation of this compound, although this is also a subject of controversy (see next section). The methylation processes occur primarily in the liver, particularly after ingestion, but have also been observed in the kidneys, lungs and brain (Healy *et al.*, 1998; Rodriguez *et al.*, 2005). These reactions produce monomethyl and dimethyl arsenicals, which are then excreted into the urine and bile (Vahter, 1999).

Biomethylation processes diverge greatly amongst mammalian species. Marmoset and tamarin monkeys, chimpanzees and guinea pigs, for example, have been shown to be unable to methylate arsenic species, while rats have demonstrated a very low secretion of methylated arsenic species due to the retention of DMAIII in the erythrocytes (Vahter *et al.*, 1984; Vahter and Marafante, 1985; Vahter *et al.*, 1995; Zakharyan *et al.*, 1996; Healy *et al.*, 1999; Shiobara *et al.*, 2001; Lu *et al.*, 2004, Lu *et al.*, 2007). Several mammals such as mice, dogs and rhesus monkeys have high rates of arsenic methylation to DMA, while humans are unique in the fact that they secrete significant amounts of MMA in the urine, although DMA is also the major arsenic metabolite excreted by humans (10 – 30% As, 10 – 20% MMA, 60 – 70% DMA) (Vahter, 1999; Zakharyan *et al.*, 1996). The specific pathways of disease causation by arsenic compounds in mammals is complicated by the fact that different arsenic compounds have greatly different toxic effects and arsenic biotransformation is not only diverse amongst mammals, but can also show much variation even amongst different human populations (Meza *et al.*, 2007). The susceptibility of individuals to arsenic exposure may be due to the variations of arsenic biotransformation in different

populations and individuals, particularly in regards to the relative rate of MMA produced, suggesting potential genetic polymorphisms influence the methylation process (Vahter and Concha, 2001).

Although trivalent arsenic species are generally regarded to be more toxic than pentavalent forms, methylated trivalent arsenite compounds are the major metabolites of inorganic arsenic in the urine (Vahter, 1999; Aposhian et al., 2000). Furthermore, trivalent arsenic compounds have also been shown to be secreted from the liver as a GSH adduct using a multidrug resistant protein 2 (MRP2) and GSH cotransport system, and the formation of these adducts are likely to play an important role in the bile secretion of trivalent arsenic compounds (Dietrich, et al., 2001; Gao et al., 2006).

The highly divergent metabolism of arsenic compounds in mammalian lineages suggests the evolution of arsenic metabolism in mammals is still a "work in progress". The high toxicity of arsenic may more than anything be due to the complex chemistry of this compound and difficulty for mammalian species to effectively metabolize such a compound, perhaps combined with low selective pressure to develop an effective arsenic secretion system. Research of arsenic metabolism is confounded by the fact that in many instances it is difficult to determine if enzymatic reactions with arsenic compounds are involved in detoxification of this compound or are in fact contributing to toxicity by creating more reactive arsenic compounds (bioactivation). In other words, reactions that have commonly been perceived as detoxification of arsenic, may just be the fortuitous interaction of arsenic with an enzyme that would otherwise perform a normal cellular function, and thus leads to increased toxicity.

5.1.3 Eukaryotic methyltransferase

Metabolism of arsenic species through methylation reactions remains a largely misunderstood process and the nature of each constituent step in the process remains unclear. However, the first step of the reaction, the conversion of AsIII to MMA-5 has been shown to be catalyzed by arsenic methyltransferase (AS3MT), a protein that is conserved in organisms as diverse as sea urchins to chickens and humans, but not in fruit flies, suggesting the gene arose before the division of chordates (Thomas *et al.*, 2007). The protein contains five conserved cysteines and it is thus perhaps not surprising that reducing agents have been shown to promote its methylating activity (Aposhian, 1997). Most AS3MT enzymes are ~350 residues in length, although in chimpanzees it is truncated to only 180 residues. The inability of chimpanzees to methylate arsenic could be accounted for by the truncated and potentially inactive protein (Vahter *et al.*, 1995).

There are two current models of the process of arsenic metabolism through methylation in mammals, both of which assume AS3MT acts as the methyl donor in the reaction. The first, and more widely recognized model, is a process by which the reduction of pentavalent arsenicals is a prerequisite for methylation/oxidation by AS3MT (Thomas *et al.*, 2007). Thus, AsV is converted to AsIII, which is methylated to form MMA-5 and subsequently reduced to produce MMA-3, which is methylated to form DMA-5 and reduced to form DMA-3 **(Figure 5.1)**.

The second model of arsenic methylation was proposed based on the observation that AS3MT methylates trivalent arsenic compounds that are bound to GSH, and is concomitantly less reliant on redox reactions (Hayakawa *et al.*, 2005).

Classic pathway of arsenic metabolism in mammals

As-5

2e⁻ → | GAPDH, GSH |

As-3

AdoMet → AdoCys | Arsenic Methyltransferase |

MMA-5

2e⁻ → | GSTO-1, GSTO-2, GSH, Grx |

MMA-3

AdoMet → AdoCys | Arsenic Methyltransferase |

DMA-5

2e⁻ → | Grx, GSTO-1, GSH |

DMA-3

New pathway of arsenic metabolism in mammals

As-5

2e⁻ → | GAPDH, GSH |

As-3

GSH

As-3(GS)$_3$

AdoMet → AdoCys +GSH | Arsenic Methyltransferase |

MMA-3(GS)$_2$

AdoMet → AdoCys + GSH | Arsenic Methyltransferase |

DMA-3(GS)

Figure 5.1. Proposed pathways of arsenic metabolism in mammals. Enzymes or molecules that have been shown to catalyze the listed reactions *in vitro*, are shown in yellow boxes. In the classic pathway, reduction of pentavalent arsenic species to trivalent arsenic species is a prerequisite for methylation by arsenic methyltransferase. In the proposed new pathway, trivalent arsenic complexes covalently bound to GSH are the substrates for arsenic methyltransferase.

115

This model is also supported by the fact that GSH has been shown to form stable complexes with trivalent arsenite complexes (Delnomdedieu *et al.*, 1994). Furthermore, depletion of GSH from rats resulted in a diminished rate of methylation in these organisms (Buchet and Lauwerys, 1988; Hirata *et al.*, 1990). Conversely, other studies have shown that the presence of GSH is not an absolute requirement for the AS3MT catalyzed methyltransferase reaction since other thiols are effective in its place (DTT, cysteine, 2-mercaptoethanol) which argues against the second model (Zakharyan *et al.*, 1996). In reality, the most biologically relevant model could in fact be a combination of both models since there is overlap in product formation and different mechanisms of each model could be utilized depending on redox status of the environment or other variables.

The metabolism of arsenic in mammalian species remains a vastly misunderstood puzzle that will likely require much research in order to put the pieces together to provide a coherent picture. The characterization of potential players in these reactions, such as reducing or oxidizing agents, or other proteins that enable arsenic detoxification, will lead to a better understanding of mammalian mechanisms of detoxification in general.

5.2 Arsenate reductases

Arsenic is ubiquitous in the environment and all organisms from bacteria to humans have evolved mechanisms of arsenic metabolism (Rosen, 2002). The reduction of arsenate to arsenite has been shown to be the initial step in arsenic detoxification for

many organisms and arsenate reductases have been characterized in bacteria, yeast, plants and protozoans (Gladysheva *et al.*, 1994; Stevens *et al.*, 1999; Li *et al.*, 2003; Mukhopadhyay *et al.*, 2000; Mukhopadhyay and Rosen, 2002; Zhou *et al.*, 2006; Duan *et al.*, 2007). Arsenate reductases have evolved independently at least three times, but the function of these enzymes is invariably linked to thiol chemistry since all arsenate reductases utilize an active site nucleophilic cysteine for catalysis (Messens and Silver, 2006). Furthermore, these enzymes are dependent on either Trx or Grx to complete their catalytic cycle (see below).

Disruption of arsenic reductase genes in both yeast and *E. coli* leads to arsenate hypersensitivity for these microorganisms (Gladysheva *et al.*, 1994; Mukhopadhyay and Rosen, 1998). Recent research has also pointed to an important role for arsenate reductases in the viability of several plant species, and the Acr2 protein of rice can effectively attenuate hypersensitivity to arsenate in arsenate reductase deficient *E. coli* and yeast (Duan *et al.*, 2007). Conversely, the discovery of a physiologically relevant arsenate reductase in higher eukaryotes such as mammals has eluded arsenic researchers, although a few mammalian enzymes have been shown to reduce both organic and inorganic pentavalent arsenic species *in vitro* (Chowdhury *et al.*, 2006; Nemeti *et al.*, 2006; Paiva *et al.*, 2008). The high rate of arsenic related disorders in human populations due to groundwater (approximately 80% of the population in Bangladesh suffers from arsenic related disorders), food sources (i.e. rice) and other anthropogenic and geochemical sources make it imperative to discover the *in vivo* source of arsenic reduction in humans in order to better understand arsenic metabolism and disorders caused by this highly toxic and carcinogenic compound (Duan *et al.*,

2007). A study of the known arsenate reductases in microorganisms and plants may lead to clues which will facilitate the discovery of arsenic reductases in mammals.

5.2.1 Prokaryotic arsenate reductases

The most extensively studied arsenate reductases are ArsC of *S. aureus*, and ArsC of *E. coli*, which serve as the prototype arsenate reductases of gram positive and gram negative bacteria, respectively (Messens and Silver, 2006). Although the enzymes share the same name and are of approximately equal size (131 amino acids for *S. aureus* and 141 for *E. coli*), their mechanisms of arsenate reduction are fundamentally different. First, while ArsC of *S. aureus* requires a Trx coupled system to complete the catalytic cycle, ArsC of *E. coli* utilizes a Grx coupled system (Gladysheva *et al.*, 1994; Messens *et al.*, 2004). Secondly, while the *S. aureus* ArsC is structurally very similar to low molecular weight protein tyrosine phosphatases (~1.4 Å CA rmsd), *E. coli* ArsC demonstrates several structural properties that are similar to Grxs including a similar tertiary structure, an active site structure close to the N-terminus (Cys12), thiolate stabilization by an α-helix dipole, and a putative GSH binding site (Zegers *et al.*, 2001; Stevens *et al.*, 1999). Thirdly, while *S. aureus* ArsC catalysis uses three active site cysteines to reduce arsenate, *E. coli* ArsC requires only one active site cysteine (Gladysheva *et al.*, 1994; Messens *et al.*, 2004). Finally, *E. coli* ArsC shows a much higher K_m (~100 fold) and lower k_{cat} (~10 fold) than *S. aureus* ArsC, and a pH optimum of 6.3-6.6 (compared to 8.0 for *S. aureus*) (Gladysheva *et al.*, 1994; Messens *et al.*, 2002). The much lower K_m of *S. aureus* ArsC for arsenate (68 μM) than *E. coli* ArsC (8

mM) has been at least partially attributed to the binding of a potassium cation by *S. aureus* ArsC, although other factors are also likely involved in the higher apparent specificity of the *S. aureus* ArsC enzyme (Lah *et al.*, 2003; Roos *et al.*, 2006a)

5.2.2 Eukaryotic arsenate reductases

The first eukaryotic arsenate reductase characterized was that of the yeast *Saccharomyces cerevisiae*, known as Acr2p (Mukhopadhyay and Rosen, 1998; Mukhopadhyay *et al.*, 2000). Acr2p arsenate reductase homologs have also been characterized in plants and the protozoan parasite *Leishmania major*, for which a crystal structure has recently been solved (Bisacchi *et al.*, 2006). This protein is characterized by an N-terminal CX(5)R motif and the arsenate reductase catalytic activity of Acr2p is also coupled to Grx and GSH (Mukhopadhyay *et al.*, 2000). Acr2p shows similar kinetics as *E. coli* ArsC with a relatively high K_m (35 mM) for arsenate. The Acr2p protein belongs to a family of oxyanion binding proteins that includes another group of protein tyrosine phosphatases, which includes human Cdc25a, and thiolsulphate transferase (rhodanese) (Fauman *et al.*, 1998; Hofmann *et al.*, 1998). The crystal structures of human Cdc25, *Azotobacter vinelandii* rhodanese and *L. major* arsenate reductase proteins demonstrated that although these proteins show only weak over all sequence homology (23% identity for *L. major* arsenate reductase to Cdc25), the enzymes share a remarkably similar active site geometry. The active site cysteine is stabilized at the centre of a strongly positively charged pocket and makes several hydrogen bonds that range in length from ~3.2 to 3.8 Å. In an analogy to Grx, the active

site cysteine pKa has been shown to be markedly reduced to 4.7 in a *Yersinia enterocolitica* protein tyrosine phosphatase (Zhang and Dixon, 1993), and to 6.5 for a sulfurtransferase (rhodanese) from *A. vinelandii* (Bordo *et al.*, 2000). The lower pKa in phosphatases and arsenate reductases has been attributed to the conservation of a histidine before the active site cysteine in these enzymes but not rhodanese proteins (Zhang and Dixon, 1993). Interestingly, Acr2p can be converted into a tyrosine phosphatase (with concomitant loss of arsenate reductase activity) by the substitution of only 3 amino acids, suggesting substrate specificity and catalysis can be easily manipulated for these proteins (Mukhopadhyay *et al.*, 2003).

In mammals, although several homologs of the tyrosine phosphatases (LMW phosphatases and Cdc25) have been characterized there is no known functional arsenate reductase enzyme that is orthologous to the bacterial and yeast enzyme and this process is much less understood than arsenate metabolism in bacteria and yeast (Messens and Silver, 2006). Thus far a physiologically relevant mammalian arsenate reductase has eluded identification, although a handful of mammalian enzymes have been shown to have arsenate reductase activities *in vitro* (Chowdhury *et al.*, 2006; Nemeti *et al.*, 2006; Paiva *et al.*, 2008). For example, a mammalian enzyme that catalyzes the reduction of methylated arsenic species has been characterized (GSTO-1) (Zakharyan *et al.*, 2001). Interestingly, GSTO-1, and the related GSTO-2, were first characterized as Glutathione S-transferases, but then subsequently found to have methyl- and dimethyl- arsenate reductase activities (Schmuck *et al.*, 2005). However, *in vivo* studies demonstrated that deletion of the GSTO-1 gene in mice resulted in only marginal differences in arsenic metabolites in the tissues of knockout and wild-type mice after acute arsenic

administration (Chowdhury *et al.*, 2006). Another mammalian enzyme, glyceraldehyde-3-phosphate dehydrogenase (GAPDH), has demonstrated GSH-dependent inorganic arsenate reductase activity *in vitro*, but *in vivo* experiments have thus far shown inconclusive results (Nemeti *et al.*, 2006).

Taken together these results might suggest that a "bona fide" arsenate reductase still remains to be found and characterized in mammalian species, since arsenate reduction is a crucial step for arsenic metabolism in yeast and bacteria. Conversely, it must also be considered that although studies of arsenic metabolism in mammals has yielded vast information about the beginning and end products of this metabolic pathway, discussions of the molecular mechanisms for these reactions have thus far remained highly speculative.

5.2.3 Glutaredoxin role in arsenic metabolism

Arsenic has not previously been shown to interact with Grx, but the covalent modification of Cys23 by DMA-3 in the reduced EVM053 structure demonstrated that the Grx active site is also a target for arsenic compounds. Furthermore, mammalian GSTOs display several structural and functional properties that are typical of Grxs including, dehydroascorbate reductase and thioltransferase activities, a catalytic cysteine (Cys32) in a Grx-like CPF sequence motif, thiolate stabilization through a helix dipole, and formation of a mixed disulfide with GSH (Schmuck *et al.*, 2005). As noted above, human GSTO-1 and GSTO-2, have also been shown to reduce monomethyl and dimethyl arsenate *in vitro* (Schmuck *et al.*, 2005).

With the finding of a dimethylarsenite adduct covalently attached to the active site of EVM053 (see section 3.2.3), it was evident that the cacodylate in the buffer must be reduced from the pentavalent to trivalent state. It is well known that DTT is capable of performing this reaction (Maignan *et al.*, 1998). However, the known involvement of strongly nucleophilic thiolates in arsenic reductase activities and the structural homology of Grx to *E. coli* ArsC, as well as the involvement of Grx as a cofactor in several arsenic reduction mechanisms, led to the hypothesis that Grx itself may be able to catalyze the reduction of dimethylarsenate.

5.3 Results & Discussion

5.3.1 Glutaredoxins have dimethylarsenate reductase activity

To test whether Grx demonstrated dimethylarsenate reductase activity, DMA-5 was used as a substrate in the standard NADPH-coupled Grx assay. Using this assay, a significant decrease in NADPH absorbance was demonstrated in the presence of EVM053 **(Figure 5.2)**. Other Grxs, including human Grx-1, also demonstrated DMA-5 reductase activity (see section 5.3.7), suggesting this is a general functional property of Grxs. Furthermore, similar to the enzyme's DHA reduction rate, the DMA-5 reduction reaction proceeded at approximately twice the rate when C26S was used as the enzyme (see next section).

The arsenate reductase activities for GSTO-1 and GSTO-2, have been reported as 0.15 and 0.03 μmol NADPH oxidized/min/mg protein, respectively, when using 10
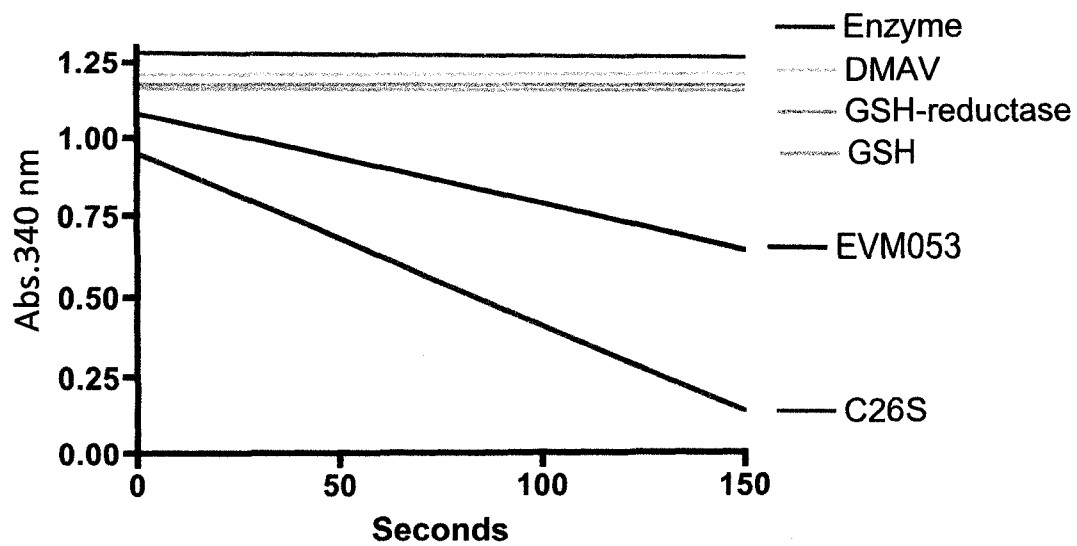
Figure 5.2. Dimethylarsenate reductase activity of EVM053 and a C26S mutant. The top four coloured lines represent the NADPH-coupled reaction rate with the indicated component absent. The bottom two rates represent the reaction rate when all components are present with either EVM053 or the C26S mutant as the enzyme.

mM DMA-5 as substrate. At the same substrate concentration and a pH of 6.8, EVM053 reduces DMA-5 with an average activity of 0.25 μmol NADPH oxidized/min/mg protein **(Figure 5.3)**. To determine if this activity was specific to DMA-5 or whether other arsenate species could be reduced by EVM053; MMA-5 and AsV were also tested as substrates. At the same concentration of arsenic species, DMA-5 shows the strongest rate of NADPH oxidation in the presence of EVM053 **(Figure 5.3)**. When MMA-5 is used as the substrate, the rate of NADPH oxidation is markedly decreased to 0.08 μmol NADPH oxidized/min/mg, while the AsV reaction rate is only 0.03 μmol NADPH oxidized/min/mg. The enhanced ability of Grx to catalyze DMA-5 reduction may be at least partially explained by the Pearson acid base concept, which states that hard acids are more likely to interact with hard bases and soft acids are more likely to interact with soft bases (Ayers *et al.*, 2006). A hard species is generally a small highly charged compound that is weakly polarizable, whereas a soft species is relatively large and highly polarizable. AsV is seen as a relatively hard acid whereas the replacement of electron withdrawing hydroxyls by methyls makes DMA-5 a softer acid. Since the thiolate of the active site cysteine is also considered a soft base, Grx may prefer dimethylated arsenic as a substrate. The binding of DMA-5 to the active site cysteine could make the substrate even softer and enhance interactions with GSH or a second Grx, which may be required for the catalytic mechanism. Although the reduction of arsenic species has for the most part shown that reduction to the trivalent state is a prerequisite for binding to GSH, a pentavalent dimethylarsenic compound that has a double bond to sulfur *in lieu* of oxygen (dimethylarsinothioyl) has been shown to complex with GSH. This demonstrated that addition of a sulfur (or thiolation) to arsenic
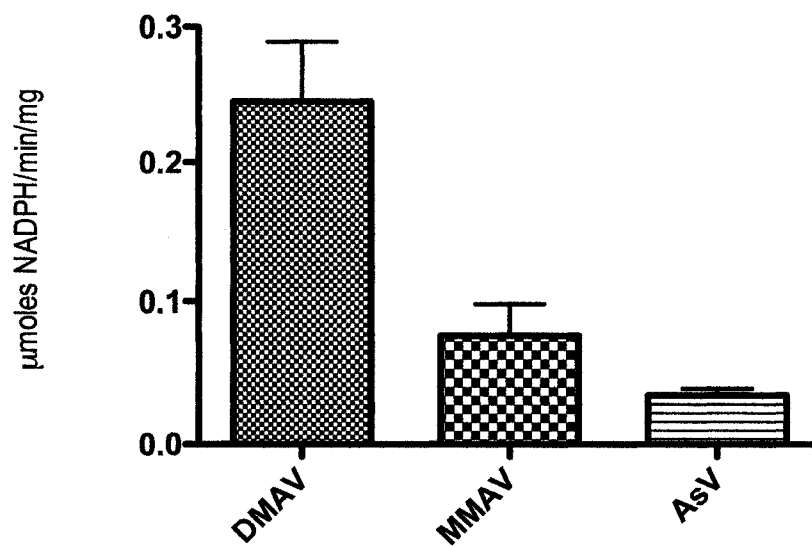
Figure 5.3. Dimethylarsenate, monomethylarsenate and arsenate reductase activity of EVM053.

compounds, promotes interactions of pentavalent arsenic compounds with other thiol compounds (Raab *et al.*, 2007). Methylation of arsenic also affects the number of protonation sites and their pKas, which may also affect substrate preference (see section 5.3.4).

5.3.2 Glutaredoxin catalyzed dimethylarsenate reduction requires only one active site cysteine

Glutaredoxins are known to catalyze the reduction of mixed disulfides through the use of only the N-terminal active site cysteine whereas reduction of protein disulfides has been shown to require both active site cysteines (Bushweller *et al.*, 1992). For the reduction of DHA, either a monothiol or dithiol mechanism may be utilized to catalyze the reaction (Washburn and Wells, 1999). In order to investigate the catalytic mechanism of Grx catalyzed DMA reductase activity, the C26S mutant of EVM053 was used to determine whether the DMA reductase activity could proceed through a monothiol mechanism. Analysis of the C26S mutant demonstrated that this reaction proceeded at a rate of approximately 2 times the rate catalyzed by wild type EVM053 **(Figure 5.2)**. Similar results were previously obtained when DHA was used as the substrate (see section 4.2.3).

This analysis provided the first evidence that the mechanism of Grx catalyzed DMA reduction resembles that of the DHA reductase mechanism. In the proposed DHA monothiol reduction mechanism, DHA first binds to the active site thiol Cys23 through a nucleophilic attack. GSH then attacks the Cys23-DHA adduct, releasing the reduced product, ascorbic acid, while a Grx-GS adduct is formed. A second GSH molecule then

interacts with the Grx-GS adduct to form GSSG and reduced Grx (see **Figure 4.5** in section 4.2.3).

5.3.3 Glutaredoxin catalyzed dimethylarsenate reduction may also proceed through a dithiol mechanism and does not require the presence of GSH

For Grx catalyzed DHA reduction it had been shown that the reaction could proceed through either a monothiol or dithiol mechanism (Washburn and Wells, 1999). While analysis with the C26S mutant demonstrated that the Grx catalyzed reduction of arsenic species was possible through the monothiol mechanism, it was still not clear whether the reaction could also proceed through a dithiol mechanism.

In order to test whether the DMA reduction mechanism could proceed through the dithiol mechanism, the Y21W mutant was used for the tryptophan fluorescence based assay in the absence of GSH (see **Figure 4.3** in section 4.2.2). The results of this analysis demonstrated that, similar to the DHA reductase mechanism, the reaction could proceed through the dithiol mechanism and that the presence of GSH was not required. In this mechanism the substrate likely binds to the catalytic Cys23, which is similar to the monothiol mechanism, but instead of receiving the second reducing equivalent from GSH, the second reducing equivalent likely comes from Cys26 and the Cys23-Cys26 disulfide bond is formed. Although this reaction demonstrated that the reaction may proceed through a dithiol mechanism, *in vivo*, GSH is in all probability required to regenerate the reduced enzyme.

5.3.4 pH profiles of glutaredoxin-catalyzed arsenate reduction reactions

Since enzyme mechanisms and interactions with substrates are intrinsically linked to the pH at which these reactions occur, it is of interest to study the reaction rate of DMA-5, MMA-5 and AsV reduction at various pH levels. In a series of experiments the pH activity profiles for reduction of DMA-5, MMA-5 and AsV were determined. As shown in **Figure 5.4**, the reaction rate for DMA-5 reduction using EVM053 and the C26S mutant shows the highest rate of activity between pH 4.8-6.0. The rising inflection point at approximately pH 4.6 is close to the expected pKa of the active site Cys23 thiol, which ranges from 3.5 to 5.0 in other Grxs (Mieyal *et al.*, 1991; Aslund *et al.*, 1997). This suggests that at low pH levels, activity may be limited by the pH dependent protonation of Cys23. The falling inflection point at approximately pH 6.2, may be related to the pKa of DMA-5, which is also 6.2. Above pH 6.2 more of the substrate will be negatively charged and may experience electrostatic repulsion by the negatively charged active site thiolate, which could reduce binding affinity. Conversely, fully protonated DMA-5 would make it more amenable for nucleophilic attack below pH 6.2.

Initial studies demonstrated only weak reductase activity at pH 6.8 when MMA-5 or AsV were used as substrates with EVM053 as the enzyme (see section 5.3.1). A stronger absorbance change could be obtained with the C26S mutant since the monothiol mechanism appears to be the faster reaction, and this enzyme was thus used to determine the pH activity profile of MMA-5 and AsV reduction. For MMA-5 reduction the pH profile was quite similar to that of DMA-5, but at a markedly lower rate of activity. AsV reductase activity was relatively stronger at very acidic pH levels. The rate of activity peaked at 4.0 and demonstrated a steady decline in activity towards
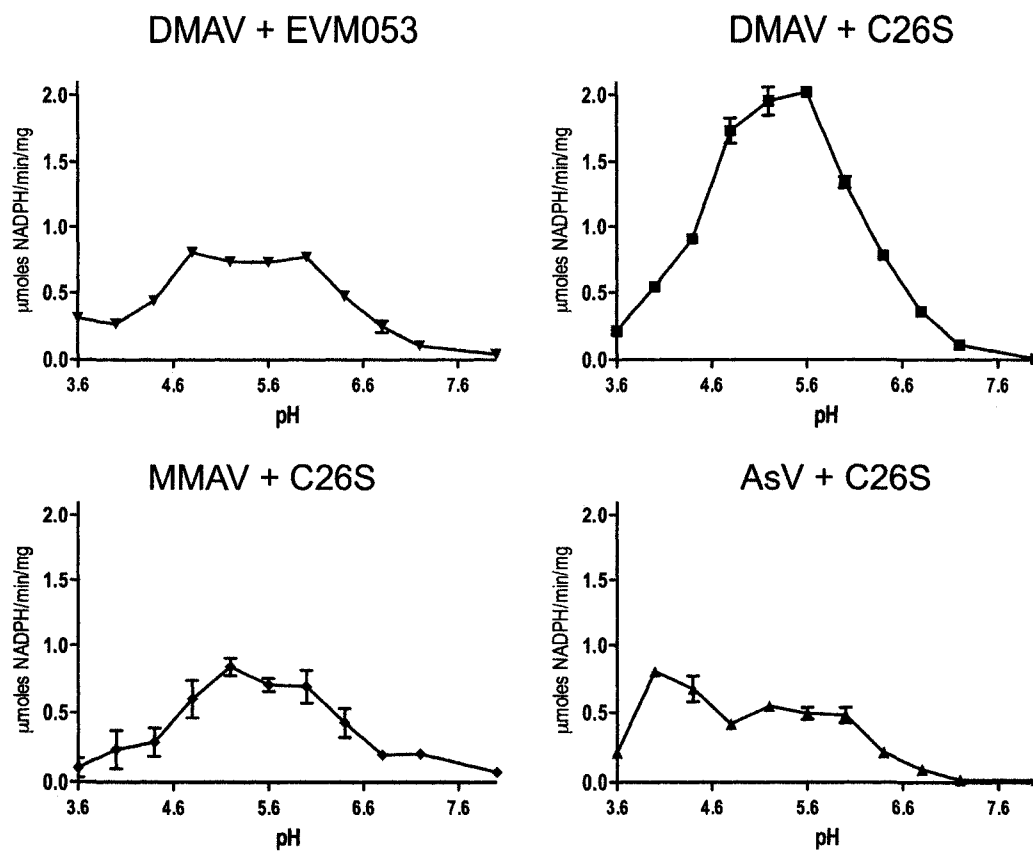
Figure 5.4. pH profiles of dimethylarsenate, monomethylarsenate and arsenate reductase activity of EVM053 and C26S.

pH neutrality (**Figure 5.4**).

MMA-5 has two protonation sites with pKa values of 3.6 and 8.2. The rising activity in the pH 4-5 region most likely again reflects the pKa of the active site cysteine because MMA-5 will be mostly monoanionic throughout this range. The negative charge would then also explain the overall lower activity in the higher pH range with the diminished reduction activity at this pH reflecting loss of the second proton to yield the dianionic state.

Inorganic arsenate has three protonation states with pKa values of 2.3, 6.8, and 11.6. The lower pKa values make AsV the most anionic of the three substrates, which accounts for it being the poorest substrate for EVM053. The much lower rate of catalysis when AsV is the substrate is not surprising considering various Grxs from *E. coli* and yeast have shown to act only as cofactors for ArsC or Acr2p catalyzed arsenate reduction (see section 5.2.1).

Catalysis of arsenate reduction is optimal at pH 8.0 for *S. aureus* ArsC (Roos *et al.*, 2006b) and 6.3-6.6 for *E. coli* ArsC (Messens *et al.*, 2002; Gladysheva *et al.*, 1994). Interestingly, the active site pKa for *E. coli* ArsC is 6.4, suggesting catalysis by this reductase is also linked to the active site thiol pKa. The similarity in active site thiol pKa and the pKa_2 of arsenate suggests *E. coli* ArsC may have evolved to couple the high reactivity of its thiol pKa at pH 6.4 with the pH at which the greatest amount of monoanionic arsenate would be present. For Grx the low pKa of its active site cysteine suggests the enzyme may only be a fortuitous dimethylarsenate reductase since the pKa of DMA-5 is 6.2.

5.3.5 Catalytic mechanism of glutaredoxin catalyzed dimethylarsenate reduction

From the above analyses, it is apparent that Grx catalyzed DMA reduction shares similar characteristics with its DHA reduction activity, since the reaction may proceed through either a mono- or dithiol mechanism and the monthiol mechanism is approximately twice as fast as the dithiol mechanism. In the proposed monothiol DHA reductase mechanism, the active site cysteine in the Grx-DHA complex is attacked directly by GSH resulting in reduced DHA and a Grx-SG adduct (see **Figure 4.5** in section 4.2.3). However, since Grx shows several structural properties similar to *E. coli* ArsC, it is also worthwhile to consider if the DMA reductase activity of Grx might also be similar to the proposed mechanism of ArsC catalyzed arsenate reduction.

Both ArsC and Acr2p enzymes have cationic substrate-binding pockets, which most likely contributes to their efficient reduction of anionic inorganic arsenate. *E. coli* ArsC crystal structures have shown that three arginine residues form a triad (Arg60, Arg94 and Arg107) surrounding the active site cysteine, which likely act to stabilize the transient interaction of the active site cysteine with anionic pentavalent arsenate, and also play a role in catalysis. In particular, Arg60, has been shown to be required for the putative formation of a unique positively charged arsenite intermediate (DeMel *et al.*, 2004). In the proposed mechanism, following glutathionylation of the ArsC-AsV intermediate and subsequent Grx assisted reduction, a positively charged thiarsahydroxy intermediate is formed. Crystallographic data of both native and mutant ArsC enzymes in the presence of several reaction intermediates support this proposed mechanism, and the formation of the unique positively charged arsenite intermediate has been suggested

to act as a mechanism to facilitate product release from the active site cysteine (Maignan *et al.*, 1998; DeMel *et al.*, 2004) **(Figure 5.5a)**.

The mechanism of Grx-1 catalyzed DMA-5 reduction could be similar to that of ArsC **(Figure 5.5b)**. However, the formation of the positively charged intermediate is not possible for DMA-3 due to the presence of the two methyl groups. Thus, for the case of the Grx catalyzed DMA-5 reduction, the production of DMA-3 could lead to greater product inhibition since it is clear form the EVM053 structures that DMA-3 is capable of forming a stable covalent bond with EVM053 Cys23 at low pH levels (see section 3.2.3). GSH has also been shown to form stable complexes with trivalent arsenic (organic and inorganic) below pH 7.5 (Delnomdedieu *et al.*, 1994). Thus GSH is likely to more effectively remove reduced arsenite species from Grx below this pH level in order to return Grx to its reduced unligated form and to complete the catalytic cycle. It is also important to note that much of the arsenic excreted into the bile is in the form of trivalent arsenite metabolites covalently linked to GSH and the formation of these complexes is considered an important step in arsenic detoxification (Cui *et al.*, 2004; Kobayashi *et al.*, 2005).

5.3.6 Role of conserved lysine in glutaredoxin catalyzed dimethylarsenate reduction

All Grxs conserve a positively charged residue that precedes the active site cysteine, (Lys20 in poxviral and mammalian Grx-1, Arg8 in *E. coli* Grx-1), that is also in close proximity to the active site cysteine. This residue was initially hypothesized to play a role in thiolate stabilization leading to the reduced pKa of Cys23,
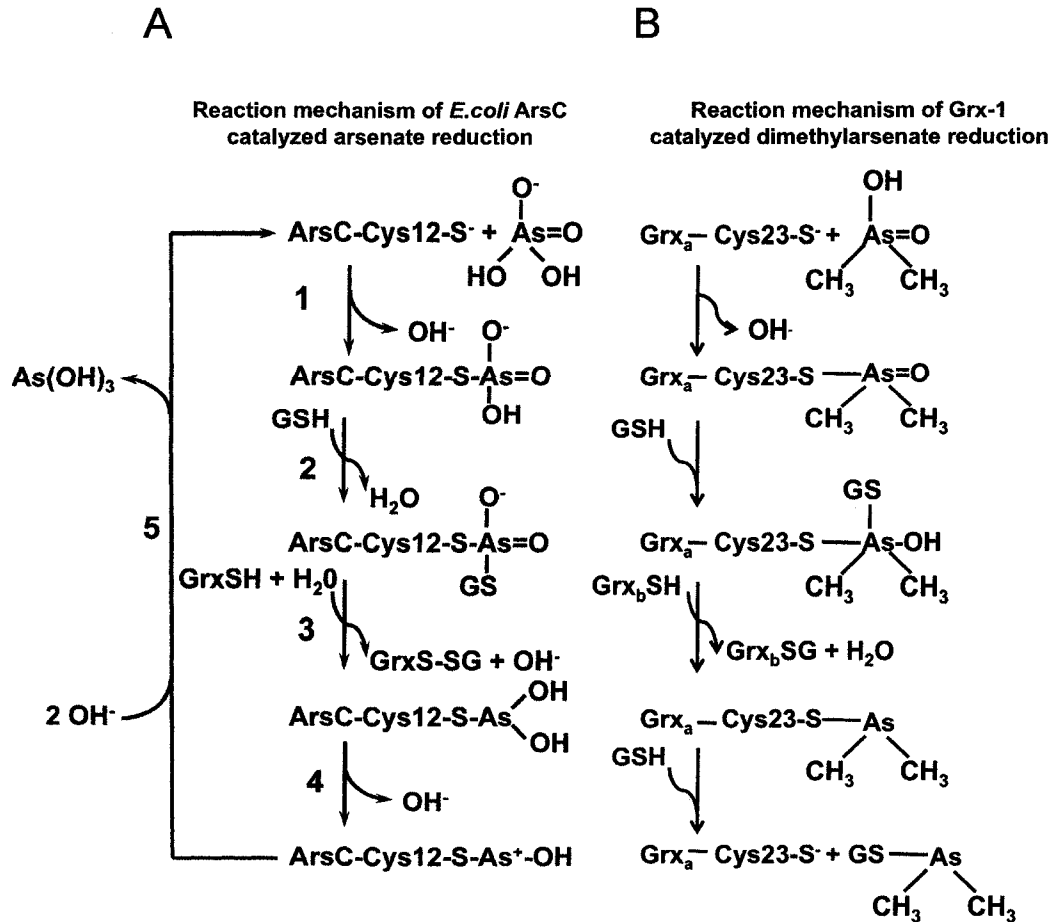
Figure 5.5. Mechanism of *E.coli* ArsC reductase and comparison to proposed Grx catalyzed mechanism. 1) Nucleophilic attack of active site thiolate on substrate. 2) Glutathionylation of covalent intermediate. 3) Reduction of substrate. 4) In the ArsC mechanism, a positively charged intermediate is proposed to be formed, but this is not possible for DMAIII. Instead GSH may be required to assist in product release for the Grx catalyzed mechanism. 5) Trivalent arsenite is released through hydrolysis only for the ArsC mechanism. ArsC reductase mechanism adapted from Demel *et al.*, 2004.

although more recent data and structural analysis does not support such a role for this residue (see section 3.3.1). In the dimethylarsenylated EVM053 structure Lys20 is in close proximity (5.6 Å) to the DMA-3 adduct and could move closer without any steric hindrance or electrostatic repulsion by other residues **(Figure 5.6)**. As noted above, the active site cysteine of *E. coli* ArsC is surrounded by three arginines, all of which are well positioned to stabilize or interact with arsenate and its reaction intermediates (Martin *et al.*, 2001). Similarly, catalysis of arsenate reduction by *S. aureus* ArsC is dependent on the presence of another arginine residue, Arg16, which is believed to act as a leaving group activator by forming a hydrogen bond with the leaving group hydroxyl and thus weakening the As-OH bond (Roos *et al.*, 2006b).

Since positively charged residues have been shown to be important for substrate interactions and catalysis for other arsenate reductases, it is worthwhile to consider the potential role of Lys20 in Grx catalyzed dimethylarsenate reduction. This residue may promote catalysis either through leaving group activation (in an analogy to Arg16), or through stabilization of the Cys23-DMA-5 intermediate during the S_N2 reaction. However, the presence of only one positively charged residue that can interact with the pentavalent arsenic substrate in Grxs might suggest why this enzyme shows high K_m values for DMA reduction (see next section) and is a relatively weaker or much weaker reducing agent for MMA-5 and AsV, respectively.
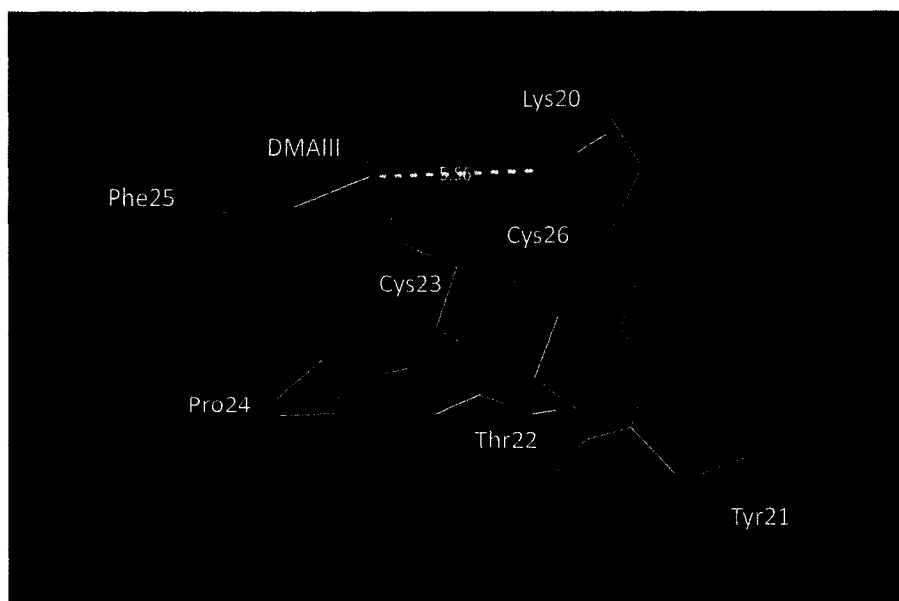
Figure 5.6. Active site structure of dimethylarsenylated EVM053. The structure shows that the positively charged side chain of Lys20 is in close proximity to the DMAIII adduct, suggesting the residue may play a role in substrate interactions during Grx catalyzed DMAV reduction.

5.3.7 Biological significance of glutaredoxin catalyzed dimethylarsenate reductase reaction

Although arsenic compounds are generally considered highly toxic and carcinogenic, low doses of arsenic compounds have been used to treat various ailments since ancient times and has been documented as an anticancer drug since the 19th century (Berenson and Yeh, 2006). The compound fell out of use in the mid-20th century due to the serious adverse side effects associated with its use as a therapeutic agent. More recently arsenic trioxide has been used successfully as a treatment for cancers such as acute promyelocytic leukemia (APL) and other arsenic compounds such as phenylarsine trioxide are also being explored for their efficacy as therapeutic agents to treat cancer (Chen *et al.*, 2002). With the knowledge that the metabolism of arsenic compounds in mammals is a poorly understood process, and that biotransformation of arsenic in humans may modulate the response of cancer patients to arsenic therapy, the study of enzymes that interact with arsenic metabolites is crucial for a better understanding of how these compounds can be more effectively used for medicinal purposes.

The dimethylarsenate reductase activity of human Grx-1 could potentially play an important role in arsenic detoxification in mammals. However, the pH profiles of poxviral Grx-1 catalyzed DMA-5, MMA-5 and AsV reduction demonstrated that maximum enzyme activity occurs well below normal physiological pH of the cell. In order to begin to evaluate the potential relevance of human Grx-1 catalyzed dimethylarsenate reduction, Michaelis-Menten kinetics for the reduction of DMA-5 were determined at pH 5.6, 6.8 and 7.4 (**Figure 5.7**). As expected, the k_{cat} for DMA-5 shows the fastest rate of activity at pH 5.6 (0.717 µmoles/min/mg), with less activity at

136
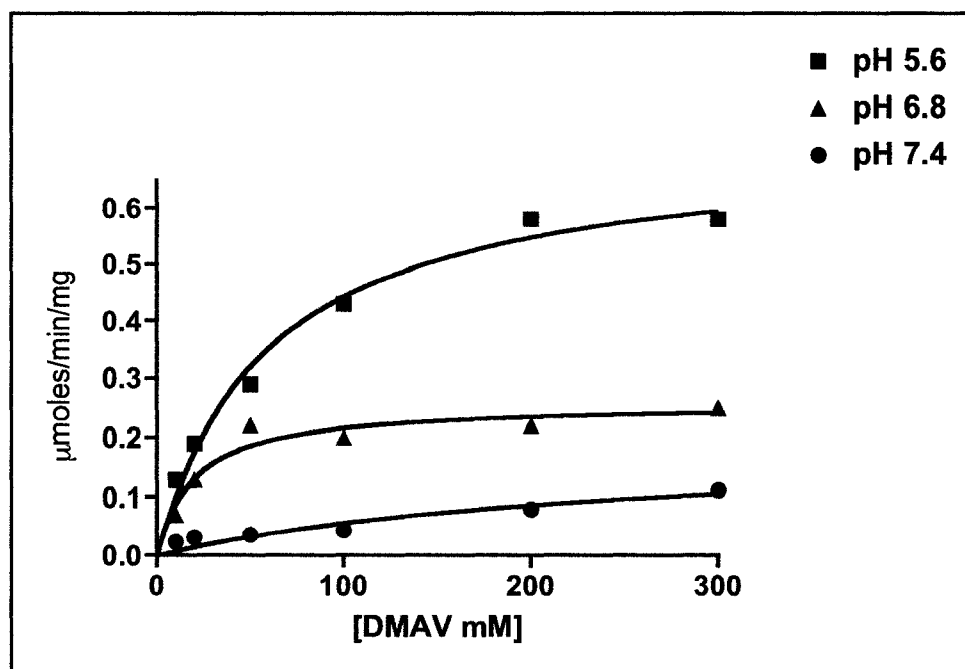
	K_m (mM)	Standard error	k_{cat} (µmoles/min/mg)	Standard error	k_{cat}/K_m
pH 5.6 ■	62.1	11.7	0.717	0.0456	0.0155
pH 6.8 ▲	19.4	6.12	0.257	0.0191	0.0132
pH 7.4 ●	237.5	188.6	0.189	0.0819	0.000796

Figure 5.7. Kinetic analysis of the DMAV reductase activity of human Grx-1 at pH 5.6, 6.8 and 7.4.

137

pH 6.8 (0.257 μmoles/min/mg) and pH 7.4 (0.189 μmoles/min/mg). Thus, the reaction shows the lowest rate of activity at a pH level that is expected to be the most physiologically relevant, since arsenic is believed to be metabolized for the most part in the liver cells where the pH is approximately 7.4. Furthermore, the results show noticeably high K_m values at all three pH levels (**Figure 5.7**). Despite this, *E. coli* ArsC and Acr2p also demonstrate pH activity profiles that are optimal at acidic pH (6.3-6.8), and these enzymes have been shown to be physiologically relevant for these organisms (see section 5.2.1). Furthermore, the bacterial arsenate reductases also demonstrate high K_m values for arsenate (8-35 mM), suggesting *in vivo* experiments will be required to more accurately determine the actual physiological significance of Grx-1 catalyzed arsenic reduction.

The methylation of arsenic is believed to be important for the metabolism of arsenic in many mammals, including humans. The existence of several enzymes that can reduce methylated arsenic species *in vitro* might suggest that the methylation of arsenic to MMA-5 or DMA-5 may facilitate the reduction of these compounds *in vivo*, and could assist in their secretion or detoxification. Methyl- or dimethylation of arsenic makes this compound a better substrate for redox enzymes which can "moonlight" as organoarsenic reductases and this list already includes at least three enzymes (GSTO-1, GSTO-2 and Grxs). Thus, several enzymes, and molecules such as GSH, may potentially act in tandem to provide this function and other redox enzymes might also have monomethyl or dimethylarsenate reductase activities that remain to be discovered.

5.3.8 A potential role for glutaredoxin in the prevention or progression of neurodegenerative diseases

Ascorbic acid is an important antioxidant in the brain and accordingly the brain has the highest concentration of this molecule, which localizes to the brain as DHA where it is then reduced (Rice, 2000; Fornai *et al.*, 1999; Fornai *et al.*, 2001). GSTO-1 and GSTO-2 are mammalian enzymes that, in addition to their MMA-5 and DMA-5 reductase activities, have both been shown to have significant DHA reductase activity (Schmuck *et al.*, 2005). Using a combination of allelic association and gene expression studies, both GSTO-1 and GSTO-2 were shown to be significantly associated with age-at-onset of Parkinson's (PD) and Alzheimer's disease (AD) (Li *et al.*, 2003; Whitbread *et al.*, 2003; Kolsch *et al.*, 2004). Since oxidative stress has been implicated in the pathogenesis of both of these diseases, the importance of GSTO enzymes to maintain an adequate basal supply of ascorbic acid in order to prevent onset of these neurodegenerative diseases must be recognized (Schmuck *et al.*, 2005). Human Grx-1 expression levels have also been shown to be dramatically increased in AD brains and thus the role of Grx-1 in the prevention or progression (see below) of neurodegenerative diseases must also be further evaluated (Akterin *et al.*, 2006).

The brain is sensitive to arsenic exposure and recent evidence has indicated that arsenite is methylated to MMA and DMA within the brain (Rodriguez *et al.*, 2005). Exposure to arsenic compounds has been shown to cause impairments of learning and memory in both children and adults as well as peripheral neuropathies that commonly occur weeks or months after initial exposure (Bolla-Wilson and Bleecker, 1987; Yip *et al.*, 2002; Tsai *et al.*, 2003; Hafeman *et al.*, 2005). Significantly lower nerve conduction

velocities in peripheral nerves of patients exposed to arsenic has been proposed to be due to changes in cytoskeleton composition leading to axonal degeneration (Le Quesne and McLeod, 1977; Tseng et al., 2006; Vahidnia et al., 2007). Furthermore, the use of arsenic trioxide to treat APL often results in severe neurotoxicity (Yip et al., 2002; Lazo et al., 2003).

Metals such as copper, zinc, and iron are concentrated in the neocortex of the brain and changes in the homeostasis of these metals are suspected to contribute to the neuropathology of AD (Lovell et al., 1998; Huang et al., 2004; Liu et al., 2006). Interestingly, the product of the DMA-5 reduction reaction, DMA-3, has been shown to cause the release of iron from ferritin purified from horse spleen and human liver, at a rate much higher than other arsenic metabolites (Ahmad et al., 2000). As well, it is known that brain ferritin iron accumulations increase with age and are also abnormally elevated in the brains of AD and PD patients (Bartzokis et al., 2004; Bartzokis et al., 2007). Iron released from ferritin subunits that are synthesized in the neuronal cell body can lead to oxidative damage and deterioration of components of the axon such as neurofilaments (LaVaute et al., 2001; Rouault, 2001). Taken together, it is interesting to speculate that the ability of human Grx-1 to act as a reducing agent for DMA-5 and thus promote the production of DMA-3, could lead to a bioactivation process that contributes to the progression of neurodegenerative diseases.

5.4 Conclusions

The results of the enzyme kinetics presented here demonstrated DMA-5 reductase activity of several Grxs including human Grx-1, suggesting this activity is common to many Grxs. Mechanistically, Grx catalyzed reduction of DMA-5 demonstrates properties similar to the proposed DHA mechanism, although a mechanism similar to that of *E. coli* ArsC is also plausible. The ability of Grx to more effectively reduce DMA-5 than MMA-5 and AsV supports the hypothesis that methylation facilitates the reduction and metabolism of arsenic species in mammals. The role of another mammalian arsenic reductase, GSTO, in the progression or prevention of neurodegenerative diseases has already been demonstrated, and these results point to an analogous role for Grx. Although the brain is the most aerobically active organ in the body and must maintain a tightly regulated oxidative balance, the role of Grx in this organ and its role in neurodegenerative diseases is largely unknown and thus demands further analysis.

CHAPTER VI

GENERAL SUMMARY & CONCLUSIONS

Protein crystallography is a method used to visually investigate protein structures at the atomic level in order to further understand biological processes. The ways in which proteins catalyze reactions and interact with different molecules can be studied at the most basic level using protein crystallography and this method becomes even more powerful when combined with functional studies. The work presented within this thesis demonstrates how protein crystallography can be used to both test hypotheses and to generate new hypotheses based on the findings of structural analysis. In addition, these results demonstrate how the study of similar proteins in otherwise dissimilar organisms not only furthers our understanding of protein evolution, but can also lead to new and unanticipated discoveries.

Poxviral enzymes acquired by HGT from their hosts were predicted to undergo viral specific adaptations as a result of the differences between the poxviral and mammalian lifecycles. A preliminary analysis of the viral sequences demonstrated intriguing evidence of these adaptations, through the loss of N- and C-terminal regions that have been shown to be required for regulation or degradation for the mammalian homologues of these enzymes. Another potential viral adaptation observed from sequence analyses was the replacement of non-catalytic cysteine residues that are conserved in many mammalian and bacterial Grx sequences, and that are also believed to play a regulatory role in these enzymes. However, since the full scope of protein evolution is seldom evident from sequence analysis alone, an analysis of these enzymes at the structural level would be required to more thoroughly investigate evidence of

viral adaptations.

A set of poxviral enzymes involved in nucleotide metabolism was targeted for structural analysis, since this group of proteins shows strong evidence of HGT and enzymes involved in nucleotide metabolism have also been shown to be effective targets for anticancer and antiviral strategies. Moreover, since the physical processes that lead to crystallization of proteins are not well understood and often vary substantially for different proteins, the targeting of several enzymes was performed in order to increase chances of obtaining crystal structures.

The screening of targets was narrowed down until focus was primarily on the poxviral Grx-1, EVM053, and this structure was solved in the reduced, oxidized and dimethylarsenylated states. By solving the EVM053 structure in different conformations, it allowed the ability to more effectively probe for residues that play a role in poxviral Grx catalysis and substrate specificity that would be difficult to detect through other biochemical methods. Comparisons of the poxviral structures to other known mammalian or bacterial Grx structures also promoted the generation of structure-based hypotheses that were further investigated using mutagenesis combined with functional studies.

Functional studies were used to both validate structure-based hypotheses and to further explore structural findings. The proposed redox-sensitive movement of Tyr21 was first validated by mutating this residue to a tryptophan and then measuring changes in protein fluorescence intensity in the presence of reducing and oxidizing agents. In addition to the biological significance of this finding, it also carries practical

implications since the Y21W mutant can be used to measure enzyme activity and presents a novel assay for future experiments. While the initial structural analysis suggested that the structural rearrangement of Tyr21 enhanced the stabilization of the reduced form over the oxidized form of the protein, functional studies in combination with mutagenesis suggested that the movement of this residue also enhances the formation of Grx-SG mixed disulfides. A similar approach was also used to evaluate the role of *cis*-Pro53 in substrate interactions with RNR R1.

The EVM053 structures represented the first example where high resolution crystal structures of both the reduced and oxidized states of a Grx have been determined. Furthermore, the unanticipated observation of a dimethylarsenylated active site cysteine in one of the EVM053 structures resulted in the discovery that Grxs can act as DMA-5 reductases. Enzyme kinetics demonstrated this activity for several Grxs including human Grx-1, and the ability of Grxs to more effectively reduce DMA-5 than MMA-5 and AsV supports the hypothesis that methylation facilitates the metabolism of arsenic in mammals.

Viral specific adaptations that appear to have evolved to promote interactions with GSH and RNR R1 have provided new insight into the molecular mechanisms of Grx function and evolution. While this work shows a high level of sequence and structural conservation between EVM053 and the known mammalian Grx-1 structures, discrete differences between the structures may reflect significant evolutionary adaptations to the viral life cycle that could be exploited for the development of antiviral therapeutics. The results of this thesis delineate features that are virus-specific adaptations and also expand our understanding of Grxs in general. The previously unrecognized role of Grxs

144

as catalysts of dimethylarsenate reduction may be of particular significance for populations exposed to high levels of arsenic or for patients that receive arsenic for chemotherapeutic purposes.

Bibliography

Afonso, C. L., Tulman, E. R., Delhon, G., Lu, Z., Viljoen, G. J., Wallace, D. B. et al. (2006). Genome of crocodilepox virus. *J Virol, 80*(10), 4978-4991.

Ahmad, S., Kitchin, K. T., & Cullen, W. R. (2000). Arsenic species that cause release of iron from ferritin and generation of activated oxygen. *Arch Biochem Biophys, 382*(2), 195-202.

Ahn, B. Y. & Moss, B. (1992). Glutaredoxin homolog encoded by vaccinia virus is a virion-associated enzyme with thioltransferase and dehydroascorbate reductase activities. *Proc Natl Acad Sci U S A, 89*(15), 7060-7064.

Akterin, S., Cowburn, R. F., Miranda-Vizuete, A., Jimenez, A., Bogdanovic, N., Winblad, B. et al. (2006). Involvement of glutaredoxin-1 and thioredoxin-1 in beta-amyloid toxicity and Alzheimer's disease. *Cell Death Differ, 13*(9), 1454-1465.

Allen, J. R., Reddy, G. P., Lasser, G. W., & Mathews, C. K. (1980). T4 ribonucleotide reductase. Physical and kinetic linkage to other enzymes of deoxyribonucleotide biosynthesis. *J Biol Chem, 255*(16), 7583-7588.

Andrew, A. S., Burgess, J. L., Meza, M. M., Demidenko, E., Waugh, M. G., Hamilton, J. W. et al. (2006). Arsenic exposure is associated with decreased DNA repair in vitro and in individuals exposed to drinking water arsenic. *Environ Health Perspect, 114*(8), 1193-1198.

Aposhian, H. V. (1997). Enzymatic methylation of arsenic species and other new approaches to arsenic toxicity. *Annu Rev Pharmacol Toxicol, 37*, 397-419.

Aposhian, H. V., Gurzau, E. S., Le, X. C., Gurzau, A., Healy, S. M., Lu, X. et al. (2000). Occurrence of monomethylarsonous acid in urine of humans exposed to inorganic arsenic. *Chem Res Toxicol, 13*(8), 693-697.

Armstrong, R. N. (1997). Structure, catalytic mechanism, and evolution of the glutathione transferases. *Chem Res Toxicol, 10*(1), 2-18.

Aslund, F., Ehn, B., Miranda-Vizuete, A., Pueyo, C., & Holmgren, A. (1994). Two additional glutaredoxins exist in Escherichia coli: glutaredoxin 3 is a hydrogen donor for ribonucleotide reductase in a thioredoxin/glutaredoxin 1 double mutant. *Proc Natl Acad Sci U S A, 91*(21), 9813-9817.

Aslund, F., Berndt, K. D., & Holmgren, A. (1997). Redox potentials of glutaredoxins and other thiol-disulfide oxidoreductases of the thioredoxin superfamily

determined by direct protein-protein redox equilibria. *J Biol Chem, 272*(49), 30780-30786.

Audette, G. F., Irvin, R. T., & Hazes, B. (2003). Purification, crystallization and preliminary diffraction studies of the Pseudomonas aeruginosa strain K122-4 monomeric pilin. *Acta Crystallogr D Biol Crystallogr, 59*(Pt 9), 1665-1667.

Ayers, P. W., Parr, R. G., & Pearson, R. G. (2006). Elucidating the hard/soft acid/base principle: a perspective based on half-reactions. *J Chem Phys, 124*(19), 194107.

Bach, R. D., Dmitrenko, O., & Thorpe, C. (2008). Mechanism of thiolate-disulfide interchange reactions in biochemistry. *J Org Chem, 73*(1), 12-21.

Bacik, J. P., Brigley, A. M., Channon, L. D., Audette, G. F., & Hazes, B. (2005). Purification, crystallization and preliminary diffraction studies of an ectromelia virus glutaredoxin. *Acta Crystallograph Sect F Struct Biol Cryst Commun, 61*(Pt 6), 550-552.

Bacik, J. P. & Hazes, B. (2007). Crystal structures of a poxviral glutaredoxin in the oxidized and reduced states show redox-correlated structural changes. *J Mol Biol, 365*(5), 1545-1558.

Balassu, T. C. & Robinson, A. J. (1987). Orf virus replication in bovine testis cells: kinetics of viral DNA, polypeptide, and infectious virus production and analysis of virion polypeptides. *Arch Virol, 97*(3-4), 267-281.

Bandyopadhyay, S., Starke, D. W., Mieyal, J. J., & Gronostajski, R. M. (1998). Thioltransferase (glutaredoxin) reactivates the DNA-binding activity of oxidation-inactivated nuclear factor I. *J Biol Chem, 273*(1), 392-397.

Barrett, W. C., DeGnore, J. P., Konig, S., Fales, H. M., Keng, Y. F., Zhang, Z. Y. et al. (1999). Regulation of PTP1B via glutathionylation of the active site cysteine 215. *Biochemistry, 38*(20), 6699-6705.

Bartzokis, G., Tishler, T. A., Lu, P. H., Villablanca, P., Altshuler, L. L., Carter, M. et al. (2007). Brain ferritin iron may influence age- and gender-related risks of neurodegeneration. *Neurobiol Aging, 28*(3), 414-423.

Bartzokis, G., Tishler, T. A., Shin, I. S., Lu, P. H., & Cummings, J. L. (2004). Brain ferritin iron as a risk factor for age at onset in neurodegenerative diseases. *Ann N Y Acad Sci, 1012*, 224-236.

Bates, M. N., Smith, A. H., & Hopenhayn-Rich, C. (1992). Arsenic ingestion and internal cancers: a review. *Am J Epidemiol, 135*(5), 462-476.

Beer, S. M., Taylor, E. R., Brown, S. E., Dahm, C. C., Costa, N. J., Runswick, M. J. et al. (2004). Glutaredoxin 2 catalyzes the reversible oxidation and glutathionylation

of mitochondrial membrane thiol proteins: implications for mitochondrial redox regulation and antioxidant DEFENSE. *J Biol Chem, 279*(46), 47939-47951.

Berardi, M. J. & Bushweller, J. H. (1999). Binding specificity and mechanistic insight into glutaredoxin-catalyzed protein disulfide reduction. *J Mol Biol, 292*(1), 151-161.

Berche, P. (2001). The threat of smallpox and bioterrorism. *Trends Microbiol, 9*(1), 15-18.

Berenson, J. R. & Yeh, H. S. (2006). Arsenic compounds in the treatment of multiple myeloma: a new role for a historical remedy. *Clin Lymphoma Myeloma, 7*(3), 192-198.

Bergfors, T. (2003). Seeds to crystals. *J Struct Biol, 142*(1), 66-76.

Birringer, M. S., Claus, M. T., Folkers, G., Kloer, D. P., Schulz, G. E., & Scapozza, L. (2005). Structure of a type II thymidine kinase with bound dTTP. *FEBS Lett, 579*(6), 1376-1382.

Bisacchi, D., Zhou, Y., Rosen, B. P., Mukhopadhyay, R., & Bordo, D. (2006). Crystallization and preliminary crystallographic characterization of LmACR2, an arsenate/antimonate reductase from Leishmania major. *Acta Crystallogr Sect F Struct Biol Cryst Commun, 62*(Pt 10), 976-979.

Black, M. E. & Hruby, D. E. (1990). Quaternary structure of vaccinia virus thymidine kinase. *Biochem Biophys Res Commun, 169*(3), 1080-1086.

Black, M. E. & Hruby, D. E. (1992). Site-directed mutagenesis of a conserved domain in vaccinia virus thymidine kinase. Evidence for a potential role in magnesium binding. *J Biol Chem, 267*(10), 6801-6806.

Bolla-Wilson, K. & Bleecker, M. L. (1987). Neuropsychological impairment following inorganic arsenic exposure. *J Occup Med, 29*(6), 500-503.

Bordo, D., Deriu, D., Colnaghi, R., Carpen, A., Pagani, S., & Bolognesi, M. (2000). The crystal structure of a sulfurtransferase from Azotobacter vinelandii highlights the evolutionary relationship between the rhodanese and phosphatase enzyme families. *J Mol Biol, 298*(4), 691-704.

Boyle, K. A., Arps, L., & Traktman, P. (2007). Biochemical and genetic analysis of the vaccinia virus d5 protein: Multimerization-dependent ATPase activity is required to support viral DNA replication. *J Virol, 81*(2), 844-859.

Bratke, K. A. & McLysaght, A. (2008). Identification of multiple independent horizontal gene transfers into poxviruses using a comparative genomics approach. *BMC Evol Biol, 8*, 67.

Broyles, S. S. (1993). Vaccinia virus encodes a functional dUTPase. *Virology, 195*(2), 863-865.

Broyles, S. S. (2003). Vaccinia virus transcription. *J Gen Virol, 84*(Pt 9), 2293-2303.

Buchet, J. P. & Lauwerys, R. (1988). Role of thiols in the in-vitro methylation of inorganic arsenic by rat liver cytosol. *Biochem Pharmacol, 37*(16), 3149-3153.

Bugert, J. J. & Darai, G. (1997). Recent advances in molluscum contagiosum virus research. *Arch Virol Suppl, 13*, 35-47.

Bugert, J. J. & Darai, G. (2000). Poxvirus homologues of cellular genes. *Virus Genes, 21*(1-2), 111-133.

Buller, R. M., Smith, G. L., Cremer, K., Notkins, A. L., & Moss, B. (1985). Decreased virulence of recombinant vaccinia virus expression vectors is associated with a thymidine kinase-negative phenotype. *Nature, 317*(6040), 813-815.

Burmeister, W. P. (2000). Structural changes in a cryo-cooled protein crystal owing to radiation damage. *Acta Crystallogr D Biol Crystallogr, 56*(Pt 3), 328-341.

Bushweller, J. H., Billeter, M., Holmgren, A., & Wuthrich, K. (1994). The nuclear magnetic resonance solution structure of the mixed disulfide between Escherichia coli glutaredoxin(C14S) and glutathione. *J Mol Biol, 235*(5), 1585-1597.

Bushweller, J. H., Aslund, F., Wuthrich, K., & Holmgren, A. (1992). Structural and functional characterization of the mutant Escherichia coli glutaredoxin (C14----S) and its mixed disulfide with glutathione. *Biochemistry, 31*(38), 9288-9293.

Buzdin, A. (2007). Human-specific endogenous retroviruses. *ScientificWorldJournal, 7*, 1848-1868.

Caradonna, S. & Muller-Weeks, S. (2001). The nature of enzymes involved in uracil-DNA repair: isoform characteristics of proteins responsible for nuclear and mitochondrial genomic integrity. *Curr Protein Pept Sci, 2*(4), 335-347.

Casadei, M., Persichini, T., Polticelli, F., Musci, G., & Colasanti, M. (2008). S-Glutathionylation of metallothioneins by nitrosative/oxidative stress. *Exp Gerontol, 43*(5), 415-422.

Cerqueira, N. M., Fernandes, P. A., Eriksson, L. A., & Ramos, M. J. (2006). Dehydration of ribonucleotides catalyzed by ribonucleotide reductase: the role of the enzyme. *Biophys J, 90*(6), 2109-2119.

Cerqueira, N. M., Fernandes, P. A., & Ramos, M. J. (2007). Ribonucleotide reductase: a critical enzyme for cancer chemotherapy and antiviral agents. *Recent Patents Anticancer Drug Discov, 2*(1), 11-29.

Chabes, A. L., Pfleger, C. M., Kirschner, M. W., & Thelander, L. (2003). Mouse ribonucleotide reductase R2 protein: a new target for anaphase-promoting complex-Cdh1-mediated proteolysis. *Proc Natl Acad Sci U S A, 100*(7), 3925-3929.

Chan, S., Segelke, B., Lekin, T., Krupka, H., Cho, U. S., Kim, M. Y. et al. (2004). Crystal structure of the Mycobacterium tuberculosis dUTPase: insights into the catalytic mechanism. *J Mol Biol, 341*(2), 503-517.

Chen, R., Wang, H., & Mansky, L. M. (2002). Roles of uracil-DNA glycosylase and dUTPase in virus replication. *J Gen Virol, 83*(Pt 10), 2339-2345.

Chen, Z., Chen, G. Q., Shen, Z. X., Sun, G. L., Tong, J. H., Wang, Z. Y. et al. (2002b). Expanding the use of arsenic trioxide: leukemias and beyond. *Semin Hematol, 39*(2 Suppl 1), 22-26.

Child, S. J., Palumbo, G. J., Buller, R. M., & Hruby, D. E. (1990). Insertional inactivation of the large subunit of ribonucleotide reductase encoded by vaccinia virus is associated with reduced virulence in vivo. *Virology, 174*(2), 625-629.

Chiu, C. S., Cook, K. S., & Greenberg, G. R. (1982). Characteristics of a bacteriophage T4-induced complex synthesizing deoxyribonucleotides. *J Biol Chem, 257*(24), 15087-15097.

Chou, W. C. & Dang, C. V. (2005). Acute promyelocytic leukemia: recent advances in therapy and molecular basis of response to arsenic therapies. *Curr Opin Hematol, 12*(1), 1-6.

Chouchane, S. & Snow, E. T. (2001). In vitro effect of arsenical compounds on glutathione-related enzymes. *Chem Res Toxicol, 14*(5), 517-522.

Chowdhury, U. K., Zakharyan, R. A., Hernandez, A., Avram, M. D., Kopplin, M. J., & Aposhian, H. V. (2006). Glutathione-S-transferase-omega [MMA(V) reductase] knockout mice: enzyme and arsenic species concentrations in tissues after arsenate administration. *Toxicol Appl Pharmacol, 216*(3), 446-457.

Condit, R. C., Moussatche, N., & Traktman, P. (2006). In a nutshell: structure and assembly of the vaccinia virion. *Adv Virus Res, 66*, 31-124.

Conway, M. E., Yennawar, N., Wallin, R., Poole, L. B., & Hutson, S. M. (2002). Identification of a peroxide-sensitive redox switch at the CXXC motif in the human mitochondrial branched chain aminotransferase. *Biochemistry, 41*(29), 9070-9078.

Cosentino, G., Lavallee, P., Rakhit, S., Plante, R., Gaudette, Y., Lawetz, C. et al. (1991). Specific inhibition of ribonucleotide reductases by peptides corresponding to the C-terminal of their second subunit. *Biochem Cell Biol, 69*(1), 79-83.

Cui, X., Kobayashi, Y., Hayakawa, T., & Hirano, S. (2004). Arsenic speciation in bile and urine following oral and intravenous exposure to inorganic and organic arsenics in rats. *Toxicol Sci, 82*(2), 478-487.

Dalle-Donne, I., Rossi, R., Giustarini, D., Colombo, R., & Milzani, A. (2007). S-glutathionylation in protein redox regulation. *Free Radic Biol Med, 43*(6), 883-898.

Darby, N. J. & Creighton, T. E. (1995). Characterization of the active site cysteine residues of the thioredoxin-like domains of protein disulfide isomerase. *Biochemistry*, *34*(51), 16770-16780.

Dauter, Z., Persson, R., Rosengren, A. M., Nyman, P. O., Wilson, K. S., & Cedergren-Zeppezauer, E. S. (1999). Crystal structure of dUTPase from equine infectious anaemia virus; active site metal binding in a substrate analogue complex. *J Mol Biol*, *285*(2), 655-673.

Davis, D. A., Newcomb, F. M., Starke, D. W., Ott, D. E., Mieyal, J. J., & Yarchoan, R. (1997). Thioltransferase (glutaredoxin) is detected within HIV-1 and can regulate the activity of glutathionylated HIV-1 protease in vitro. *J Biol Chem*, *272*(41), 25935-25940.

Davis, R. E. & Mathews, C. K. (1993). Acidic C terminus of vaccinia virus DNA-binding protein interacts with ribonucleotide reductase. *Proc Natl Acad Sci U S A*, *90*(2), 745-749.

Davis, R. E. (1992). Oregon State University, Corvallis, OR.

De Clercq, E. (2003). Clinical potential of the acyclic nucleoside phosphonates cidofovir, adefovir, and tenofovir in treatment of DNA virus and retrovirus infections. *Clin Microbiol Rev*, *16*(4), 569-596.

De Silva, F. S., Lewis, W., Berglund, P., Koonin, E. V., & Moss, B. (2007). Poxvirus DNA primase. *Proc Natl Acad Sci U S A*, *104*(47), 18724-18729.

De Silva, F. S. & Moss, B. (2003). Vaccinia virus uracil DNA glycosylase has an essential role in DNA synthesis that is independent of its glycosylase activity: catalytic site mutations reduce virulence but not virus replication in cultured cells. *J Virol*, *77*(1), 159-166.

Delnomdedieu, M., Basti, M. M., Otvos, J. D., & Thomas, D. J. (1994). Reduction and binding of arsenate and dimethylarsinate by glutathione: a magnetic resonance study. *Chem Biol Interact*, *90*(2), 139-155.

DeMel, S., Shi, J., Martin, P., Rosen, B. P., & Edwards, B. F. (2004). Arginine 60 in the ArsC arsenate reductase of E. coli plasmid R773 determines the chemical nature of the bound As(III) product. *Protein Sci*, *13*(9), 2330-2340.

Derewenda, Z. S. (2004). The use of recombinant methods and molecular engineering in protein crystallization. *Methods*, *34*(3), 354-363.

Di Giulio, D. B. & Eckburg, P. B. (2004). Human monkeypox: an emerging zoonosis. *Lancet Infect Dis*, *4*(1), 15-25.

Dietrich, C. G., Ottenhoff, R., de Waart, D. R., & Oude Elferink, R. P. (2001). Role of MRP2 and GSH in intrahepatic cycling of toxins. *Toxicology*, *167*(1), 73-81.

Domi, A. & Beaud, G. (2000). The punctate sites of accumulation of vaccinia virus early proteins are precursors of sites of viral DNA synthesis. *J Gen Virol, 81*(Pt 5), 1231-1235.

Doublie, S., Tabor, S., Long, A. M., Richardson, C. C., & Ellenberger, T. (1998). Crystal structure of a bacteriophage T7 DNA replication complex at 2.2 A resolution. *Nature, 391*(6664), 251-258.

Duan, G. L., Zhou, Y., Tong, Y. P., Mukhopadhyay, R., Rosen, B. P., & Zhu, Y. G. (2007). A CDC25 homologue from rice functions as an arsenate reductase. *New Phytol, 174*(2), 311-321.

Duan, G. L., Zhu, Y. G., Tong, Y. P., Cai, C., & Kneer, R. (2005). Characterization of arsenate reductase in the extract of roots and fronds of Chinese brake fern, an arsenic hyperaccumulator. *Plant Physiol, 138*(1), 461-469.

Dunlop, K. V. & Hazes, B. (2003). When less is more: a more efficient vapour-diffusion protocol. *Acta Crystallogr D Biol Crystallogr, 59*(Pt 10), 1797-1800.

Dyson, H. J., Jeng, M. F., Tennant, L. L., Slaby, I., Lindell, M., Cui, D. S. et al. (1997). Effects of buried charged groups on cysteine thiol ionization and reactivity in Escherichia coli thioredoxin: structural and functional characterization of mutants of Asp 26 and Lys 57. *Biochemistry, 36*(9), 2622-2636.

Eklund, H., Ingelman, M., Soderberg, B. O., Uhlin, T., Nordlund, P., Nikkola, M. et al. (1992). Structure of oxidized bacteriophage T4 glutaredoxin (thioredoxin). Refinement of native and mutant proteins. *J Mol Biol, 228*(2), 596-618.

El Omari, K., Solaroli, N., Karlsson, A., Balzarini, J., & Stammers, D. K. (2006). Structure of vaccinia virus thymidine kinase in complex with dTTP: insights for drug design. *BMC Struct Biol, 6*, 22.

Elledge, S. J., Zhou, Z., & Allen, J. B. (1992). Ribonucleotide reductase: regulation, regulation, regulation. *Trends Biochem Sci, 17*(3), 119-123.

Ellis, D. R., Gumaelius, L., Indriolo, E., Pickering, I. J., Banks, J. A., & Salt, D. E. (2006). A novel arsenate reductase from the arsenic hyperaccumulating fern Pteris vittata. *Plant Physiol, 141*(4), 1544-1554.

Ellison, K. S., Peng, W., & McFadden, G. (1996). Mutations in active-site residues of the uracil-DNA glycosylase encoded by vaccinia virus are incompatible with virus viability. *J Virol, 70*(11), 7965-7973.

Engstrom, Y., Eriksson, S., Jildevik, I., Skog, S., Thelander, L., & Tribukait, B. (1985). Cell cycle-dependent expression of mammalian ribonucleotide reductase. Differential regulation of the two subunits. *J Biol Chem, 260*(16), 9114-9116.

Eriksson, M., Uhlin, U., Ramaswamy, S., Ekberg, M., Regnstrom, K., Sjoberg, B. M. et al. (1997). Binding of allosteric effectors to ribonucleotide reductase protein R1:

reduction of active-site cysteines promotes substrate binding. *Structure, 5*(8), 1077-1092.

Eriksson, S., Graslund, A., Skog, S., Thelander, L., & Tribukait, B. (1984). Cell cycle-dependent regulation of mammalian ribonucleotide reductase. The S phase-correlated increase in subunit M2 is regulated by de novo protein synthesis. *J Biol Chem, 259*(19), 11695-11700.

Esposito, J. J., Sammons, S. A., Frace, A. M., Osborne, J. D., Olsen-Rasmussen, M., Zhang, M. et al. (2006). Genome sequence diversity and clues to the evolution of variola (smallpox) virus. *Science, 313*(5788), 807-812.

Evans, E., Klemperer, N., Ghosh, R., & Traktman, P. (1995). The vaccinia virus D5 protein, which is required for DNA replication, is a nucleic acid-independent nucleoside triphosphatase. *J Virol, 69*(9), 5353-5361.

Fauman, E. B., Cogswell, J. P., Lovejoy, B., Rocque, W. J., Holmes, W., Montana, V. G. et al. (1998). Crystal structure of the catalytic domain of the human cell cycle control phosphatase, Cdc25A. *Cell, 93*(4), 617-625.

Fenner, F. (2000). Adventures with poxviruses of vertebrates. *FEMS Microbiol Rev, 24*(2), 123-133.

Fernandes, A. P. & Holmgren, A. (2004). Glutaredoxins: glutathione-dependent redox enzymes with functions far beyond a simple thioredoxin backup system. *Antioxid Redox Signal, 6*(1), 63-74.

Filomeni, G., Aquilano, K., Rotilio, G., & Ciriolo, M. R. (2005). Glutathione-related systems and modulation of extracellular signal-regulated kinases are involved in the resistance of AGS adenocarcinoma gastric cells to diallyl disulfide-induced apoptosis. *Cancer Res, 65*(24), 11735-11742.

Fleming, S. B., Lyttle, D. J., Sullivan, J. T., Mercer, A. A., & Robinson, A. J. (1995). Genomic analysis of a transposition-deletion variant of orf virus reveals a 3.3 kbp region of non-essential DNA. *J Gen Virol, 76*(Pt 12), 2969-2978.

Flora, S. J., Bhadauria, S., Kannan, G. M., & Singh, N. (2007). Arsenic induced oxidative stress and the role of antioxidant supplementation during chelation: a review. *J Environ Biol, 28*(2 Suppl), 333-347.

Foloppe, N. & Nilsson, L. (2004). The glutaredoxin -C-P-Y-C- motif: influence of peripheral residues. *Structure, 12*(2), 289-300.

Foloppe, N. & Nilsson, L. (2007). Stabilization of the catalytic thiolate in a mammalian glutaredoxin: structure, dynamics and electrostatics of reduced pig glutaredoxin and its mutants. *J Mol Biol, 372*(3), 798-816.

Forman-Kay, J. D., Clore, G. M., & Gronenborn, A. M. (1992). Relationship between electrostatics and redox function in human thioredoxin: characterization of pH

titration shifts using two-dimensional homo- and heteronuclear NMR. *Biochemistry, 31*(13), 3442-3452.

Fornai, F., Piaggi, S., Gesi, M., Saviozzi, M., Lenzi, P., Paparelli, A. et al. (2001). Subcellular localization of a glutathione-dependent dehydroascorbate reductase within specific rat brain regions. *Neuroscience, 104*(1), 15-31.

Fornai, F., Saviozzi, M., Piaggi, S., Gesi, M., Corsini, G. U., Malvaldi, G. et al. (1999). Localization of a glutathione-dependent dehydroascorbate reductase within the central nervous system of the rat. *Neuroscience, 94*(3), 937-948.

Freedman, R. B., Brockway, B. E., & Lambert, N. (1984). Protein disulphide-isomerase and the formation of native disulphide bonds. *Biochem Soc Trans, 12*(6), 929-932.

Gao, Y., Pei, Q. L., Li, G. X., Han, G., Tian, F. J., Qin, X. J. et al. (2006). [Effects of MRP2-GSH cotransport system on hepatic arsenic metabolism in rats]. *Zhonghua Lao Dong Wei Sheng Zhi Ye Bing Za Zhi, 24*(5), 278-280.

Gilbert, H. F. (1984). Redox control of enzyme activities by thiol/disulfide exchange. *Methods Enzymol, 107*, 330-351.

Gilbert, H. F. (1995). Thiol/disulfide exchange equilibria and disulfide bond stability. *Methods Enzymol, 251*, 8-28.

Gladysheva, T., Liu, J., & Rosen, B. P. (1996). His-8 lowers the pKa of the essential Cys-12 residue of the ArsC arsenate reductase of plasmid R773. *J Biol Chem, 271*(52), 33256-33260.

Gladysheva, T. B., Oden, K. L., & Rosen, B. P. (1994). Properties of the arsenate reductase of plasmid R773. *Biochemistry, 33*(23), 7288-7293.

Gravina, S. A. & Mieyal, J. J. (1993). Thioltransferase is a specific glutathionyl mixed disulfide oxidoreductase. *Biochemistry, 32*(13), 3368-3376.

Gubser, C., Hue, S., Kellam, P., & Smith, G. L. (2004). Poxvirus genomes: a phylogenetic analysis. *J Gen Virol, 85*(Pt 1), 105-117.

Guddat, L. W., Bardwell, J. C., Glockshuber, R., Huber-Wunderlich, M., Zander, T., & Martin, J. L. (1997). Structural analysis of three His32 mutants of DsbA: support for an electrostatic role of His32 in DsbA stability. *Protein Sci, 6*(9), 1893-1900.

Guddat, L. W., Bardwell, J. C., & Martin, J. L. (1998). Crystal structures of reduced and oxidized DsbA: investigation of domain motion and thiolate stabilization. *Structure, 6*(6), 757-767.

Gvakharia, B. O., Koonin, E. K., & Mathews, C. K. (1996). Vaccinia virus G4L gene encodes a second glutaredoxin. *Virology, 226*(2), 408-411.

154

Hafeman, D. M., Ahsan, H., Louis, E. D., Siddique, A. B., Slavkovich, V., Cheng, Z. et al. (2005). Association between arsenic exposure and a measure of subclinical sensory neuropathy in Bangladesh. *J Occup Environ Med*, *47*(8), 778-784.

Han, Y. H., Kim, S. H., Kim, S. Z., & Park, W. H. (2008). Apoptosis in arsenic trioxide-treated Calu-6 lung cells is correlated with the depletion of GSH levels rather than the changes of ROS levels. *J Cell Biochem*.

Hawkes, N. (1979). Smallpox death in Britain challenges presumption of laboratory safety. *Science*, *203*(4383), 855-856.

Hayakawa, T., Kobayashi, Y., Cui, X., & Hirano, S. (2005). A new metabolic pathway of arsenite: arsenic-glutathione complexes are substrates for human arsenic methyltransferase Cyt19. *Arch Toxicol*, *79*(4), 183-191.

Hazes, B., Sastry, P. A., Hayakawa, K., Read, R. J., & Irvin, R. T. (2000). Crystal structure of Pseudomonas aeruginosa PAK pilin suggests a main-chain-dominated mode of receptor binding. *J Mol Biol*, *299*(4), 1005-1017.

Hazes, B. & Dijkstra, B. W. (1988). Model building of disulfide bonds in proteins with known three-dimensional structure. *Protein Eng*, *2*(2), 119-125.

Healy, S. M., Casarez, E. A., Ayala-Fierro, F., & Aposhian, H. (1998). Enzymatic methylation of arsenic compounds. V. Arsenite methyltransferase activity in tissues of mice. *Toxicol Appl Pharmacol*, *148*(1), 65-70.

Healy, S. M., Wildfang, E., Zakharyan, R. A., & Aposhian, H. V. (1999). Diversity of inorganic arsenite biotransformation. *Biol Trace Elem Res*, *68*(3), 249-266.

Hirata, M., Tanaka, A., Hisanaga, A., & Ishinishi, N. (1990). Effects of glutathione depletion on the acute nephrotoxic potential of arsenite and on arsenic metabolism in hamsters. *Toxicol Appl Pharmacol*, *106*(3), 469-481.

Hofmann, K., Bucher, P., & Kajava, A. V. (1998). A model of Cdc25 phosphatase catalytic domain and Cdk-interaction surface based on the presence of a rhodanese homology domain. *J Mol Biol*, *282*(1), 195-208.

Holm, L. & Park, J. (2000). DaliLite workbench for protein structure comparison. *Bioinformatics*, *16*(6), 566-567.

Holmgren, A. (1972). Tryptophan fluorescence study of conformational transitions of the oxidized and reduced form of thioredoxin. *J Biol Chem*, *247*(7), 1992-1998.

Holmgren, A. (1976). Hydrogen donor system for Escherichia coli ribonucleoside-diphosphate reductase dependent upon glutathione. *Proc Natl Acad Sci U S A*, *73*(7), 2275-2279.

Holmgren, A. (1979). Glutathione-dependent synthesis of deoxyribonucleotides. Purification and characterization of glutaredoxin from Escherichia coli. *J Biol Chem*, *254*(9), 3664-3671.

Hopper, S., Johnson, R. S., Vath, J. E., & Biemann, K. (1989). Glutaredoxin from rabbit bone marrow. Purification, characterization, and amino acid sequence determined by tandem mass spectrometry. *J Biol Chem, 264*(34), 20438-20447.

Hruby, D. E. (1985). Inhibition of vaccinia virus thymidine kinase by the distal products of its own metabolic pathway. *Virus Res, 2*(2), 151-156.

Hruby, D. E., Maki, R. A., Miller, D. B., & Ball, L. A. (1983). Fine structure analysis and nucleotide sequence of the vaccinia virus thymidine kinase gene. *Proc Natl Acad Sci U S A, 80*(11), 3411-3415.

Huang, S. H., Tang, A., Drisco, B., Zhang, S. Q., Seeger, R., Li, C. et al. (1994). Human dTMP kinase: gene expression and enzymatic activity coinciding with cell cycle progression and cell growth. *DNA Cell Biol, 13*(5), 461-471.

Huang, X., Moir, R. D., Tanzi, R. E., Bush, A. I., & Rogers, J. T. (2004). Redox-active metals, oxidative stress, and Alzheimer's disease pathology. *Ann N Y Acad Sci, 1012*, 153-163.

Hughes, A. L. & Friedman, R. (2005). Poxvirus genome evolution by gene gain and loss. *Mol Phylogenet Evol, 35*(1), 186-195.

Hughes, S. J., Johnston, L. H., de Carlos, A., & Smith, G. L. (1991). Vaccinia virus encodes an active thymidylate kinase that complements a cdc8 mutant of Saccharomyces cerevisiae. *J Biol Chem, 266*(30), 20103-20109.

Ishmael, F. T., Trakselis, M. A., & Benkovic, S. J. (2003). Protein-protein interactions in the bacteriophage T4 replisome. The leading strand holoenzyme is physically linked to the lagging strand holoenzyme and the primosome. *J Biol Chem, 278*(5), 3145-3152.

Iyer, L. M., Aravind, L., & Koonin, E. V. (2001). Common origin of four diverse families of large eukaryotic DNA viruses. *J Virol, 75*(23), 11720-11734.

Iyer, L. M., Balaji, S., Koonin, E. V., & Aravind, L. (2006). Evolutionary genomics of nucleo-cytoplasmic large DNA viruses. *Virus Res, 117*(1), 156-184.

Jao, S. C., English Ospina, S. M., Berdis, A. J., Starke, D. W., Post, C. B., & Mieyal, J. J. (2006). Computational and mutational analysis of human glutaredoxin (thioltransferase): probing the molecular basis of the low pKa of cysteine 22 and its role in catalysis. *Biochemistry, 45*(15), 4785-4796.

Johansson, C., Kavanagh, K. L., Gileadi, O., & Oppermann, U. (2007). Reversible sequestration of active site cysteines in a 2Fe-2S-bridged dimer provides a mechanism for glutaredoxin 2 regulation in human mitochondria. *J Biol Chem, 282*(5), 3077-3082.

Johansson, C., Lillig, C. H., & Holmgren, A. (2004). Human mitochondrial glutaredoxin reduces S-glutathionylated proteins with high affinity accepting electrons from either glutathione or thioredoxin reductase. *J Biol Chem, 279*(9), 7537-7543.

156

Johnson, G. P., Goebel, S. J., Perkus, M. E., Davis, S. W., Winslow, J. P., & Paoletti, E. (1991). Vaccinia virus encodes a protein with similarity to glutaredoxins. *Virology*, *181*(1), 378-381.

Jones, D. P., Go, Y. M., Anderson, C. L., Ziegler, T. R., Kinkade, J. M. J., & Kirlin, W. G. (2004). Cysteine/cystine couple is a newly recognized node in the circuitry for biologic redox signaling and control. *FASEB J*, *18*(11), 1246-1248.

Jung, C. H. & Thomas, J. A. (1996). S-glutathiolated hepatocyte proteins and insulin disulfides as substrates for reduction by glutaredoxin, thioredoxin, protein disulfide isomerase, and glutathione. *Arch Biochem Biophys*, *335*(1), 61-72.

Kapust, R. B. & Waugh, D. S. (1999). Escherichia coli maltose-binding protein is uncommonly effective at promoting the solubility of polypeptides to which it is fused. *Protein Sci*, *8*(8), 1668-1674.

Kashlan, O. B. & Cooperman, B. S. (2003). Comprehensive model for allosteric regulation of mammalian ribonucleotide reductase: refinements and consequences. *Biochemistry*, *42*(6), 1696-1706.

Kasrayan, A., Birgander, P. L., Pappalardo, L., Regnstrom, K., Westman, M., Slaby, A. et al. (2004). Enhancement by effectors and substrate nucleotides of R1-R2 interactions in Escherichia coli class Ia ribonucleotide reductase. *J Biol Chem*, *279*(30), 31050-31057.

Katsafanas, G. C. & Moss, B. (2007). Colocalization of transcription and translation within cytoplasmic poxvirus factories coordinates viral expression and subjugates host functions. *Cell Host Microbe*, *2*(4), 221-228.

Katti, S. K., Robbins, A. H., Yang, Y., & Wells, W. W. (1995). Crystal structure of thioltransferase at 2.2 A resolution. *Protein Sci*, *4*(10), 1998-2005.

Kauffman, M. G. & Kelly, T. J. (1991). Cell cycle regulation of thymidine kinase: residues near the carboxyl terminus are essential for the specific degradation of the enzyme at mitosis. *Mol Cell Biol*, *11*(5), 2538-2546.

Kauffman, M. G., Rose, P. A., & Kelly, T. J. (1991). Mutations in the thymidine kinase gene that allow expression of the enzyme in quiescent (G0) cells. *Oncogene*, *6*(8), 1427-1435.

Kauppi, B., Nielsen, B. B., Ramaswamy, S., Larsen, I. K., Thelander, M., Thelander, L. et al. (1996). The three-dimensional structure of mammalian ribonucleotide reductase protein R2 reveals a more-accessible iron-radical site than Escherichia coli R2. *J Mol Biol*, *262*(5), 706-720.

Kavli, B., Otterlei, M., Slupphaug, G., & Krokan, H. E. (2007). Uracil in DNA--general mutagen, but normal intermediate in acquired immunity. *DNA Repair (Amst)*, *6*(4), 505-516.

Kawalek, A. & Rudikoff, D. (2002). A spotlight on smallpox. *Clin Dermatol*, *20*(4), 376-387.

Kim, J., Shen, R., Olcott, M. C., Rajagopal, I., & Mathews, C. K. (2005). Adenylate kinase of Escherichia coli, a component of the phage T4 dNTP synthetase complex. *J Biol Chem*, *280*(31), 28221-28229.

Kim, J., Wheeler, L. J., Shen, R., & Mathews, C. K. (2005b). Protein-DNA interactions in the T4 dNTP synthetase complex dependent on gene 32 single-stranded DNA-binding protein. *Mol Microbiol*, *55*(5), 1502-1514.

Klatt, P. & Lamas, S. (2000). Regulation of protein function by S-glutathiolation in response to oxidative and nitrosative stress. *Eur J Biochem*, *267*(16), 4928-4944.

Klintrot, I. M., Hoog, J. O., Jornvall, H., Holmgren, A., & Luthman, M. (1984). The primary structure of calf thymus glutaredoxin. Homology with the corresponding Escherichia coli protein but elongation at both ends and with an additional half-cystine/cysteine pair. *Eur J Biochem*, *144*(3), 417-423.

Kobayashi, Y., Cui, X., & Hirano, S. (2005). Stability of arsenic metabolites, arsenic triglutathione [As(GS)3] and methylarsenic diglutathione [CH3As(GS)2], in rat bile. *Toxicology*, *211*(1-2), 115-123.

Kochneva, G. V., Urmanov, I. H., Ryabchikova, E. I., Streltsov, V. V., & Serpinsky, O. I. (1994). Fine mechanisms of ectromelia virus thymidine kinase-negative mutants avirulence. *Virus Res*, *34*(1), 49-61.

Kolsch, H., Linnebank, M., Lutjohann, D., Jessen, F., Wullner, U., Harbrecht, U. et al. (2004). Polymorphisms in glutathione S-transferase omega-1 and AD, vascular dementia, and stroke. *Neurology*, *63*(12), 2255-2260.

Krause, G., Lundstrom, J., Barea, J. L., Pueyo de la Cuesta, C., & Holmgren, A. (1991). Mimicking the active site of protein disulfide-isomerase by substitution of proline 34 in Escherichia coli thioredoxin. *J Biol Chem*, *266*(15), 9494-9500.

Krauth-Siegel, R. L., Arscott, L. D., Schonleben-Janas, A., Schirmer, R. H., & Williams, C. H. J. (1998). Role of active site tyrosine residues in catalysis by human glutathione reductase. *Biochemistry*, *37*(40), 13968-13977.

Kren, B., Parsell, D., & Fuchs, J. A. (1988). Isolation and characterization of an Escherichia coli K-12 mutant deficient in glutaredoxin. *J Bacteriol*, *170*(1), 308-315.

Kwon, Y. W., Masutani, H., Nakamura, H., Ishii, Y., & Yodoi, J. (2003). Redox regulation of cell growth and cell death. *Biol Chem*, *384*(7), 991-996.

Ladner, R. D. & Caradonna, S. J. (1997). The human dUTPase gene encodes both nuclear and mitochondrial isoforms. Differential expression of the isoforms and characterization of a cDNA encoding the mitochondrial species. *J Biol Chem*, *272*(30), 19072-19080.

Lah, N., Lah, J., Zegers, I., Wyns, L., & Messens, J. (2003). Specific potassium binding stabilizes pI258 arsenate reductase from Staphylococcus aureus. *J Biol Chem*, *278*(27), 24673-24679.

Lalezari, J. P. (1997). Cidofovir: a new therapy for cytomegalovirus retinitis. *J Acquir Immune Defic Syndr Hum Retrovirol*, *14 Suppl 1*, S22-6.

Larsson, G., Svensson, L. A., & Nyman, P. O. (1996). Crystal structure of the Escherichia coli dUTPase in complex with a substrate analogue (dUDP). *Nat Struct Biol*, *3*(6), 532-538.

Larsson, K. M., Jordan, A., Eliasson, R., Reichard, P., Logan, D. T., & Nordlund, P. (2004). Structural mechanism of allosteric substrate specificity regulation in a ribonucleotide reductase. *Nat Struct Mol Biol*, *11*(11), 1142-1149.

Laskowski, R.A., MacArthur, M.W., Moss, D.S., & Thornton, J. M. (1993). PROCHECK: a program to check the stereochemical quality of protein structures. *J. Appl. Crystallogr*, *26*, 283-291.

LaVaute, T., Smith, S., Cooperman, S., Iwai, K., Land, W., Meyron-Holtz, E. et al. (2001). Targeted deletion of the gene encoding iron regulatory protein-2 causes misregulation of iron metabolism and neurodegenerative disease in mice. *Nat Genet*, *27*(2), 209-214.

Lazo, G., Kantarjian, H., Estey, E., Thomas, D., O'Brien, S., & Cortes, J. (2003). Use of arsenic trioxide (As2O3) in the treatment of patients with acute promyelocytic leukemia: the M. D. Anderson experience. *Cancer*, *97*(9), 2218-2224.

Le Quesne, P. M. & McLeod, J. G. (1977). Peripheral neuropathy following a single exposure to arsenic. Clincal course in four patients with electrophysiological and histological studies. *J Neurol Sci*, *32*(3), 437-451.

Lee, M. S., Roos, J. M., McGuigan, L. C., Smith, K. A., Cormier, N., Cohen, L. K. et al. (1992). Molecular attenuation of vaccinia virus: mutant generation and animal characterization. *J Virol*, *66*(5), 2617-2630.

Lefkowitz, E. J., Wang, C., & Upton, C. (2006). Poxviruses: past, present and future. *Virus Res*, *117*(1), 105-118.

Lennon, B. W., Williams, C. H., Jr., & Ludwig, M. L. (1999). Crystal structure of reduced thioredoxin reductase from Escherichia coli: structural flexibility in the isoalloxazine ring of the flavin adenine dinucleotide cofactor. *Protein Sci*, *8*(11), 2366-2379.

Leslie, A. G. W. (1992). *Joint CCP4.ESF-EACMB Newsl. Protein Crystallogr. 26.*

Li, Y., Carroll, D. S., Gardner, S. N., Walsh, M. C., Vitalis, E. A., & Damon, I. K. (2007). On the origin of smallpox: correlating variola phylogenics with historical smallpox records. *Proc Natl Acad Sci U S A*, *104*(40), 15787-15792.

Li, Y. J., Oliveira, S. A., Xu, P., Martin, E. R., Stenger, J. E., Scherzer, C. R. et al. (2003). Glutathione S-transferase omega-1 modifies age-at-onset of Alzheimer disease and Parkinson disease. *Hum Mol Genet, 12*(24), 3259-3267.

Liu, G., Huang, W., Moir, R. D., Vanderburg, C. R., Lai, B., Peng, Z. et al. (2006). Metal exposure and Alzheimer's pathogenesis. *J Struct Biol, 155*(1), 45-51.

Lovell, M. A., Robertson, J. D., Teesdale, W. J., Campbell, J. L., & Markesbery, W. R. (1998). Copper, iron and zinc in Alzheimer's disease senile plaques. *J Neurol Sci, 158*(1), 47-52.

Lu, J., Chew, E. H., & Holmgren, A. (2007). Targeting thioredoxin reductase is a basis for cancer therapy by arsenic trioxide. *Proc Natl Acad Sci U S A, 104*(30), 12288-12293.

Lu, M., Wang, H., Li, X. F., Arnold, L. L., Cohen, S. M., & Le, X. C. (2007). Binding of dimethylarsinous acid to cys-13alpha of rat hemoglobin is responsible for the retention of arsenic in rat blood. *Chem Res Toxicol, 20*(1), 27-37.

Lu, M., Wang, H., Li, X. F., Lu, X., Cullen, W. R., Arnold, L. L. et al. (2004). Evidence of hemoglobin binding to arsenic as a basis for the accumulation of arsenic in rat blood. *Chem Res Toxicol, 17*(12), 1733-1742.

Lundberg, M., Johansson, C., Chandra, J., Enoksson, M., Jacobsson, G., Ljung, J. et al. (2001). Cloning and expression of a novel human glutaredoxin (Grx2) with mitochondrial and nuclear isoforms. *J Biol Chem, 276*(28), 26269-26275.

Lundstrom, J. & Holmgren, A. (1993). Determination of the reduction-oxidation potential of the thioredoxin-like domains of protein disulfide-isomerase from the equilibrium with glutathione and thioredoxin. *Biochemistry, 32*(26), 6649-6655.

Lycksell, P. O., Ingemarson, R., Davis, R., Graslund, A., & Thelander, L. (1994). 1H NMR studies of mouse ribonucleotide reductase: the R2 protein carboxyl-terminal tail, essential for subunit interaction, is highly flexible but becomes rigid in the presence of protein R1. *Biochemistry, 33*(10), 2838-2842.

Mahy, B. W. (2003). An overview on the use of a viral pathogen as a bioterrorism agent: why smallpox? *Antiviral Res, 57*(1-2), 1-5.

Maignan, S., Guilloteau, J. P., Zhou-Liu, Q., Clement-Mella, C., & Mikol, V. (1998). Crystal structures of the catalytic domain of HIV-1 integrase free and complexed with its metal cofactor: high level of similarity of the active site with other viral integrases. *J Mol Biol, 282*(2), 359-368.

Martin, J. L. (1995). Thioredoxin--a fold for all reasons. *Structure, 3*(3), 245-250.

Martin, P., DeMel, S., Shi, J., Gladysheva, T., Gatti, D. L., Rosen, B. P. et al. (2001). Insights into the structure, solvation, and mechanism of ArsC arsenate reductase, a novel arsenic detoxification enzyme. *Structure, 9*(11), 1071-1081.

Matthews, B. W. (1968). Solvent content of protein crystals. *J Mol Biol, 33*(2), 491-497.

McLysaght, A., Baldi, P. F., & Gaut, B. S. (2003). Extensive gene gain associated with adaptive evolution of poxviruses. *Proc Natl Acad Sci U S A, 100*(26), 15655-15660.

McRee, D. E. (1999). XtalView/Xfit--A versatile program for manipulating atomic coordinates and electron density. *J Struct Biol, 125*(2-3), 156-165.

Messens, J., Martins, J. C., Brosens, E., Van Belle, K., Jacobs, D. M., Willem, R. et al. (2002). Kinetics and active site dynamics of Staphylococcus aureus arsenate reductase. *J Biol Inorg Chem, 7*(1-2), 146-156.

Messens, J. & Silver, S. (2006). Arsenate reduction: thiol cascade chemistry with convergent evolution. *J Mol Biol, 362*(1), 1-17.

Messens, J., Van Molle, I., Vanhaesebrouck, P., Limbourg, M., Van Belle, K., Wahni, K. et al. (2004). How thioredoxin can reduce a buried disulphide bond. *J Mol Biol, 339*(3), 527-537.

Meyer, H., Perrichot, M., Stemmler, M., Emmerich, P., Schmitz, H., Varaine, F. et al. (2002). Outbreaks of disease suspected of being due to human monkeypox virus infection in the Democratic Republic of Congo in 2001. *J Clin Microbiol, 40*(8), 2919-2921.

Meza, M., Gandolfi, A. J., & Klimecki, W. T. (2007). Developmental and genetic modulation of arsenic biotransformation: a gene by environment interaction? *Toxicol Appl Pharmacol, 222*(3), 381-387.

Mieyal, J. J., Starke, D. W., Gravina, S. A., & Hocevar, B. A. (1991). Thioltransferase in human red blood cells: kinetics and equilibrium. *Biochemistry, 30*(36), 8883-8891.

Mol, C. D., Arvai, A. S., Sanderson, R. J., Slupphaug, G., Kavli, B., Krokan, H. E. et al. (1995). Crystal structure of human uracil-DNA glycosylase in complex with a protein inhibitor: protein mimicry of DNA. *Cell, 82*(5), 701-708.

Mol, C. D., Harris, J. M., McIntosh, E. M., & Tainer, J. A. (1996). Human dUTP pyrophosphatase: uracil recognition by a beta hairpin and active sites formed by three separate subunits. *Structure, 4*(9), 1077-1092.

Moss, B. (2006). Poxvirus entry and membrane fusion. *Virology, 344*(1), 48-54.

Moss, B. & Salzman, N. P. (1968). Sequential protein synthesis following vaccinia virus infection. *J Virol, 2*(10), 1016-1027.

Moss, B., Shisler, J. L., Xiang, Y., & Senkevich, T. G. (2000). Immune-defense molecules of molluscum contagiosum virus, a human poxvirus. *Trends Microbiol, 8*(10), 473-477.

Moss, B. & Ward, B. M. (2001). High-speed mass transit for poxviruses on microtubules. *Nat Cell Biol, 3*(11), E245-6.

Moss, B. (2001). Poxviruses. In D. M. Knipe, Howley, D.E., Griffin, R.A., Lamb, M.A., Martin, B., Roizman, Straus, S.E. (Ed.), *Fields virology*. (4 ed., Vol. 2, pp. 2849-2884). Philadelphia: Lippincott Williams & Wilkins.

Mossner, E., Huber-Wunderlich, M., & Glockshuber, R. (1998). Characterization of Escherichia coli thioredoxin variants mimicking the active-sites of other thiol/disulfide oxidoreductases. *Protein Sci, 7*(5), 1233-1244.

Mukherjee, A., Sengupta, M. K., Hossain, M. A., Ahamed, S., Das, B., Nayak, B. et al. (2006). Arsenic contamination in groundwater: a global perspective with emphasis on the Asian scenario. *J Health Popul Nutr, 24*(2), 142-163.

Mukhopadhyay, R. & Rosen, B. P. (1998). Saccharomyces cerevisiae ACR2 gene encodes an arsenate reductase. *FEMS Microbiol Lett, 168*(1), 127-136.

Mukhopadhyay, R., Shi, J., & Rosen, B. P. (2000). Purification and characterization of ACR2p, the Saccharomyces cerevisiae arsenate reductase. *J Biol Chem, 275*(28), 21149-21157.

Mukhopadhyay, R., Zhou, Y., & Rosen, B. P. (2003). Directed evolution of a yeast arsenate reductase into a protein-tyrosine phosphatase. *J Biol Chem, 278*(27), 24476-24480.

Mukhopadhyay, R. & Rosen, B. P. (2002). Arsenate reductases in prokaryotes and eukaryotes. *Environ Health Perspect, 110 Suppl 5*, 745-748.

Murshudov, G. N., Vagin, A. A., & Dodson, E. J. (1997). Refinement of macromolecular structures by the maximum-likelihood method. *Acta Crystallogr D Biol Crystallogr, 53*(Pt 3), 240-255.

Murthy, S. & Reddy, G. P. (2006). Replitase: complete machinery for DNA synthesis. *J Cell Physiol, 209*(3), 711-717.

Nelson, J. W. & Creighton, T. E. (1994). Reactivity and ionization of the active site cysteine residues of DsbA, a protein required for disulfide bond formation in vivo. *Biochemistry, 33*(19), 5974-5983.

Nemeti, B., Csanaky, I., & Gregus, Z. (2006). Effect of an inactivator of glyceraldehyde-3-phosphate dehydrogenase, a fortuitous arsenate reductase, on disposition of arsenate in rats. *Toxicol Sci, 90*(1), 49-60.

Nielsen, B. B., Kauppi, B., Thelander, M., Thelander, L., Larsen, I. K., & Eklund, H. (1995). Crystallization and crystallographic investigations of the small subunit of mouse ribonucleotide reductase. *FEBS Lett, 373*(3), 310-312.

Noiva, R. & Lennarz, W. J. (1992). Protein disulfide isomerase. A multifunctional protein resident in the lumen of the endoplasmic reticulum. *J Biol Chem*, *267*(6), 3553-3556.

Nordlund, P. & Eklund, H. (1993). Structure and function of the Escherichia coli ribonucleotide reductase protein R2. *J Mol Biol*, *232*(1), 123-164.

Nordlund, P., Sjoberg, B. M., & Eklund, H. (1990). Three-dimensional structure of the free radical protein of ribonucleotide reductase. *Nature*, *345*(6276), 593-598.

Nordstrand, K., Sandstrom, A., Aslund, F., Holmgren, A., Otting, G., & Berndt, K. D. (2000). NMR structure of oxidized glutaredoxin 3 from Escherichia coli. *J Mol Biol*, *303*(3), 423-432.

Nordstrand, K., slund, F., Holmgren, A., Otting, G., & Berndt, K. D. (1999). NMR structure of Escherichia coli glutaredoxin 3-glutathione mixed disulfide complex: implications for the enzymatic mechanism. *J Mol Biol*, *286*(2), 541-552.

Ostermann, N., Schlichting, I., Brundiers, R., Konrad, M., Reinstein, J., Veit, T. et al. (2000). Insights into the phosphoryltransfer mechanism of human thymidylate kinase gained from crystal structures of enzyme complexes along the reaction coordinate. *Structure*, *8*(6), 629-642.

Ostermann, N., Segura-Pena, D., Meier, C., Veit, T., Monnerjahn, C., Konrad, M. et al. (2003). Structures of human thymidylate kinase in complex with prodrugs: implications for the structure-based design of novel compounds. *Biochemistry*, *42*(9), 2568-2577.

Padilla, C. A., Martinez-Galisteo, E., Barcena, J. A., Spyrou, G., & Holmgren, A. (1995). Purification from placenta, amino acid sequence, structure comparisons and cDNA cloning of human glutaredoxin. *Eur J Biochem*, *227*(1-2), 27-34.

Padilla, C. A., Spyrou, G., & Holmgren, A. (1996). High-level expression of fully active human glutaredoxin (thioltransferase) in E. coli and characterization of Cys7 to Ser mutant protein. *FEBS Lett*, *378*(1), 69-73.

Pai, E. F., Karplus, P. A., & Schulz, G. E. (1988). Crystallographic analysis of the binding of NADPH, NADPH fragments, and NADPH analogues to glutathione reductase. *Biochemistry*, *27*(12), 4465-4474.

Pai, E. F. & Schulz, G. E. (1983). The catalytic mechanism of glutathione reductase as derived from x-ray diffraction analyses of reaction intermediates. *J Biol Chem*, *258*(3), 1752-1757.

Paiva, L., Marcos, R., Creus, A., Coggan, M., Oakley, A. J., & Board, P. G. (2008). Polymorphism of glutathione transferase Omega 1 in a population exposed to a high environmental arsenic burden. *Pharmacogenet Genomics*, *18*(1), 1-10.

Parke, D. V. & Sapota, A. (1996). Chemical toxicity and reactive oxygen species. *Int J Occup Med Environ Health*, *9*(4), 331-340.

Pereira, S., Fernandes, P. A., & Ramos, M. J. (2004). Mechanism for ribonucleotide reductase inactivation by the anticancer drug gemcitabine. *J Comput Chem*, *25*(10), 1286-1294.

Perrakis, A., Harkiolaki, M., Wilson, K. S., & Lamzin, V. S. (2001). ARP/wARP and molecular replacement. *Acta Crystallogr D Biol Crystallogr*, *57*(Pt 10), 1445-1450.

Persson, R., Cedergren-Zeppezauer, E. S., & Wilson, K. S. (2001). Homotrimeric dUTPases; structural solutions for specific recognition and hydrolysis of dUTP. *Curr Protein Pept Sci*, *2*(4), 287-300.

Piskurek, O. & Okada, N. (2007). Poxviruses as possible vectors for horizontal transfer of retroposons from reptiles to mammals. *Proc Natl Acad Sci U S A*, *104*(29), 12046-12051.

Prasad, G. S., Stura, E. A., Elder, J. H., & Stout, C. D. (2000). Structures of feline immunodeficiency virus dUTP pyrophosphatase and its nucleotide complexes in three crystal forms. *Acta Crystallogr D Biol Crystallogr*, *56*(Pt 9), 1100-1109.

Quenelle, D. C., Collins, D. J., & Kern, E. R. (2003). Efficacy of multiple- or single-dose cidofovir against vaccinia and cowpox virus infections in mice. *Antimicrob Agents Chemother*, *47*(10), 3275-3280.

Raab, A., Wright, S. H., Jaspars, M., Meharg, A. A., & Feldmann, J. (2007). Pentavalent arsenic can bind to biomolecules. *Angew Chem Int Ed Engl*, *46*(15), 2594-2597.

Rabenstein, D. L. & Millis, K. K. (1995). Nuclear magnetic resonance study of the thioltransferase-catalyzed glutathione/glutathione disulfide interchange reaction. *Biochim Biophys Acta*, *1249*(1), 29-36.

Rajagopal, I., Ahn, B. Y., Moss, B., & Mathews, C. K. (1995). Roles of vaccinia virus ribonucleotide reductase and glutaredoxin in DNA precursor biosynthesis. *J Biol Chem*, *270*(46), 27415-27418.

Reddy, G. P. & Fager, R. S. (1993). Replitase: a complex integrating dNTP synthesis and DNA replication. *Crit Rev Eukaryot Gene Expr*, *3*(4), 255-277.

Reichard, P. (1997). The evolution of ribonucleotide reduction. *Trends Biochem Sci*, *22*(3), 81-85.

Rice, M. E. (2000). Ascorbate regulation and its neuroprotective role in the brain. *Trends Neurosci*, *23*(5), 209-216.

Rochester, S. C. & Traktman, P. (1998). Characterization of the single-stranded DNA binding protein encoded by the vaccinia virus I3 gene. *J Virol*, *72*(4), 2917-2926.

Rodriguez, V. M., Del Razo, L. M., Limon-Pacheco, J. H., Giordano, M., Sanchez-Pena, L. C., Uribe-Querol, E. et al. (2005). Glutathione reductase inhibition and

methylated arsenic distribution in Cd1 mice brain and liver. *Toxicol Sci, 84*(1), 157-166.

Roos, G., Buts, L., Van Belle, K., Brosens, E., Geerlings, P., Loris, R. et al. (2006a). Interplay between ion binding and catalysis in the thioredoxin-coupled arsenate reductase family. *J Mol Biol, 360*(4), 826-838.

Roos, G., Loverix, S., Brosens, E., Van Belle, K., Wyns, L., Geerlings, P. et al. (2006b). The activation of electrophile, nucleophile and leaving group during the reaction catalysed by pI258 arsenate reductase. *Chembiochem, 7*(6), 981-989.

Rosen, B. P. (2002). Biochemistry of arsenic detoxification. *FEBS Lett, 529*(1), 86-92.

Rossman, T. G. (1981). Effect of metals on mutagenesis and DNA repair. *Environ Health Perspect, 40*, 189-195.

Rouault, T. A. (2001). Iron on the brain. *Nat Genet, 28*(4), 299-300.

Roy, B., Chambert, S., Lepoivre, M., Aubertin, A. M., Balzarini, J., & Decout, J. L. (2003). Deoxyribonucleoside 2'- or 3'-mixed disulfides: prodrugs to target ribonucleotide reductase and/or to inhibit HIV reverse transcription. *J Med Chem, 46*(13), 2565-2568.

Roy, B., Chambert, S., Lepoivre, M., & Decout, J. L. (2003b). Thionucleotides as inhibitors of ribonucleotide reductase. *Nucleosides Nucleotides Nucleic Acids, 22*(5-8), 883-885.

Sagemark, J., Elgan, T. H., Burglin, T. R., Johansson, C., Holmgren, A., & Berndt, K. D. (2007). Redox properties and evolution of human glutaredoxins. *Proteins, 68*(4), 879-892.

Samal, A., Schormann, N., Cook, W. J., DeLucas, L. J., & Chattopadhyay, D. (2007). Structures of vaccinia virus dUTPase and its nucleotide complexes. *Acta Crystallogr D Biol Crystallogr, 63*(Pt 5), 571-580.

Scaramozzino, N., Sanz, G., Crance, J. M., Saparbaev, M., Drillien, R., Laval, J. et al. (2003). Characterisation of the substrate specificity of homogeneous vaccinia virus uracil-DNA glycosylase. *Nucleic Acids Res, 31*(16), 4950-4957.

Schafer, F. Q. & Buettner, G. R. (2001). Redox environment of the cell as viewed through the redox state of the glutathione disulfide/glutathione couple. *Free Radic Biol Med, 30*(11), 1191-1212.

Schmelz, M., Sodeik, B., Ericsson, M., Wolffe, E. J., Shida, H., Hiller, G. et al. (1994). Assembly of vaccinia virus: the second wrapping cisterna is derived from the trans Golgi network. *J Virol, 68*(1), 130-147.

Schmuck, E. M., Board, P. G., Whitbread, A. K., Tetlow, N., Cavanaugh, J. A., Blackburn, A. C. et al. (2005). Characterization of the monomethylarsonate reductase and dehydroascorbate reductase activities of Omega class glutathione

transferase variants: implications for arsenic metabolism and the age-at-onset of Alzheimer's and Parkinson's diseases. *Pharmacogenet Genomics, 15*(7), 493-501.

Schormann, N., Grigorian, A., Samal, A., Krishnan, R., DeLucas, L., & Chattopadhyay, D. (2007). Crystal structure of vaccinia virus uracil-DNA glycosylase reveals dimeric assembly. *BMC Struct Biol, 7*, 45.

Schramm, B. & Locker, J. K. (2005). Cytoplasmic organization of POXvirus DNA replication. *Traffic, 6*(10), 839-846.

Senkevich, T. G., White, C. L., Koonin, E. V., & Moss, B. (2002). Complete pathway for protein disulfide bond formation encoded by poxviruses. *Proc Natl Acad Sci U S A, 99*(10), 6667-6672.

Sheldrick, G. M. (1997). SHELXL-97 Program for crystal structure refinement.

Shenton, D., Perrone, G., Quinn, K. A., Dawes, I. W., & Grant, C. M. (2002). Regulation of protein S-thiolation by glutaredoxin 5 in the yeast Saccharomyces cerevisiae. *J Biol Chem, 277*(19), 16853-16859.

Shiobara, Y., Ogra, Y., & Suzuki, K. T. (2001). Animal species difference in the uptake of dimethylarsinous acid (DMA(III)) by red blood cells. *Chem Res Toxicol, 14*(10), 1446-1452.

Shisler, J. L., Senkevich, T. G., Berry, M. J., & Moss, B. (1998). Ultraviolet-induced cell death blocked by a selenoprotein from a human dermatotropic poxvirus. *Science, 279*(5347), 102-105.

Sikorska, M., Brewer, L. M., Youdale, T., Richards, R., Whitfield, J. F., Houghten, R. A. et al. (1990). Evidence that mammalian ribonucleotide reductase is a nuclear membrane associated glycoprotein. *Biochem Cell Biol, 68*(5), 880-888.

Singh, N., Kumar, D., & Sahu, A. P. (2007). Arsenic in the environment: effects on human health and possible prevention. *J Environ Biol, 28*(2 Suppl), 359-365.

Slabaugh, M. B., Davis, R. E., Roseman, N. A., & Mathews, C. K. (1993). Vaccinia virus ribonucleotide reductase expression and isolation of the recombinant large subunit. *J Biol Chem, 268*(24), 17803-17810.

Slabaugh, M. B. & Mathews, C. K. (1984). Vaccinia virus-induced ribonucleotide reductase can be distinguished from host cell activity. *J Virol, 52*(2), 501-506.

Sliva, K. & Schnierle, B. (2007). From actually toxic to highly specific--novel drugs against poxviruses. *Virol J, 4*, 8.

Smee, D. F., Bailey, K. W., Wong, M. H., Wandersee, M. K., & Sidwell, R. W. (2004). Topical cidofovir is more effective than is parenteral therapy for treatment of progressive vaccinia in immunocompromised mice. *J Infect Dis, 190*(6), 1132-1139.

Smee, D. F., Sidwell, R. W., Kefauver, D., Bray, M., & Huggins, J. W. (2002). Characterization of wild-type and cidofovir-resistant strains of camelpox, cowpox, monkeypox, and vaccinia viruses. *Antimicrob Agents Chemother, 46*(5), 1329-1335.

Smith, G. L., de Carlos, A., & Chan, Y. S. (1989). Vaccinia virus encodes a thymidylate kinase gene: sequence and transcriptional mapping. *Nucleic Acids Res, 17*(19), 7581-7590.

Smith, G. L. & Law, M. (2004). The exit of vaccinia virus from infected cells. *Virus Res, 106*(2), 189-197.

Sodano, P., Xia, T. H., Bushweller, J. H., Bjornberg, O., Holmgren, A., Billeter, M. et al. (1991). Sequence-specific 1H n.m.r. assignments and determination of the three-dimensional structure of reduced Escherichia coli glutaredoxin. *J Mol Biol, 221*(4), 1311-1324.

Sousa, M. M., Krokan, H. E., & Slupphaug, G. (2007). DNA-uracil and human pathology. *Mol Aspects Med, 28*(3-4), 276-306.

Srinivasan, U., Mieyal, P. A., & Mieyal, J. J. (1997). pH profiles indicative of rate-limiting nucleophilic displacement in thioltransferase catalysis. *Biochemistry, 36*(11), 3199-3206.

Stahl, R. L., Liebes, L. F., Farber, C. M., & Silber, R. (1983). A spectrophotometric assay for dehydroascorbate reductase. *Anal Biochem, 131*(2), 341-344.

Stanitsa, E. S., Arps, L., & Traktman, P. (2006). Vaccinia virus uracil DNA glycosylase interacts with the A20 protein to form a heterodimeric processivity factor for the viral DNA polymerase. *J Biol Chem, 281*(6), 3439-3451.

Stevens, R. C. (2000). High-throughput protein crystallization. *Curr Opin Struct Biol, 10*(5), 558-563.

Stevens, S. Y., Hu, W., Gladysheva, T., Rosen, B. P., Zuiderweg, E. R., & Lee, L. (1999). Secondary structure and fold homology of the ArsC protein from the Escherichia coli arsenic resistance plasmid R773. *Biochemistry, 38*(31), 10178-10186.

Stone, R. (2002). Smallpox. WHO puts off destruction of U.S., Russian caches. *Science, 295*(5555), 598-599.

Storoni, L. C., McCoy, A. J., & Read, R. J. (2004). Likelihood-enhanced fast rotation functions. *Acta Crystallogr D Biol Crystallogr, 60*(Pt 3), 432-438.

Strahler, J. R., Zhu, X. X., Hora, N., Wang, Y. K., Andrews, P. C., Roseman, N. A. et al. (1993). Maturation stage and proliferation-dependent expression of dUTPase in human T cells. *Proc Natl Acad Sci U S A, 90*(11), 4991-4995.

Stubbe, J. (1990). Ribonucleotide reductases: amazing and confusing. *J Biol Chem*, *265*(10), 5329-5332.

Studebaker, A. W., Balendiran, G. K., & Williams, M. V. (2001). The herpesvirus encoded dUTPase as a potential chemotherapeutic target. *Curr Protein Pept Sci*, *2*(4), 371-379.

Su, H. P., Lin, D. Y., & Garboczi, D. N. (2006). The structure of g4, the poxvirus disulfide oxidoreductase essential for virus maturation and infectivity. *J Virol*, *80*(15), 7706-7713.

Sun, C., Berardi, M. J., & Bushweller, J. H. (1998). The NMR solution structure of human glutaredoxin in the fully reduced form. *J Mol Biol*, *280*(4), 687-701.

Taylor, G., Stott, E. J., Wertz, G., & Ball, A. (1991). Comparison of the virulence of wild-type thymidine kinase (tk)-deficient and tk+ phenotypes of vaccinia virus recombinants after intranasal inoculation of mice. *J Gen Virol*, *72*(Pt 1), 125-130.

Tengelsen, L. A., Slabaugh, M. B., Bibler, J. K., & Hruby, D. E. (1988). Nucleotide sequence and molecular genetic analysis of the large subunit of ribonucleotide reductase encoded by vaccinia virus. *Virology*, *164*(1), 121-131.

Thomas, D. J., Li, J., Waters, S. B., Xing, W., Adair, B. M., Drobna, Z. et al. (2007). Arsenic (+3 oxidation state) methyltransferase and the methylation of arsenicals. *Exp Biol Med (Maywood)*, *232*(1), 3-13.

Tinkelenberg, B. A., Fazzone, W., Lynch, F. J., & Ladner, R. D. (2003). Identification of sequence determinants of human nuclear dUTPase isoform localization. *Exp Cell Res*, *287*(1), 39-46.

Topalis, D., Collinet, B., Gasse, C., Dugue, L., Balzarini, J., Pochet, S. et al. (2005). Substrate specificity of vaccinia virus thymidylate kinase. *FEBS J*, *272*(24), 6254-6265.

Tsai, S. Y., Chou, H. Y., The, H. W., Chen, C. M., & Chen, C. J. (2003). The effects of chronic arsenic exposure from drinking water on the neurobehavioral development in adolescence. *Neurotoxicology*, *24*(4-5), 747-753.

Tseng, H. P., Wang, Y. H., Wu, M. M., The, H. W., Chiou, H. Y., & Chen, C. J. (2006). Association between chronic exposure to arsenic and slow nerve conduction velocity among adolescents in Taiwan. *J Health Popul Nutr*, *24*(2), 182-189.

Tseng, M., Palaniyar, N., Zhang, W., & Evans, D. H. (1999). DNA binding and aggregation properties of the vaccinia virus I3L gene product. *J Biol Chem*, *274*(31), 21637-21644.

Tseng, W. P. (1977). Effects and dose--response relationships of skin cancer and blackfoot disease with arsenic. *Environ Health Perspect*, *19*, 109-119.

Vahidnia, A., van der Voet, G. B., & de Wolff, F. A. (2007). Arsenic neurotoxicity--a review. *Hum Exp Toxicol, 26*(10), 823-832.

Vahter, M. (1999). Methylation of inorganic arsenic in different mammalian species and population groups. *Sci Prog, 82*(Pt 1), 69-88.

Vahter, M. & Concha, G. (2001). Role of metabolism in arsenic toxicity. *Pharmacol Toxicol, 89*(1), 1-5.

Vahter, M., Couch, R., Nermell, B., & Nilsson, R. (1995). Lack of methylation of inorganic arsenic in the chimpanzee. *Toxicol Appl Pharmacol, 133*(2), 262-268.

Vahter, M. & Marafante, E. (1985). Reduction and binding of arsenate in marmoset monkeys. *Arch Toxicol, 57*(2), 119-124.

Vahter, M., Marafante, E., & Dencker, L. (1984). Tissue distribution and retention of 74As-dimethylarsinic acid in mice and rats. *Arch Environ Contam Toxicol, 13*(3), 259-264.

Vivian, J. T. & Callis, P. R. (2001). Mechanisms of tryptophan fluorescence shifts in proteins. *Biophys J, 80*(5), 2093-2109.

Wang, Y., Amegbey, G., & Wishart, D. S. (2004). Solution structures of reduced and oxidized bacteriophage T4 glutaredoxin. *J Biomol NMR, 29*(1), 85-90.

Washburn, M. P. & Wells, W. W. (1999). The catalytic mechanism of the glutathione-dependent dehydroascorbate reductase activity of thioltransferase (glutaredoxin). *Biochemistry, 38*(1), 268-274.

Wheeler, L. J., Ray, N. B., Ungermann, C., Hendricks, S. P., Bernard, M. A., Hanson, E. S. et al. (1996). T4 phage gene 32 protein as a candidate organizing factor for the deoxyribonucleoside triphosphate synthetase complex. *J Biol Chem, 271*(19), 11156-11162.

Whitbread, A. K., Tetlow, N., Eyre, H. J., Sutherland, G. R., & Board, P. G. (2003). Characterization of the human Omega class glutathione transferase genes and associated polymorphisms. *Pharmacogenetics, 13*(3), 131-144.

White, C. L., Senkevich, T. G., & Moss, B. (2002). Vaccinia virus G4L glutaredoxin is an essential intermediate of a cytoplasmic disulfide bond pathway required for virion assembly. *J Virol, 76*(2), 467-472.

Whitesides, G. M., Houk, I., & Patterson, M. A. K. (1983). Activation parameters for thiolate-disulfide interchange reactions in aqueous solution. *Journal of Organic Chemistry, 48*, 112-115.

Whitley, R. J. (2003). Smallpox: a potential agent of bioterrorism. *Antiviral Res, 57*(1-2), 7-12.

Wildfang, E., Radabaugh, T. R., & Vasken Aposhian, H. (2001). Enzymatic methylation of arsenic compounds. IX. Liver arsenite methyltransferase and arsenate reductase activities in primates. *Toxicology*, *168*(3), 213-221.

Wilson, W. W. (2003). Light scattering as a diagnostic for protein crystal growth--a practical approach. *J Struct Biol*, *142*(1), 56-65.

Winn, M. D., Isupov, M. N., & Murshudov, G. N. (2001). Use of TLS parameters to model anisotropic displacements in macromolecular refinement. *Acta Crystallogr D Biol Crystallogr*, *57*(Pt 1), 122-133.

Wunderlich, M. & Glockshuber, R. (1993). Redox properties of protein disulfide isomerase (DsbA) from Escherichia coli. *Protein Sci*, *2*(5), 717-726.

Xia, T. H., Bushweller, J. H., Sodano, P., Billeter, M., Bjornberg, O., Holmgren, A. et al. (1992). NMR structure of oxidized Escherichia coli glutaredoxin: comparison with reduced E. coli glutaredoxin and functionally related proteins. *Protein Sci*, *1*(3), 310-321.

Xiao, R., Lundstrom-Ljung, J., Holmgren, A., & Gilbert, H. F. (2005). Catalysis of thiol/disulfide exchange. Glutaredoxin 1 and protein-disulfide isomerase use different mechanisms to enhance oxidase and reductase activities. *J Biol Chem*, *280*(22), 21099-21106.

Xu, H., Faber, C., Uchiki, T., Fairman, J. W., Racca, J., & Dealwis, C. (2006a). Structures of eukaryotic ribonucleotide reductase I provide insights into dNTP regulation. *Proc Natl Acad Sci U S A*, *103*(11), 4022-4027.

Xu, H., Faber, C., Uchiki, T., Racca, J., & Dealwis, C. (2006b). Structures of eukaryotic ribonucleotide reductase I define gemcitabine diphosphate binding and subunit assembly. *Proc Natl Acad Sci U S A*, *103*(11), 4028-4033.

Yang, F. D., Spanevello, R. A., Celiker, I., Hirschmann, R., Rubin, H., & Cooperman, B. S. (1990). The carboxyl terminus heptapeptide of the R2 subunit of mammalian ribonucleotide reductase inhibits enzyme activity and can be used to purify the R1 subunit. *FEBS Lett*, *272*(1-2), 61-64.

Yang, Y., Jao, S., Nanduri, S., Starke, D. W., Mieyal, J. J., & Qin, J. (1998). Reactivity of the human thioltransferase (glutaredoxin) C7S, C25S, C78S, C82S mutant and NMR solution structure of its glutathionyl mixed disulfide intermediate reflect catalytic specificity. *Biochemistry*, *37*(49), 17145-17156.

Yang, Y. F. & Wells, W. W. (1991). Identification and characterization of the functional amino acids at the active center of pig liver thioltransferase by site-directed mutagenesis. *J Biol Chem*, *266*(19), 12759-12765.

Yang, Z. (1997). PAML: a program package for phylogenetic analysis by maximum likelihood. *Comput Appl Biosci*, *13*(5), 555-556.

Yip, S. F., Yeung, Y. M., & Tsui, E. Y. (2002). Severe neurotoxicity following arsenic therapy for acute promyelocytic leukemia: potentiation by thiamine deficiency. *Blood, 99*(9), 3481-3482.

Zakharyan, R. A., Sampayo-Reyes, A., Healy, S. M., Tsaprailis, G., Board, P. G., Liebler, D. C. et al. (2001). Human monomethylarsonic acid (MMA(V)) reductase is a member of the glutathione-S-transferase superfamily. *Chem Res Toxicol, 14*(8), 1051-1057.

Zakharyan, R. A., Wildfang, E., & Aposhian, H. V. (1996). Enzymatic methylation of arsenic compounds. III. The marmoset and tamarin, but not the rhesus, monkeys are deficient in methyltransferases that methylate inorganic arsenic. *Toxicol Appl Pharmacol, 140*(1), 77-84.

Zapun, A., Bardwell, J. C., & Creighton, T. E. (1993). The reactive and destabilizing disulfide bond of DsbA, a protein required for protein disulfide bond formation in vivo. *Biochemistry, 32*(19), 5083-5092.

Zegers, I., Martins, J. C., Willem, R., Wyns, L., & Messens, J. (2001). Arsenate reductase from S. aureus plasmid pI258 is a phosphatase drafted for redox duty. *Nat Struct Biol, 8*(10), 843-847.

Zhang, Z., Yang, K., Chen, C. C., Feser, J., & Huang, M. (2007). Role of the C terminus of the ribonucleotide reductase large subunit in enzyme regeneration and its inhibition by Sml1. *Proc Natl Acad Sci U S A, 104*(7), 2217-2222.

Zhang, Z. Y. & Dixon, J. E. (1993). Active site labeling of the Yersinia protein tyrosine phosphatase: the determination of the pKa of the active site cysteine and the function of the conserved histidine 402. *Biochemistry, 32*(36), 9340-9345.

Zhou, Y., Bhattacharjee, H., & Mukhopadhyay, R. (2006). Bifunctional role of the leishmanial antimonate reductase LmACR2 as a protein tyrosine phosphatase. *Mol Biochem Parasitol, 148*(2), 161-168.

A.1 Poxvirus structural genomics

A.1.1 Protein target selection

Ten EVM enzymes involved in or associated with nucleotide metabolism **(Table A.1)** were initially tested for expression and solubility. Targets that demonstrated the highest levels of expression in the soluble fraction were then purified and tested for abilities to crystallize. Crystals that grew to a size large enough to mount in a crystallization loop were subjected to X-ray diffraction analysis. After this first broad screening approach, the target selection was narrowed down based on observations of protein characteristics such as protein expression levels, protein solubility, protein polydispersity and other characteristics that might suggest the protein is amenable for crystallization. More importantly, targets were pursued based on the estimated impact of the protein structure. Thus, proteins that did not exhibit high sequence homology to other proteins of known structure (i.e. I3L SSB), were preferentially pursued. In addition, the overall perceived importance of the protein to poxviral and mammalian biology was also used as a criterion for focusing efforts on these proteins. RNR R1 and Grx-1 are two proteins that would certainly fit this criterion since the function of RNR is essential for the *de novo* production of dNTPs and these proteins show only 25% and 45% sequence identity, respectively, to other known structures. It was predicted that by targeting several proteins, chances of obtaining crystal structures would be greatly

Gene target	EVM	Vaccinia
RNR R1	EVM057	I4L
RNR R2	EVM028	F4L
Grx-1	EVM053	O2L
TK	EVM078	J2R
TMPK	EVM147	A48R
dUTPase	EVM026	F2L
SSB	EVM056	I3L
UDG	EVM093	D4R
NTPase/Primase	EVM094	D5R
Grx-2	EVM065	G4L

Table A.1. EVM enzymes targeted for structural analysis. I3L was the only vaccinia virus enzyme targeted. Since vaccinia nomenclature is often used for orthopoxviral enzymes, all the vaccinia enzyme names are also listed.

enhanced, and such an approach is used in high-throughput structural genomics laboratories. All targets were initially screened using standardized protocols, which were described in chapter 2. More detailed methodologies for each target are described in the following section.

A.1.2 Individual poxviral protein targets

A.1.2.1 RNR R1 (EVM057)

EVM R1 protein was expressed according to a protocol used by Mathews and colleagues (Slabaugh *et al.*, 1993). This protein does not express well at higher temperatures and must be induced at a low initial cell density (OD_{600} = ~0.2) and low concentration of IPTG (0.05 mM) in order to obtain protein in the soluble fraction. Soluble expression is also enhanced by the presence of 5-10 mM hydroxurea. Hydroxyurea is a known inhibitor of RNR R2, and the presence of this molecule likely decreases the production of dATP, and perhaps leads to an improved environment for R1 protein folding. Although the presence of substrates is generally believed to improve protein folding, it is possible that the binding of dATP to the allosteric activity site before the protein is completely folded could lead to premature interactions with other R1 subunits, leading to aberrant folding or aggregation. Following induction these cells were grown at 4° C for 20h. It is thought that by performing expression in the presence of a low concentration of inducing agent and at a low temperature, the metabolism of the cells and processes leading to proper folding are slowed down, resulting in more soluble and correctly folded protein (Derewenda, 2004). However, although this protocol

resulted in an increased concentration of R1 in the soluble fraction, it still rarely produced enough protein for extensive crystallization experiments.

Since RNR R1 was an important target for this project, but it proved difficult to produce sufficient protein for crystallization screening, a panel of N- and C-terminal truncations of this protein was generated. Flexible N- or C-terminal regions can greatly reduce the ability of proteins to crystallize (Derewenda, 2004). These regions often do not form part of the protein structure and thus are the first choice of regions to delete. Other regions such as an abundance of hydrophobic residues can affect the solubility of the protein in addition to the ability to form crystals. For example, the Hazes laboratory previously used truncations of hydrophobic regions of PAK and K122-4 pilin proteins of *Pseudomonas aeruginosa* to obtain high resolution diffraction data, (0.78 and 1.54 Å, respectively) (Hazes, *et al.*, 2000; Audette *et al.*, 2003).

A panel of 5 N- and C-terminal R1 truncations were thus constructed (residues 1-214, 1-649, 98-771,170-771, 215-771) based on both the *E. coli* and yeast R1 structures and through analysis of orthopoxviral R1 sequence alignments. Although only 1 of these constructs was found to express well (1-214), this was an interesting construct to pursue since it formed the complete N-terminal domain of R1 (NTD), which is responsible for allosteric regulation of R1 and binds both ATP and dATP (see section 1.1.4.1). In order to obtain soluble R1 NTD protein, the N-terminal domain also had to be expressed in the presence of 5-10 mM hydroxyurea, and expression was improved when performed at lower temperatures. Following induction at an OD_{600} of 0.3-0.4, the protein was expressed at 23° C for 6 hours. The NTD protein preparation was initially purified using IMAC followed by size exclusion chromatography. Despite evidence of high

polydispersity, and moderate precipitation at high concentrations, small plate crystals could be grown from this preparation using PEG3350 as a precipitant **(Figure A.1a)**, although diffraction quality crystals were not obtained.

A.1.2.2 RNR R2 (EVM028)

Recombinant EVM028 was expressed from arabinose inducible *E. coli* cell clones that were kindly provided by Brianne Wilton and Shauna deVarrenes (Laboratory of Dr. Michele Barry, University of Alberta). The protein was purified using IMAC followed by anion exchange chromatography. Purified EVM028 was highly soluble at low salt concentrations, showed very low polydispersity, and small needle like crystals could be obtained in the presence of various salts. The crystals obtained for EVM028 were grown in similar conditions (2.5 M NaCl, 0.1 M sodium acetate pH 4.5, 0.1 M Li_2SO_4) to those found for the mouse R2, which demonstrates 80% sequence identity (Nielsen *et al.*, 1995). The crystals would also grow with different salts such as sodium formate in lieu of sodium chloride. However, the crystals were for the most part very small (<50 μm in length, 5-10 μm in width) and did not diffract to beyond 7-8 Å. Although larger crystals could be obtained for EVM028 using seeding (up to 1 mm in length), the larger size of the crystals did not result in improved diffraction. Other attempts using additive screens were also unsuccessful in obtaining useable diffraction data. **Figure A.1b** shows crystal rods of EVM028 that were acquired using seeds of smaller needles.
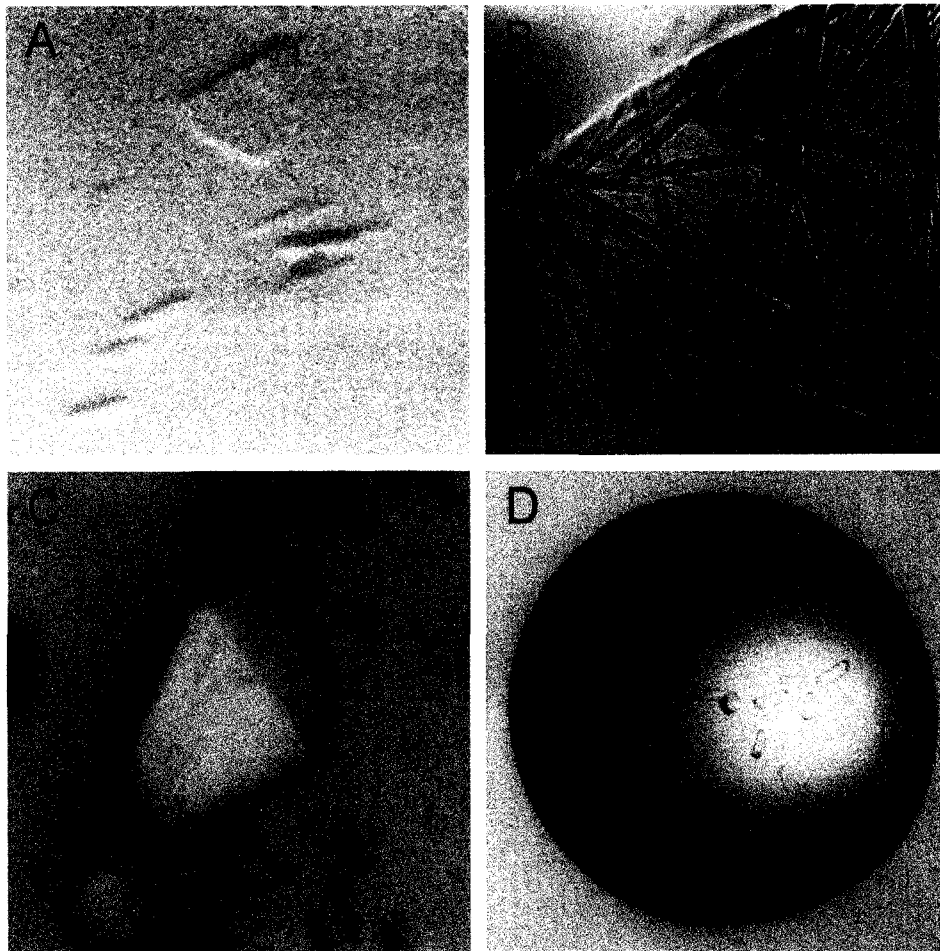
Figure A.1a. EVM057 N-Terminal domain crystals were grown with well conditions of 0.1 M Tris pH 8.7, and 4% PEG 3350.

Figure A.1b. EVM028 crystals were grown with well conditions of 0.1 M sodium acetate pH 5.4, 1.3 M NaCl, and 0.2 M Li_2SO_4.

Figure A.1c. EVM053 crystal was grown in the presence of 5mM DTT, and well conditions of 0.1 M NaCacodylate pH 6.0 and 20% MPD.

Figure A.1d. I3L crystals were grown with well conditions of 0.1 M HEPES pH 8.1, 15% PEG 3350, and 3% ethylene glycol.

Since the C-terminal region of I3L had been shown to be required for binding interactions with orthopoxviral R2 (Davis and Mathews, 1993), a peptide for the C-terminus of I3L was synthesized (Alberta Peptide Institute), and attempts were made to co-crystallize this peptide with R2. This however did not result in an improvement of crystal size, morphology or diffraction.

A.1.2.3 Grx-1 (EVM053)

EVM053 was cloned into the pET-Blue2-based COMPASS plasmid with an N-terminal His6-tag sequence (MHHHHHH) followed by the entire EVM053 open reading frame (Bacik *et al.*, 2005). As the first purification step, the filtered supernatant was loaded onto an Ni^{2+}-charged HiTrap affinity column equilibrated with column buffer on an Akta Purifier (GE Healthcare) at 277 K. The column was washed with ten column volumes of wash buffer (10 mM Tris pH 8.0, 20 mM sodium chloride, 5 mM imidazole), after which the protein was eluted with a linear gradient of wash and elution buffers (10 mM Tris pH 8.0, 20 mM sodium chloride, 200 mM imidazole) over 20 column volumes. By eluting the protein in the low ionic strength buffer, the peak fraction could be loaded directly onto an anion-exchange chromatography column filled with Resource 30Q resin (GE Healthcare), which was pre-equilibrated with loading buffer (20 mM sodium chloride, 10 mM Tris pH 8.0). After washing the column with three column volumes of loading buffer, the protein was eluted with a linear gradient of loading buffer and elution buffer (250 mM sodium chloride, 10 mM Tris pH 8.0). Interestingly, the protein would elute in two peaks off the anion exchange column

suggesting oxidized and reduced protein eluted at different points off the anion exchange column. SDS–PAGE analysis of the purified recombinant EVM053 product revealed a single band at the expected molecular weight of 13.3 kDa. A 5K NMWL membrane centrifugal filter device (Millipore) was used to exchange the buffer to 100 mM sodium chloride, 10 mM Tris pH 8.0 and to concentrate the sample. Protein concentration was assessed by amino-acid composition analysis prior to crystallization trials.

Initial crystallization screens were set up with the Honeybee crystallization robot (Genomic Solutions) using both in-house and commercial crystallization screens (Hampton Research, Emerald BioSystems). Crystals grew in several conditions of the commercial screens, but were too small to be used without optimization. Using a lab based screen, bipyramidal crystals (0.075 x 0.05 x 0.02 mm) were grown in 2–4 h using the sitting-drop vapor-diffusion method at 295 K from drops containing 200 nl protein solution (10 mg ml^{-1} in 50 mM Tris pH 8.0, 100 mM sodium chloride, 5 mM DTT), 200 nl water and 200 nl reservoir solution (20% MPD, 0.1 M sodium cacodylate pH 6.0). Larger crystals with typical dimensions of 0.30 × 0.20 × 0.075 mm were obtained in hanging drops by increasing reagent volumes to 1 μl protein sample, 2 μl water and 2 μl reservoir solution at 295 K using 24-well plates **(Figure A.1c)**.

The MPD present in the crystallization condition was sufficient for successful flash-cooling and thus no further cryoprotectants were added. Crystals were mounted in cryoloops (Hampton Research) and flash-cooled by direct immersion into liquid nitrogen prior to X-ray diffraction analysis. Crystals grown in this manner yielded the structure in the oxidized state. These crystals were also soaked for 5 min, just before

flash cooling, in a solution containing reservoir solution, 50 mM GSH, and 40% MPD, to yield the structure in the reduced and dimethylarsenylated states (see section 3.2.3).

The EVM053 crystals were first screened for their ability to diffract on an X-ray source at the University of Alberta. If diffraction was observed, the crystals were sent to collect complete diffraction data sets at the Advanced Light Source (ALS) synchrotron in Berkeley, California (Beamline 8.3.1).

The presence of two or more lattices in the diffraction pattern of several crystals indicated a problem with non-merohedral twinning. By using a 30 μm collimator and systematic translation of a crystal using a scripted procedure (J. Holton, unpublished results) a region near the edge of a crystal that was not twinned was found **(Figure A.2a)**. Two data sets of 180 images each (1 s and 10 s exposures) were collected on an ADSC Quantum 210 CCD detector with a crystal-to-detector distance of 150 mm. Intensity data were collected at 100 K using a wavelength of 1.1 Å and a 0.5° oscillation angle per image was chosen based on the relatively low mosaicity of ~0.3°. Diffraction data were integrated with MOSFLM (Leslie, 1992), followed by scaling and merging with SCALA from the CCP4 suite of programs (Collaborative Computational Project, Number 4, 1994). Based on systematic absences, the space group was assigned as C2221, with unit-cell parameters a = 61.98, b = 67.57, c = 108.55 Å, $\alpha = \beta = \gamma = 90°$. Analysis of the self-rotation function revealed a significant non-origin peak at 5.1σ above the background, indicating that there are two EVM053 monomers per asymmetric unit. This gives a Matthews volume of 2.2 Å^3 Da^{-1} (Matthews, 1968) and an estimated solvent content of 42.6% within the asymmetric unit. The NCS operation is a 90° rotation around the c axis, resulting in a pseudo-tetrameric space group. However,
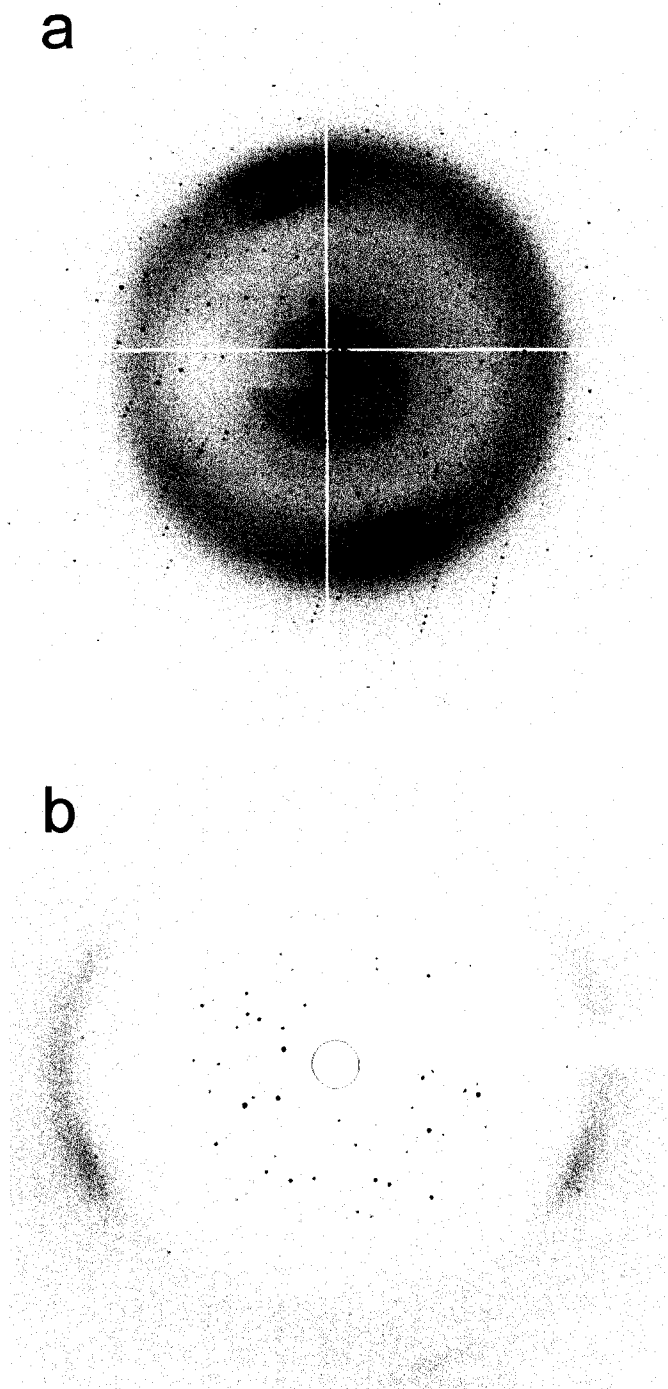
Figure A.2. X-ray diffraction images for (a) EVM053 and (b) I3L. Diffraction data was visible to 1.8 and 4.3 Å, respectively.

imposing a tetrameric space group during integration failed to yield a usable data set. The pseudo-symmetry may have also contributed to the observed non-merohedral twinning.

The EVM053 structure was solved by molecular replacement using the program PHASER (Storoni, *et al.*, 2004) and a search model based on the pig liver Grx-1 crystal structure (Katti *et al.*, 1995). The initial model was built by ARP/wARP (Perrakis *et al.*, 2001) based on the pig liver Grx-1 structural template. Refinement was performed using REFMAC (Murshudov *et al.*, 1997) using standard protocols with 5% of the data omitted to monitor Rfree. Non-crystallographic symmetry restraints were always applied and a TLS atomic displacement model (Winn *et al.*, 2001) was used in the later stages of refinement. The occupancy of residues with dual side-chain conformations was refined by SHELXL (Sheldrick, 1997). Water molecules were automatically added using ARP/wARP followed by visual inspection with Xfit (McRee, 1999). Xfit was also used for manual model building and structure analysis. Stereochemical quality of the final models was assessed by PROCHECK (Laskowski *et al.*, 1993). Diffraction data, refinement statistics and model parameters are summarized in **Table A.2**. All structural alignments were performed using DaliLite (Holm and Park, 2000). Atomic coordinates for reduced and oxidized EVM053 have been deposited in the RCSB Protein Data Bank with accession codes 2HZE and 2HZF, respectively.

A.1.2.4 Poxviral SSB (I3L)

Recombinant I3L was expressed from arabinose inducible *E. coli* cell clones that were kindly provided by Wendy Magee (Laboratory of Dr. David Evans, University of

	Oxidized	Reduced
Diffraction data statistics[1]		
Space group	$C222_1$	$C222_1$
Unit cell dimensions	a= 61.98, b=67.57, c=108.55	a= 62.63, b=66.67, c=108.10
Resolution range (Å)	36.20-1.80 (1.90-1.80)	54.07-1.80 (1.87-1.80)
Measured reflections	113946 (6928)	82915 (7496)
Unique reflections	20896 (2737)	21297 (2305)
Completeness (%)	96.7 (88.0)	99.6 (97.3)
R_{sym}	0.135 (0.655)	0.076 (0.473)
Mean (I)/sd(I)	10.6 (1.8)	11.5 (2.2)
B_{wilson} (Å^2)	19.2	24.6
Refinement statistics		
R-factor	0.180	0.183
R-free	0.219	0.208
Number of waters	149	129
Backbone average B-factor (Å^2)	18.3	29.0
All atoms average B-factor (Å^2)	21.1	32.2
RMSD bond lengths (Å)	0.022	0.019
RMSD bond angles (°)	1.772	1.845

[1] Values in parentheses indicate statistics for the highest resolution shell.

Table A.2. EVM053 diffraction data and refinement statistics.

chromatography. This construct expressed well and would crystallize easily in the presence of PEG. However, these crystals did not diffract beyond about 7 Å at cryogenic temperatures. Attempts to improve the diffraction using techniques such as crystal annealing and a wide screening of standard and alternate cryoprotectants was unsuccessful. In an attempt to obtain crystals that diffracted to a higher resolution, I performed an additive screen using the pre-existing crystallization conditions as a starting point. Additives such as metals, salts, reducing agents and organic molecules can influence crystal formation and result in higher resolution diffraction. This was evident in the Grx-1 crystals where the presence of DTT was required for crystal formation. Use of ligands in the crystallization set-up or other cofactors not commonly included in additive screens also often provides increased stabilization to the protein crystal lattice and is often used in both initial screening experiments as well as an optimization technique. Since I3L shows strong affinity for single stranded DNA, many poly-dT oligonucleotides of various length (10-34 nucleotides) and composition (GC clamps, 5' phosphorylated) were also used in both screening and optimization.

Buffer pH and PEG concentrations for the I3L crystallization experiments were varied using a matrix of these variables and bipyramid microcrystals would appear approximately 1 hour following the setup in 15% PEG 3350 and 0.1 M HEPES pH 8.1. An additive screen composed of 96 different reagents (Hampton Research) was added to the well solution in 96-well square bottom sitting drop plates and experiments were set up with a well volume of 50 µl and drops of 0.6 µl. Initially about half the drops had microcrystals similar to what was found without additives, while the other drops were clear or precipitated. The following day all of the original microcrystals had gone back

into solution. However, there were now several drops (7 of 96 additives) that had much larger, rectangular crystals, with fewer nucleations. The most promising additives were 3% ethylene glycol and 4% 1,3-propanediol **(Figure A.1d)**. These conditions resulted in rectangular crystals about 100 x 60 µm directly from the robot screens and could be optimized using manual hanging drop set-ups to obtain crystals of 600 x 300 x 300 µm. Other additives that resulted in crystals were, 0.2 M NDSB-201, 5% Jeffamine, 4% 1,3-butanediol, 4% 1-propanol, and 4% 2,2,2-trifluoroethanol.

One of the crystals grown in the presence of 3% ethylene glycol demonstrated a dramatic increase in diffraction to 4.3 Å when collected at room temperature in the presence of a 10mer poly-dT oligonucleotide **(Figure A.2b)**. Unfortunately, this crystal deteriorated due to radiation damage after 20 images and thus a complete diffraction data set could not be obtained. Similar crystals were subsequently screened at room temperature, but failed to diffract to a useable resolution.

A.1.2.5 Grx-2 (EVM065)

EVM Grx-2 was targeted for structural analysis after obtaining crystals for EVM053. EVM065 (G4L in vaccinia) was expressed for the most part in the insoluble fraction but a sufficiently large amount of protein was also present in the soluble form **(Figure A.3)**. Highly pure soluble protein could be obtained using IMAC followed by ion exchange chromatography. Microcrystals were obtained for this protein and optimization of crystallization conditions had been initiated. However, at this time, the structure was solved by another group, which halted any further crystallization
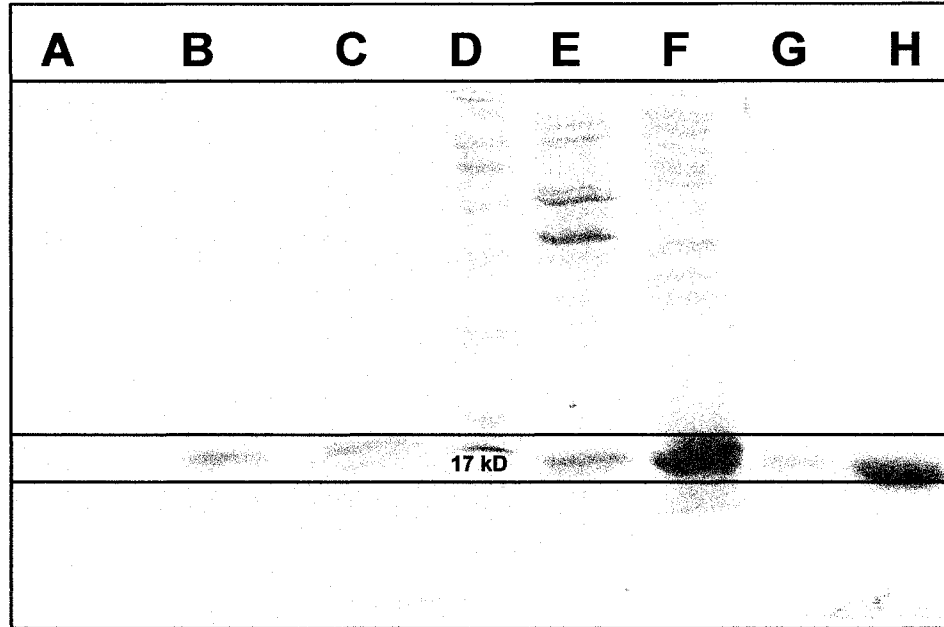
Figure A.3. SDS-PAGE of EVM065 gene product expression and purification.
Expected molecular weight is 14.8 kDa. a) t=0 expression; b) t=2 h; c) t=3 h; d)
Protein standards ladder; e) soluble fraction; f) insoluble fraction; g-h) Anion
exchange column elute.

experiments for this protein. The protein structure of G4L solved by Su and colleagues was solved from the insoluble fraction that was refolded following expression in inclusion bodies (Su *et al.*, 2006).

A.1.2.6 TK (EVM078)

Although EVM078 protein expressed well and could be purified relatively easily using IMAC followed by ion exchange chromatography, when purified it would precipitate out of solution at high concentrations after a few hours and attempts to solubilise this protein with many additives (glycerol, detergents, reducing agents) were generally unsuccessful, although the protein did show higher solubility in the presence of relatively high salt concentrations (~500 mM NaCl). Since only low yields of soluble EVM078 could be obtained, attempts to crystallize EVM078 were performed at lower concentrations than normally used for screening (<3mg/ml), and no diffraction quality crystals were obtained for this protein. The aggregation tendency of this protein may have also impeded the crystallization process. TK is known to form predominantly a tetramer, but the presence of monomers, dimers or higher aggregates may have caused the precipitation of EMV078 at high concentrations.

This structure was recently solved by another group and the use of size exclusion chromatography may have allowed for a greater stability of this protein at high concentrations since this was the final purification step used by this group (El Omari *et al.*, 2006). The crystals grown by the El Omari group were also not very robust since

they were small needle crystals (<50 μm), required the presence of thymidine triphosphate, MgCl$_2$ and DTT and only diffracted to 3.1 Å.

A.1.2.7 dUTPase (EVM026)

dUTPase fused to MBP was purified on an amylose affinity column, and further purified using cation exchange chromatography following cleavage. Although the protein was found to form aggregates when cleaved from MBP, the protein aggregates could be re-solubilised in the presence of the reducing agent DTT, and thus the aggregation was likely due to aberrant disulfide bond formation. However, no crystals were obtained from this preparation.

The vaccinia dUTPase structure recently solved by Samal and colleagues was purified using IMAC and the his$_6$-tag was removed prior to a second purification step using size exclusion chromatography in the presence of 10 mM DTT. The addition of MgCl$_2$ (5-10 mM) to the protein solution immediately prior to crystallization was also required to obtain crystals used for structure determination (Samal *et al.*, 2007).